## General Disclaimer

## One or more of the Following Statements may affect this Document

- This document has been reproduced from the best copy furnished by the organizational source. It is being released in the interest of making available as much information as possible.

- This document may contain data, which exceeds the sheet parameters. It was furnished in this condition by the organizational source and is the best copy available.

- This document may contain tone-on-tone or color graphs, charts and/or pictures, which have been reproduced in black and white.

- This document is paginated as submitted by the original source.

- Portions of this document are not fully legible due to the historical nature of some of the material. However, it is the best reproduction available from the original submission.

NGR-09-015-002

# SITE EVALUATION FOR LASER SATELLITE-TRACKING STATIONS

N. H. MAO and P. A. MOHR



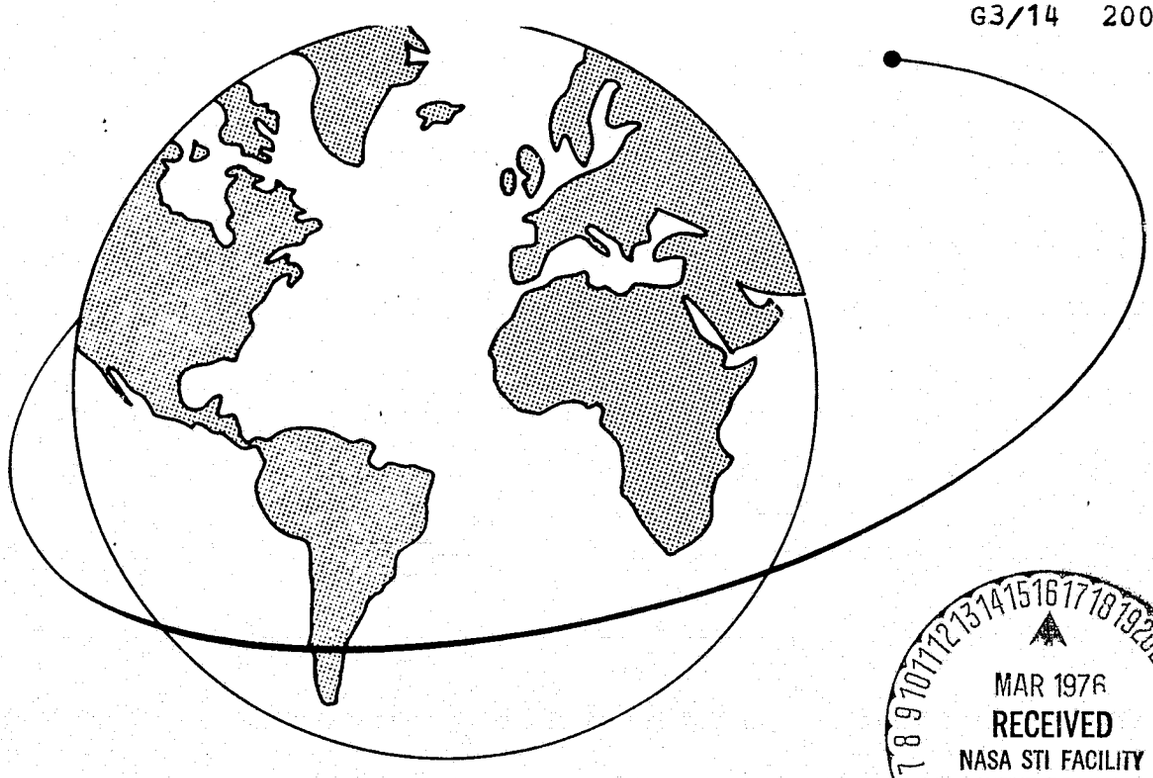




Smithsonian Astrophysical Observatory
SPECIAL REPORT 371

Research in Space Science
SAO Special Report No. 371

# SITE EVALUATION FOR LASER SATELLITE-TRACKING STATIONS

N. H. Mao and P. A. Mohr

February 6, 1976

Smithsonian Institution
Astrophysical Observatory
Cambridge, Massachusetts 02138

TABLE OF CONTENTS

TABLE OF CONTENTS (Cont.)

ILLUSTRATIONS

ILLUSTRATIONS (Cont.)



TABLES

## ABSTRACT

Twenty-six locations for potential laser satellite-tracking stations, four of them actually already occupied in this role, have been reviewed in terms of their known local and regional geology and geophysics. Laser tracking techniques are now reaching a precision where tectonic motions of station sites can be significant.

The chosen sites are scattered over the globe such that every major plate, except only for Antarctica, carries at least one site. In selecting the locations, preference has been given to shield areas stable since the early history (> 2 G.y.) of the earth. Other favorable criteria include remoteness from active plate margins or intraplate deformation zones and from recently glaciated areas and coastal margins. The station sites have been classified in a simple scheme incorporating strain-accumulation and strain-release (earthquake) risks.

Fifteen of the 26 sites qualify as suitable for a stable station whose motions are likely to reflect only gross plate motion. The others, including two of the present laser station sites (Arequipa and Athens), fail to qualify unless extra monitoring schemes can be included, such as precise geodetic surveying of ground deformation.

Additional to their geological and geophysical constraints, the sites are considered briefly in terms of weather and operational factors.

# SITE EVALUATION FOR LASER SATELLITE-TRACKING STATIONS

N. H. Mao and P. A. Mohr

## 1. INTRODUCTION

This report gives a preliminary evaluation of 26 existing or proposed laser-station sites from the point of view of their susceptibility to significant, local tectonic displacements. Operational and cloud-cover data are also included. The distribution of these sites is global (Figure 1) and, at least in the case of the existing stations, has been determined by factors that have not included consideration of tectonic stability. However, for the forthcoming generation of laser tracking stations, from which ranging precisions of only a few centimeters are expected, significant ground displacements within a regional reference frame of a few hundred kilometers can be effected, especially by seismic phenomena.

In order for a station site to be considered reasonably free from tectonic risk sufficient to impinge on the expected precision of laser observations made over a period of some years, it is desirable that the site be

A. On a shield area, free from regional crustal deformation, gentle epeirogenic movements excepted, since about 2500 to 2000 m.y. These shield areas are indicated on Figure 1.

B. Away from (> 100 km) currently active plate boundaries, especially the wider zones of deformation that occur on continents, as compared with the ocean floor.

C. Away from known intraplate deformation zones, marked both by historical seismicity and by Holocene faulting.

This work was supported in part by grant NGR 09-015-002 from the National Aeronautics and Space Administration.

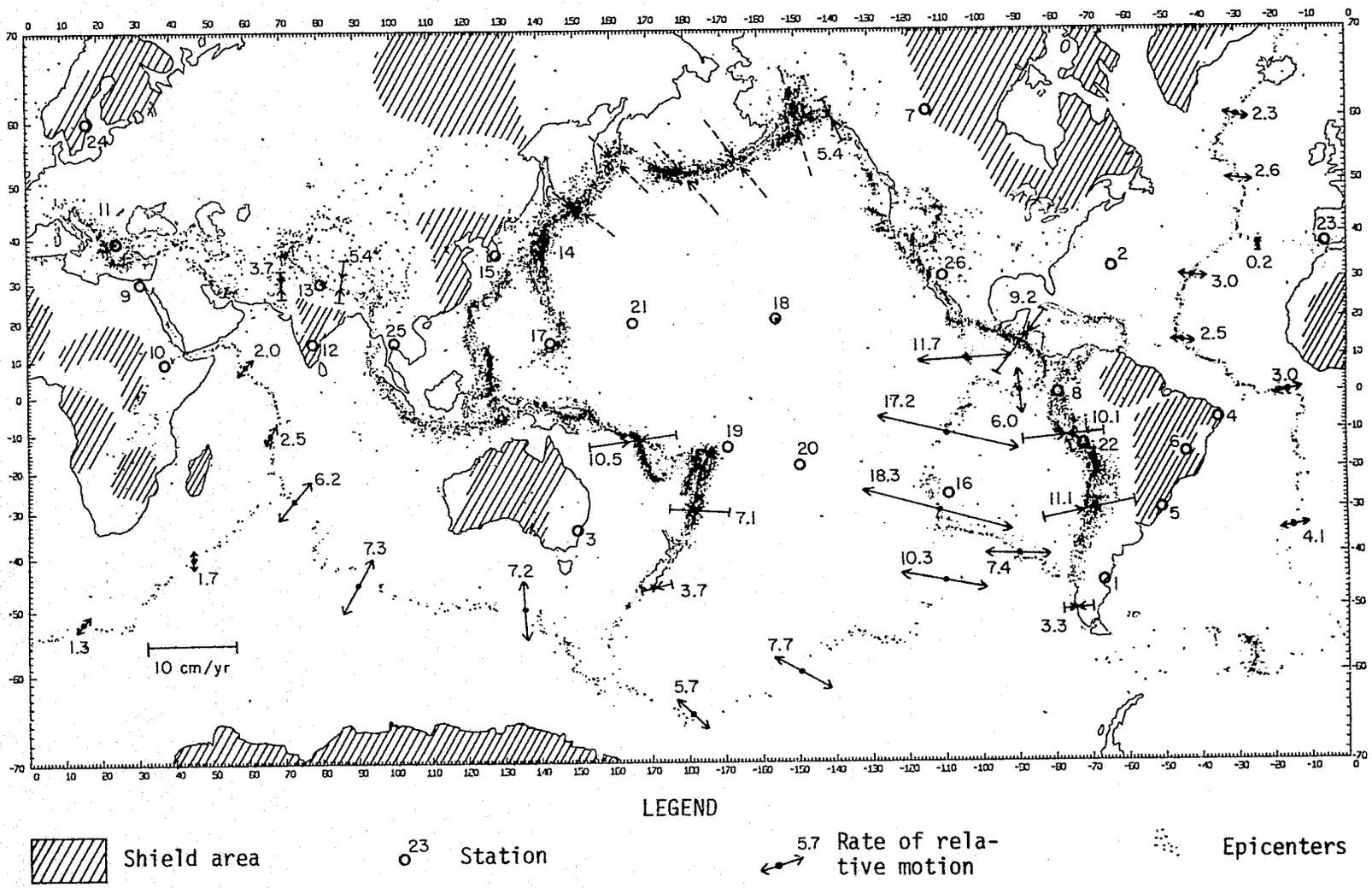


Figure 1. World map showing station sites (the number ascribed to each station is the same as indicated in Table 1), earthquake epicenters for the period 1961 through 1967 (after Barazangi and Dorman, 1969), relative motions of plates (after Minster, Jordan, Molnar, and Haines, 1974, model RM1), and shield areas (cross-hatched).

D. Away from recently glaciated areas, now subject to rapid isostatic uplift.

E. Away from coastal regions, where ocean tidal-loading effects are liable to be large.

In addition, it is necessary to have accurate geological and seismological maps for a good site evaluation, but these are regrettably not available for some areas. It is particularly desirable for each station site to be established within a precise geodetic network in order to measure both horizontal and vertical crustal motions out to a distance of at least 50 km from the site. At present, only a few stations are so equipped.

We have classified the station sites according to the estimated strain characteristics of each region, as described below.

A. Strain-rate risk. Strain refers to the amount of deformation in the crust; its units are dimensionless, and thus, for example, $10^{-6}$ in a terminal strain field signifies an extension of 1 mm $km^{-1}$. Strain rate is a measure of the buildup of strain.

good = almost certainly less than $10^{-6}$ $yr^{-1}$
poor = could be of the order of $10^{-6}$ $yr^{-1}$
bad = likely to be more than $10^{-6}$ $yr^{-1}$

B. Strain-release risk. Here we ignore aseismic strain release and refer to the likelihood of an earthquake producing a surface displacement greater than 10 cm. The time interval to contain this event is arbitrarily set at a century.

0 = minimal
1 = unlikely
2 = possible
3 = probable

C. Density of Holocene faulting around the station site (within a radius of 50 km). This is a crude but valid method of extending our estimates of

strain-rate risk and strain-release risk back from modern times to cover the last 10,000 years.

sparse = fault spacing more than 20 km
medium = fault spacing less than 20 km
dense = fault spacing less than 2 km

This scheme is applied in Table 1 to each of the stations under investigation. The geology and geophysics of the station sites are discussed individually in more detail in the ensuing sections.

Reliable meteorological data are available for the station sites (or nearby large towns) evaluated here. For present purposes, the crucial factor is cloud cover. In Table 2, monthly and mean annual cloud-cover percentages have been obtained from published meteorological records or from Smithsonian Astrophysical Observatory (SAO) files (see especially Thorp, Bush, and Pearlman, 1974; Pearlman, Hogan, Goodwin, and Kurtenbach, 1972). Where data are available only for a nearby town, the name of that town is given in parentheses after the station name.

The last column is Table 2 lists the number of months in the year when cloud cover averages 50% or more. These data require qualification. For example, although mean cloud cover at Porto Alegre exceeds 50% for 8 months in the year, not only is the excess small but the range about the mean is relatively small. This signifies that a given observing program at Porto Alegre is unlikely to be completely blotted out, and so this station is rated favorably.

Table 3 outlines operational factors, largely based on SAO experience, that concern transportation, communication, and accommodation facilities, as well as national considerations that may affect a long-term observing program. In the individual station evaluations that follow, we shall refrain from constant reference to Tables 1, 2, and 3, it being understood that the tables are based on these and SAO field observations. A final summary synthesis is given in the conclusions.

Table 1. Strain-rate and strain-release risks of the stations investigated for potential laser sites (see text for explanation).

| Station number* | Station location | Strain-rate risk | Strain-release risk | Holocene faulting |
|---|---|---|---|---|
| 1 | Argentina, Comodoro Rivadavia | good | 0 | sparse? |
| 2 | Atlantic Ocean, Bermuda | good | 0 | sparse |
| 3 | Australia, Orroral Valley | good | 1 | medium |
| 4 | Brazil, Natal | good | 0 | sparse? |
| 5 | Brazil, Porto Alegre | good | 0 | sparse? |
| 6 | Brazil, São Francisco | good | 0 | sparse? |
| 7 | Canada, Fort Resolution | good | 0 | sparse |
| 8 | Ecuador, Quito | poor | 3 | dense? |
| 9 | Egypt, Cairo | poor | 1 | medium? |
| 10 | Ethiopia, Debre Zeit | poor | 2 | dense |
| 11 | Greece, Athens | poor | 2 | medium? |
| 12 | India, Bangalore | good | 0 | sparse |
| 13 | India, Naini Tal | bad | 2 | dense? |
| 14 | Japan, Tokyo | bad | 3 | dense |
| 15 | Korea, Pusan | good | 1 | sparse? |
| 16 | Pacific Ocean, Rapa Nui | good | 1 | medium? |
| 17 | Pacific Ocean, Guam | poor | 3 | dense |
| 18 | Pacific Ocean, Maui, Hawaii | poor | 1 | medium |
| 19 | Pacific Ocean, Tutuila, Samoa | poor | 1 | medium? |
| 20 | Pacific Ocean, Tahiti | good | 1 | sparse? |
| 21 | Pacific Ocean, Wake Island | good | 0 | sparse? |
| 22 | Peru, Arequipa | bad | 3 | dense |
| 23 | Spain, San Fernando | poor | 1 | medium? |
| 24 | Sweden, Uppsala | good | 0 | sparse |
| 25 | Thailand, Bangkok | good | 1 | medium? |
| 26 | USA, Mt. Hopkins, Arizona | good | 1 | medium? |

*The code number ascribed to each station is the same as indicated in Figure 1.

Table 2. Monthly and annual mean-cloudiness data (in percent).

| Station number* | Station location | Jan. | Feb. | Mar. | Apr. | May | June | July | Aug. | Sept. | Oct. | Nov. | Dec. | Yearly mean | No. of months > 50% |
|---|---|---|---|---|---|---|---|---|---|---|---|---|---|---|---|
| 1 | Argentina, Comodoro Rivadavia | 51.9 | 35.1 | 32.8 | 44.8 | 53.4 | 44.7 | 58.2 | 58.3 | 58.0 | 46.0 | 42.1 | 60.2 | 48.8 | 6 |
| 2 | Atlantic Ocean, Bermuda | 51.0 | 51.0 | 47.0 | 42.0 | 41.0 | 40.0 | 30.0 | 33.0 | 36.0 | 45.0 | 45.0 | 51.0 | 42.7 | 3 |
| 3 | Australia, Orroral Valley (Canberra) | 45.0 | 51.7 | 45.2 | 46.0 | 48.1 | 50.9 | 44.6 | 44.3 | 40.5 | 50.2 | 50.0 | 44.4 | 46.7 | 2 |
| 4 | Brazil, Natal | 65.2 | 69.7 | 74.6 | 71.7 | 66.4 | 70.7 | 69.9 | 64.6 | 58.9 | 58.8 | 58.7 | 63.3 | 66.0 | 12 |
| 5 | Brazil, Porto Alegre | 51.0 | 49.0 | 50.0 | 49.0 | 53.0 | 54.0 | 56.0 | 54.0 | 60.0 | 54.0 | 55.0 | 49.0 | 52.8 | 8 |
| 6 | Brazil, São Francisco | 62.0 | 44.0 | 49.0 | 40.0 | 26.0 | 25.0 | 18.0 | 23.0 | 23.0 | 45.0 | 60.0 | 65.0 | 40.0 | 3 |
| 7 | Canada, Fort Resolution (Hay River) | 51.0 | 48.0 | 49.0 | 45.0 | 59.0 | 51.0 | 45.0 | 44.0 | 67.0 | 68.0 | 63.0 | 48.0 | 53.0 | 6 |
| 8 | Ecuador, Quito | 64.0 | 67.0 | 75.0 | 74.0 | 68.0 | 54.0 | 42.0 | 39.0 | 56.0 | 62.0 | 59.0 | 65.0 | 60.4 | 11 |
| 9 | Egypt, Cairo | 44.0 | 40.0 | 38.0 | 35.0 | 34.0 | 12.0 | 14.0 | 15.0 | 16.0 | 25.0 | 31.0 | 44.0 | 29.0 | 0 |
| 10 | Ethiopia, Debre Zeit | 38.8 | 56.2 | 52.5 | 55.4 | 55.7 | 62.4 | 80.3 | 75.3 | 66.9 | 42.1 | 35.1 | 28.9 | 54.2 | 8 |
| 11 | Greece, Athens | 55.0 | 56.0 | 52.0 | 41.0 | 36.0 | 24.0 | 10.0 | 11.0 | 23.0 | 40.0 | 56.0 | 57.0 | 38.4 | 5 |
| 12 | India, Bangalore | 30.0 | 18.0 | 17.0 | 39.0 | 49.0 | 69.0 | 83.0 | 83.0 | 79.0 | 61.0 | 42.0 | 44.0 | 51.2 | 5 |
| 13 | India, Naini Tal | 49.5 | 39.5 | 32.5 | 48.7 | 43.2 | 77.3 | 92.0 | 87.8 | 63.5 | 23.3 | 24.3 | 31.9 | 51.1 | 4 |
| 14 | Japan, Tokyo | 44.0 | 51.0 | 59.0 | 69.0 | 71.0 | 81.0 | 75.0 | 69.0 | 75.0 | 63.0 | 51.0 | 40.0 | 62.3 | 10 |
| 15 | Korea, Pusan | 39.0 | 41.0 | 49.0 | 55.0 | 58.0 | 70.0 | 69.0 | 54.0 | 64.0 | 44.0 | 39.0 | 30.0 | 51.0 | 6 |
| 16 | Pacific Ocean, Rapa Nui | 45.0 | 46.0 | 51.0 | 51.0 | 62.0 | 64.0 | 72.0 | 69.0 | 68.0 | 59.0 | 64.0 | 57.0 | 59.0 | 10 |
| 17 | Pacific Ocean, Guam | 72.0 | 71.0 | 70.0 | 67.0 | 65.0 | 69.0 | 79.0 | 82.0 | 80.0 | 76.0 | 66.0 | 65.0 | 71.8 | 12 |
| 18 | Pacific Ocean, Maui, Hawaii | 52.3 | 48.2 | 56.6 | 52.0 | 40.8 | 35.8 | 42.3 | 38.1 | 44.1 | 41.5 | 49.0 | 59.5 | 46.7 | 4 |
| 19 | Pacific Ocean, Tutuila, Samoa | 71.0 | 64.0 | 63.0 | 57.0 | 48.0 | 49.0 | 46.0 | 42.0 | 51.0 | 54.0 | 61.0 | 68.0 | 56.2 | 9 |
| 20 | Pacific Ocean, Tahiti (Papeete) | 60.0 | 57.0 | 50.0 | 49.0 | 54.0 | 52.0 | 44.0 | 50.0 | 42.0 | 49.0 | 51.0 | 62.0 | 51.7 | 6 |
| 21 | Pacific Ocean, Wake Island (Uselang Island) | 44.0 | 43.0 | 42.0 | 50.0 | 50.0 | 50.0 | 51.0 | 49.0 | 54.0 | 53.0 | 50.0 | 45.0 | 48.4 | 3 |
| 22 | Peru, Arequipa | 85.2 | 87.2 | 80.9 | 57.6 | 35.4 | 26.3 | 36.7 | 22.8 | 33.7 | 36.4 | 48.1 | 63.3 | 51.1 | 5 |
| 23 | Spain, San Fernando | 44.8 | 54.8 | 51.3 | 46.5 | 36.4 | 28.4 | 22.5 | 22.6 | 31.3 | 40.6 | 49.5 | 41.6 | 39.2 | 2 |
| 24 | Sweden, Uppsala (Stockholm) | 76.0 | 73.0 | 64.0 | 59.0 | 55.0 | 51.0 | 58.0 | 57.0 | 59.0 | 69.0 | 72.0 | 80.0 | 64.4 | 12 |
| 25 | Thailand, Bangkok (Rangsit) | 27.0 | 28.0 | 34.0 | 41.0 | 53.0 | 64.0 | 74.0 | 70.0 | 60.0 | 49.0 | 34.0 | 29.0 | 46.9 | 5 |
| 26 | USA, Mt. Hopkins, Arizona | 42.8 | 43.9 | 39.5 | 21.3 | 23.8 | 26.7 | 67.2 | 56.9 | 33.1 | 29.2 | 34.5 | 40.3 | 38.3 | 2 |

*The code number ascribed to each station is the same as indicated in Figure 1.

# Table 3. Operational factors.

| Station number* | Station location | Air transportation | Freight | Communications | Local living conditions | Local help | Utilities | National considerations |
|---|---|---|---|---|---|---|---|---|
| 1 | Argentina, Comodoro Rivadavia | Daily | Seafreight with delays | Via radio | Difficult | Difficult | Available | No present problem |
| 2 | Atlantic Ocean, Bermuda | Frequent | Seafreight monthly | NASA, Kindley AFB, U.S. Naval Station, commercial | No problem | Unskilled available | Available | NASA already there |
| 3 | Australia, Orroral Valley | Frequent | Regular | NASA | No problem | Available | Available | NASA already there |
| 4 | Brazil, Natal | Available | Difficult | Direct via radio | No problem | Available | Available | SAO already there |
| 5 | Brazil, Porto Alegre | Frequent | Monthly through Rio de Janeiro | Commercial, radio | No problem | Unskilled available | Available | No problem |
| 6 | Brazil, São Francisco | None | Truck | Radio | Difficult | Unskilled probably available | Probably irregular | No problem |
| 7 | Canada, Fort Resolution | Infrequent | None | Commercial, expensive; occasionally via radio | Difficult, cold | Impossible | No power, water plentiful | No problem |
| 8 | Ecuador, Quito | Frequent | Seafreight monthly through Guayaquil | Commercial, radio | No problem | Unskilled available | Available near city | Potential problem |
| 9 | Egypt, Cairo | Frequent | Monthly | Commercial | Difficult | Available | Available | Possible problem |
| 10 | Ethiopia, Debre Zeit | Frequent | Very seldom | Telex, Autodin, expensive | No problem, expensive | Difficult | Available | SAO there, but possible problem |
| 11 | Greece, Athens | Frequent | Regular | Autodin | No problem | Available | Available | No problem |
| 12 | India, Bangalore | Frequent | Extremely slow, through U.S. Embassy | Probably commercial, Autodin to New Delhi | Very difficult | Unskilled probably available | Probably available near city | Possible problem, many petty controls |
| 13 | India, Naini Tal | No direct flights | Seafreight with long delays | Commercial in India, Autodin to India | Difficult | Probably available | Available | SAO already there |
| 14 | Japan, Tokyo | Frequent | Regular | Autodin | No problem | Available | Available | No problem |
| 15 | Korea, Pusan | Frequent | Probably through Sasebo or Yokohama | Commercial, expensive | Very difficult | Unskilled probably available | Probably available | Probably no problem |
| 16 | Pacific Ocean, Rapa Nui | Twice weekly | Infrequent | Possibly commercial | Very difficult | Unskilled probably available | Power is scarce | Possible problem |
| 17 | Pacific Ocean, Guam | Frequent | Military seafreight | Autodin | No problem | Impossible | Available | No problem |
| 18 | Pacific Ocean, Maui, Hawaii | Frequent | Seafreight | Autodin, relay | No problem | Difficult | Available | SAO already there |
| 19 | Pacific Ocean, Tutuila, Samoa | Daily | Infrequent | Commercial | Difficult | Unskilled possibly available | Probably available near city | No problem |
| 20 | Pacific Ocean, Tahiti | Frequent | Infrequent | Probably commercial | Difficult | Difficult | Available close to city | Possible problem |
| 21 | Pacific Ocean, Wake Island | Less frequent | Military seafreight from Hawaii | Unknown, probably military | Difficult, confining | Impossible | From U.S. military | Probably no problem |
| 22 | Peru, Arequipa | Frequent | Twice per month | Direct via radio | No problem | Available | Available | SAO already there but possible problem |
| 23 | Spain, San Fernando | No direct flights | Seafreight via JUSMAG | Autodin | No problem | No problem | Available | SAO already there |
| 24 | Sweden, Uppsala | Frequent | Seafreight monthly | Commercial, expensive | No problem | Available | Available | No problem |
| 25 | Thailand, Bangkok | Frequent | Seafreight, poor | Commercial, expensive; Autodin, probable | Difficult | Difficult | Available near city only | No problem |
| 26 | USA, Mt. Hopkins, Arizona | Frequent to Tucson | Overland, air; regular | Telephone, teletype | No problem | Available | Available | SAO already there |

*The code number ascribed to each station is the same as indicated in Figure 1.

## 2. COMODORO RIVADAVIA, ARGENTINA

Comodoro Rivadavia (45°50'S, 67°30'W) is located on the shores of the Golfo de San Jorge, southern Argentina, a bay forming part of the structural unit known as the San Jorge Basin. South from the Rio del Plata, the San Jorge Basin is the third of four basins initiated during the late Jurassic-early Cretaceous* along the present coastal margin of Argentina. This initiation coincided with the breakup of Gondwanaland and radically modified the preexisting tectonic pattern of the region.

The coastal margin of Argentina, including the San Jorge Basin, has developed through several long-term oscillatory epeirogenic episodes of uplift and subsidence. These vertical movements have been more emphatic in the basins than in the relatively stable massifs separating the basins. The San Jorge Basin lies between the North Patagonian massif to the north and the Deseado massif to the south. The differential movement between basin and massifs has been accomplished partly by broad warping, but also by controlling WNW–ESE faults. To the west, the San Jorge Basin is cut by north–south faults, which, near the Preandes, form the linear Rio Mayo Basin of meridional trend: The Rio Mayo Basin marks the easternmost influence of Nazca-South American plate subduction, evidenced by three episodes of granitic plutonism during the late-Jurassic-mid-Tertiary interval in the Andes themselves, followed by crustal compression and folding during the Miocene (Halpern, 1973).

The San Jorge Basin contains a maximum of over 5000 m of sediments, of which the greatest thickness is of Cretaceous age, showing that vertical movements were correspondingly greater at that time than during the Cenozoic. Lower Cretaceous pyroclastics are unconformably overlain by nonmarine, petroliferous Cretaceous sediments (Chubut Group). At the close of the Cretaceous, a reversal of the regional down slope — from the Pacific to the Atlantic — occurred, apparently without interrupting deposition. A marine transgression

*See Appendix A for absolute ages.

across the basin in the Paleocene was followed by regression and nonmarine pyroclastic sedimentation during the Eocene. Total withdrawal of the sea from present Argentina during the Oligocene was followed by an equally general subsidence and marine transgression in the Miocene. The Miocene subsidence was probably related to volcanism in central-west Argentina and to an important phase of uplift of the Andes. Once more, emergence followed, during the Pliocene. In the Quaternary, there have been several short-lived advances of the sea in the present coastal region. Basaltic volcanism covered extensive areas during the Pliocene-Quaternary, indicating crustal tension in addition to the on-going, regional vertical movements (Zambrano and Urien, 1970).

The present boundaries of the San Jorge Basin with the adjoining massifs may possibly be fault-controlled (Zambrano and Urien, 1970; also see Figure 2). A postulated transcurrent fault, of sinistral sense, marks the Falkland-Malvinas escarpment on the continental shelf, extends WNW along the northern margin of the San Jorge Basin with the North Patagonian massif, and thus projects directly toward the Nazca-west Antarctic-South American plate triple junction into the Chile Rise. If the fault exists and is still potentially active, it has no recorded seismicity (magnitude $M > 4.5$). The virtual absence of seismicity in Argentina away from the Andes attests to a stability that excludes local strain accumulation but not regional epeirogeny.

Comodoro Rivadavia is thus unlikely to be hazarded by strain accumulation or release. Mean annual cloud cover is a little less than 50%, with 6 months of the year averaging above that value (Thorp et al., 1974). However, operational considerations are a difficulty for this station.

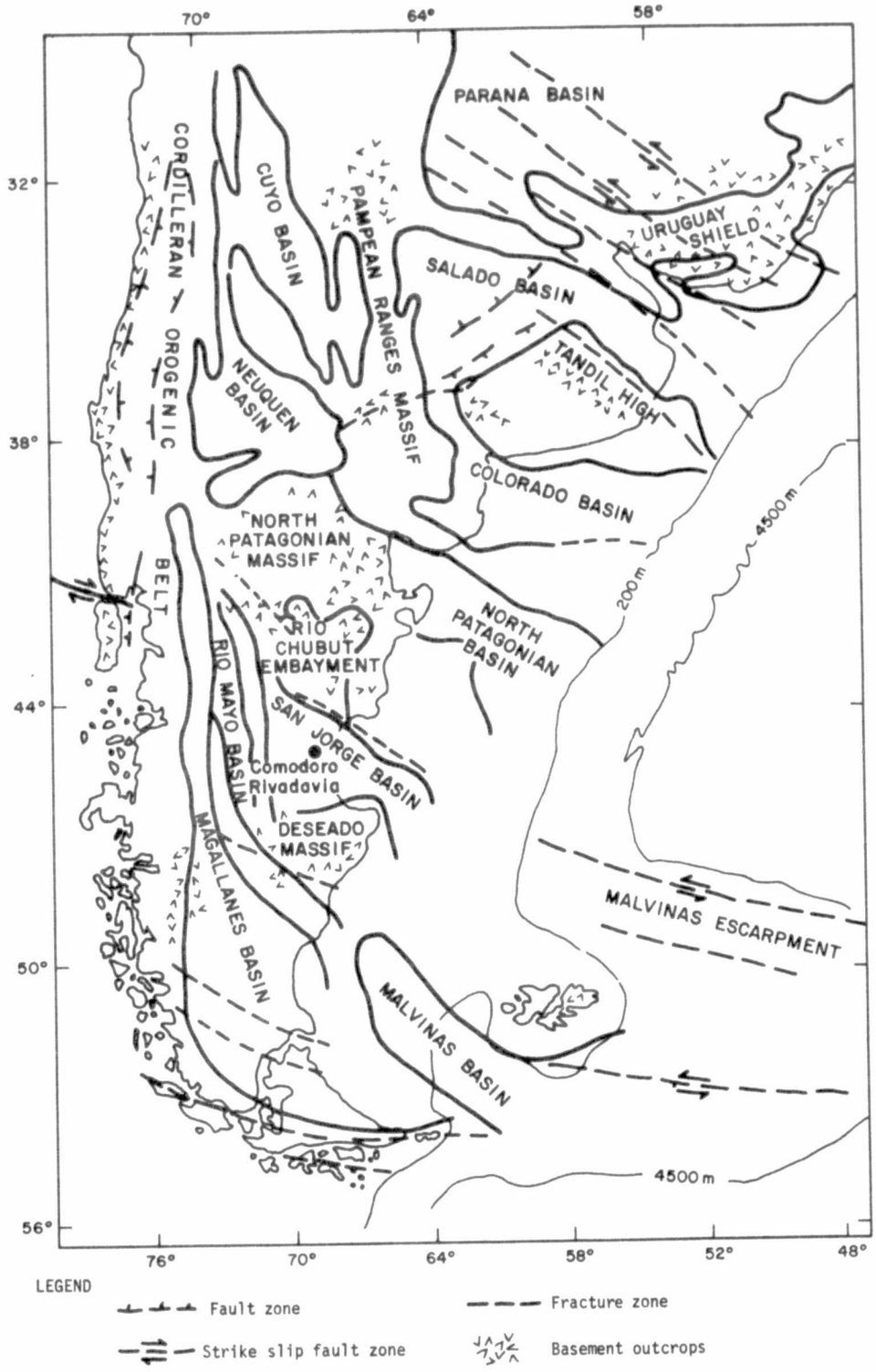


Figure 2. Tectonic map of southern Argentina (modified from Zambrano and Urien, 1970).

## 3. BERMUDA, ATLANTIC OCEAN

Bermuda (32°N, 65°W) is a volcanic pile capped with coralline limestone and dune deposits. It is the only above-sea-level expression of a 100-km-long line of volcanic seamounts, trending northeast–southwest. Farther north lies the New England seamount chain (Jacobs, Russell, and Wilson, 1974).

According to identification of magnetic stripes, the Atlantic Ocean floor around Bermuda is about 130 m.y. old (Figure 3); Bermuda itself is much younger. The original seamount resulted from a few-thousand-meter buildup of tholeiitic lavas near the axis of the mid-Atlantic ridge at least 90 m.y. ago. The pile remained dormant for the next 60 m.y. and subsided well below sea level as a result of lateral transport away from the ridge. Reactivation by unknown forces 33 m.y. ago led to intense intrusion of thin lamprophyric sheets into the old lava pile, increasing the volume of the seamount by almost 40% and resulting in the renewed emergence of an island (Reynolds and Aumento, 1973; Aumento, Reynolds, and Gunn, 1974).

Heat-flow values on Bermuda are close to 1.2 heat-flow units (HFU), which, though typical of old, stable ocean floors, is distinctly low considering the Oligocene intrusive activity that swelled the pile. It implies low radioactive heat production in the basalts (Hyndman and Aumento, 1973).

From data on resonant coupling of ocean Rayleigh waves to atmospheric shock waves from Apollo rockets, Donn and Ewing (1972) estimated that the Moho depth under Bermuda is about 11 km and the seismic-wave velocities $P_n$ and $S_n$ are 8.10 and 4.68 km $sec^{-1}$, respectively.

Bermuda is 800 km from the American continental margin and 2000 km from the mid-Atlantic ridge, the nearest plate boundary. In this northwestern Atlantic sector, no earthquakes ($M > 4.5$) have been recorded, and it seems a safe bet that the Bermuda region is tectonically stable.

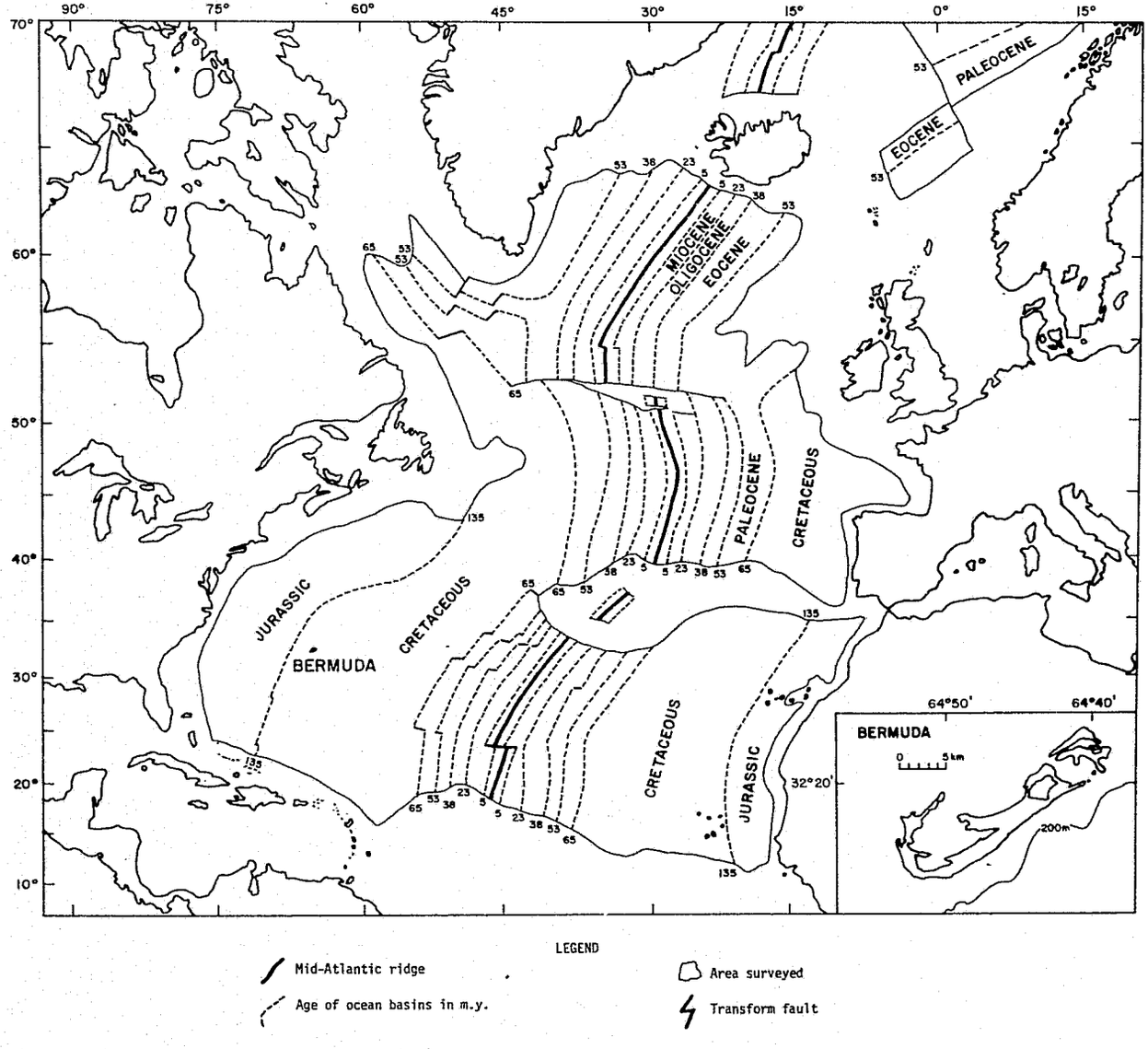


Figure 3. Age of ocean basins of the North Atlantic, with inset of Bermuda (modified from Pitman Larson, and Herron, 1974).

Operational and meteorological considerations for Bermuda are favorable. Only for 3 months of the year is cloud cover greater than 50%; the annual mean is 43%.

## 4. ORRORAL VALLEY, AUSTRALIA

Orroral Valley (35°38'S, 148°57'E, 940 m) is situated within the Paleozoic Tasman geosyncline of eastern Australia (Figure 4). The local rock types are granites and silicic volcanics of the Lachlan orogenic domain.

Whereas western and central Australia have remained essentially free from major crustal deformation since the Precambrian, eastern Australia was the site of subduction and orogeny during the Paleozoic. Subduction, directed westward, began in the early Ordovician at a previously stable, Cambrian continental margin. An andesitic volcanic arc developed (Figure 4), and Orroral Valley lies on the line of this ancient arc. The subduction zone migrated slowly eastward with time, and tectonism culminated in the mid-Devonian Tabberabberan orogeny. From then on, the area west of the subduction zone formed a relatively stable block called the Lachlan orogen. The subduction zone moved east to the present eastern margin of New South Wales, with development of the New England geosyncline culminating in a second major orogeny in the Permian. Subduction then moved east to the New Zealand-New Caledonia line (Oversby, 1971; Solomon and Griffiths, 1972).

The seismicity of Australia is concentrated into three belts (Stewart and Denham, 1974): a belt in western Australia, along the eastern margin of the Carnarvon Basin, where some 1968 earthquakes exceeded magnitude 7.0; an orthogonal system of transcurrent fault zones in central Australia (Figure 4), which Cleary and Simpson (1971) connect with the seismic belt of the Canning Basin to form a "subplate" boundary dividing the Australian continent; and a belt of epicenters following the Tasman orogenic zone between latitudes 25° and 40°S (Figure 4). In this third belt, earthquakes of magnitude 6 have occurred less than 100 km north of Orroral Valley, in a region marked by Quaternary fault scarps with east–west tensional displacements of the order of 1 m. The relationship of this contemporary tensional tectonism to the earlier major thrusts of the region is poorly understood (Geological Society of Australia, 1971).

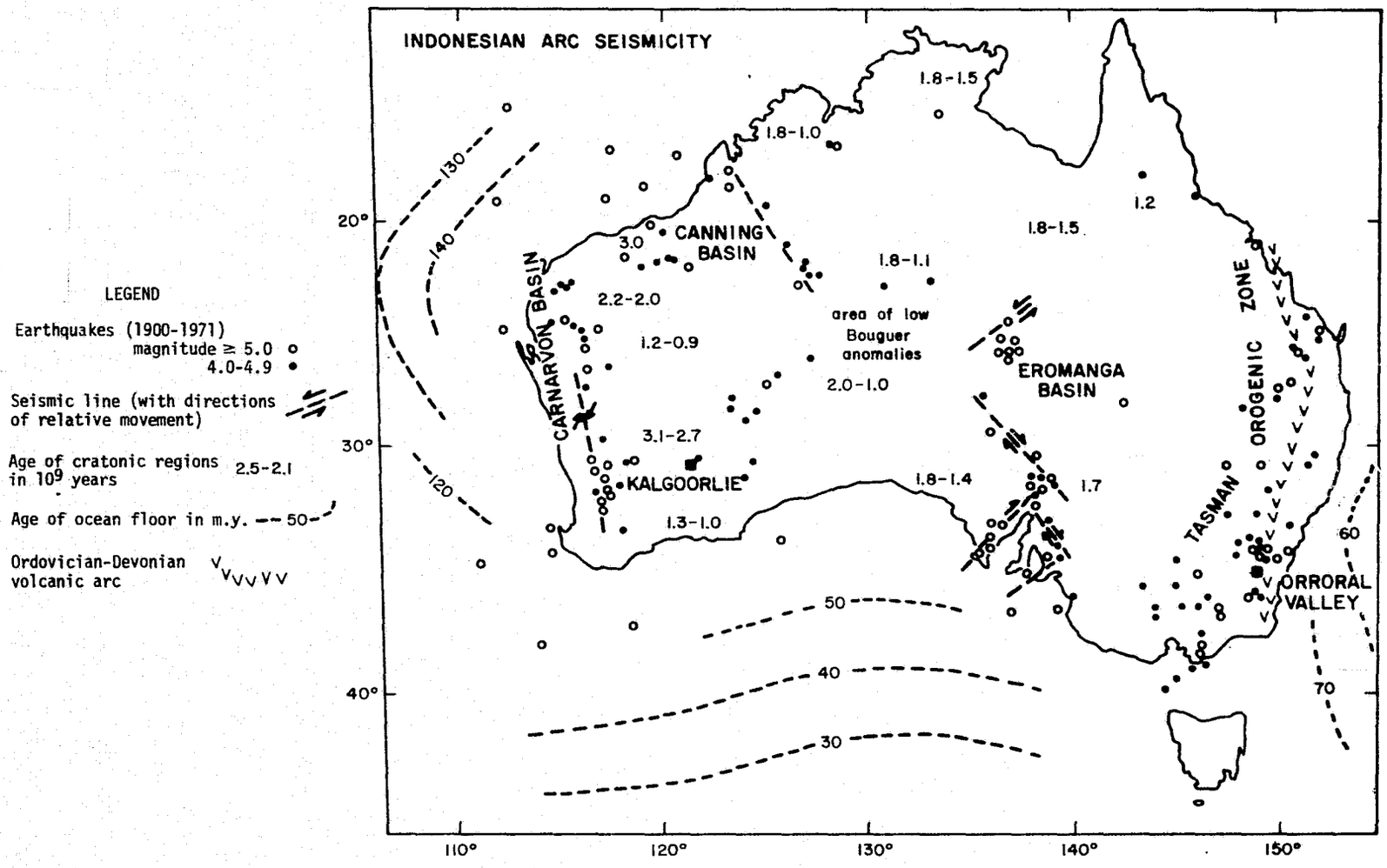


Figure 4. The Australian Shield, showing its provinces, some geophysical parameters, and its present seismicity (modified from McElhinny, 1973).

High $P_n$ and $P_i$ velocities are measured under the Australian Shield: The former increase from 8.05 km $sec^{-1}$ in central Australia to 8.40 km $sec^{-1}$ in western Australia, concomitant with increasing Precambrian age and probable thickness of the shield. Under the Tasman orogenic zone, in the Sydney-Canberra-Melbourne region, $P_n$ is measured at 7.86 km $sec^{-1}$. These figures are reflected in teleseismic P-wave arrival times: For central and western Australian stations, the arrivals are early, but for southeastern stations, they are delayed (McElhinny, 1973). It therefore appears that the mantle under the Tasman orogenic zone retains some of its low-velocity features from when the zone was active.

The average crustal thickness in the Orroral region is 40 km, and the depth to the Conrad discontinuity is about 20 km. Heat flow is highest in eastern Australia (1.2 to 2.8 HFU) and lowest under the western Australian Shield (0.69 to 1.3 HFU). The highest conductivity zone in the lower crust/upper mantle of Australia lies under western Victoria, about 700 km southwest of Orroral Valley, and is marked by concentrated seismicity.

In conclusion, Orroral Valley is situated well within the Indian plate on one of the least seismically active continents (Figure 1). However, it is not located on a Precambrian shield, but on a late Paleozoic orogenic belt that still preserves, to a rather unusual degree (cf. the Caledonides of Europe and North America), some of its original geophysical parameters and is seismically moderately active in response to a new, extensional tectonism.

Cloud-cover and operational considerations are good. The yearly mean cloudiness over Orroral Valley is $\sim$ 47%, with only 2 months of the year suffering 50% or more. Air transportation is frequent and regular, and there seem to be no communications problems.

## 5. NATAL AND PORTO ALEGRE, BRAZIL

Although separated by 3000 km, both Natal (5°46'S, 35°15'W) and Porto Alegre (30°03'S, 51°10'W) are on the Brazilian platform. This platform is a mosaic of possibly five ancient cratonic nuclei, the rocks of which are older than 2200 m.y., separated by foldbelts formed during the Trans-Amazonian (2200 to 1800 m.y.) and Braziliano (700 to 450 m.y.) orogenic cycles (de Almeida, Amaral, Cordani, and Kawashita, 1973). Natal lies on the Caririan foldbelt, which belongs to the Braziliano cycle, and Porto Alegre on the Ribeira foldbelt, which belongs to the cycle that is also identified as the Pan-African orogenic cycle along the West African coast (with which the Brazilian coast was united at that time) (see Figure 5).

Minor Phanerozoic epeirogenic movements are reflected in the deposition of largely clastic sediments on the Brazilian platform, but they remain flat-lying and undeformed, testifying to the stability typical of ancient continental shields. Both locations therefore appear tectonically stable. Nevertheless, occasional seismicity has been recorded along the continental margin of Brazil (Tarr, 1974), and an even better security against tectonic disturbance could be sought by an inland site, such as São Francisco (see Section 6).

Operationally, both sites are favorable, the only possible problem being with freight. The two locations differ, however, in the amount of cloudiness; Natal has greater than 50% cloud cover all months of the year, with an annual mean of 66%, whereas Porto Alegre has an annual mean of 53%.

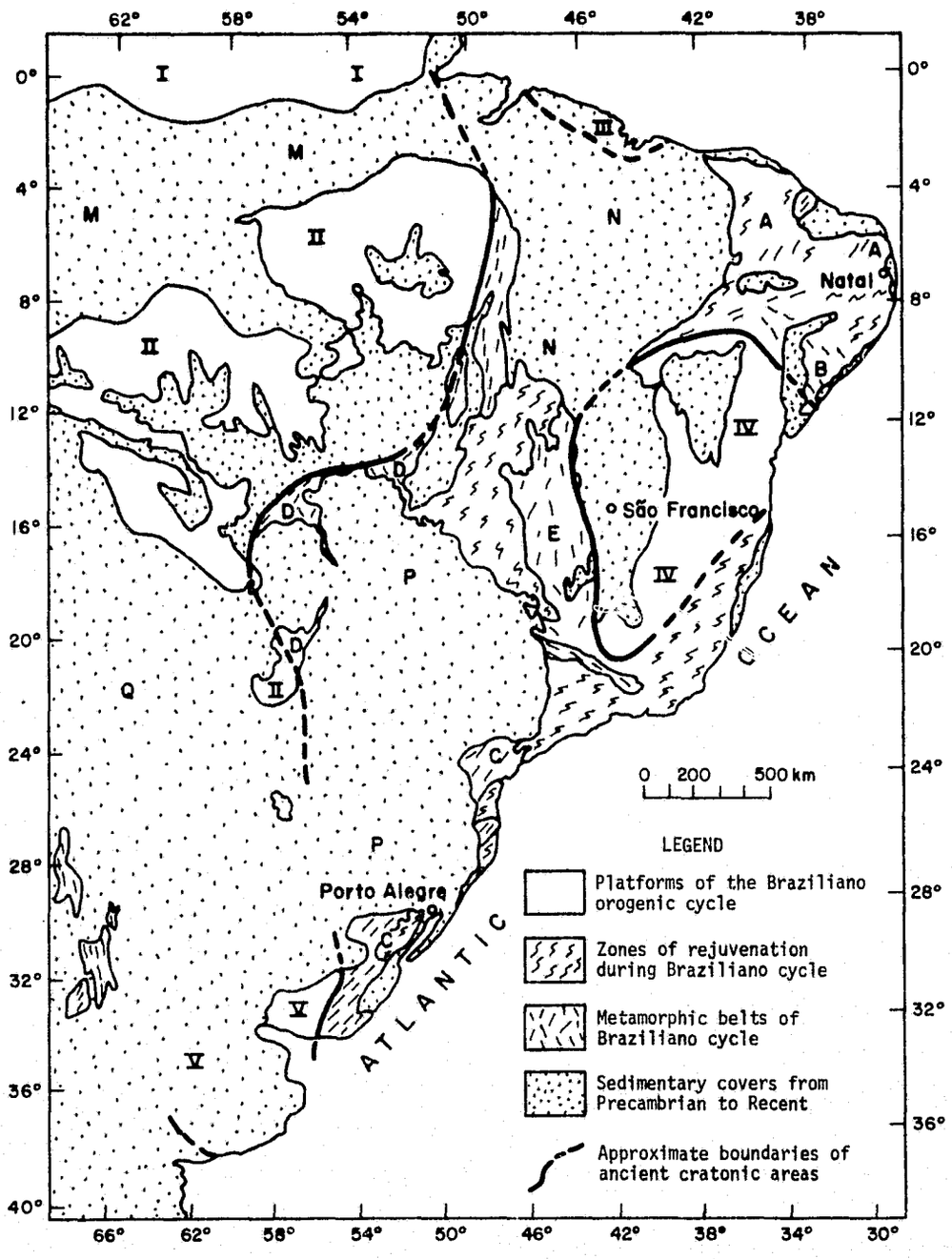


Figure 5. Tectonic outline of the Brazilian platform: (I) Guyana Shield, (II) Guapore platform, (III) São Luiz cratonic area, (IV) São Francisco platform, (V) La Plata cratonic area, (A) Caririan foldbelt, (B) Propria foldbelt, (C) Ribeira foldbelt, (D) Paraguay-Araguaia foldbelt, (E) Braziliano foldbelt, (M) Amazon sedimentary basin, (N) Parnaiba sedimentary basin, (P) Parana sedimentary basin, and (Q) Chaco sedimentary basin (simplified from de Almeida et al., 1973).

## 6. SÃO FRANCISCO, BRAZIL

Detailed geological and geophysical information is generally not available for most parts of Brazil, except for some mining districts. The whole of Brazil, east of the Andean orogenic zone, lies within the Brazilian platform, a geotectonic unit extending from eastern Venezuela to northern Argentina. This platform had obtained its present identity by early Paleozoic times.

The Brazilian platform is a mosaic of ancient cratonic nuclei comprising the Guyana Shield in the north; the Guapore craton in central Brazil; the São Luiz craton, forming a small region along the coast east of Belem; the São Francisco craton in east central Brazil; and a cratonic area extending through southern Uruguay and northeastern Argentina (de Almeida et al., 1973).

São Francisco (15°51'S, 44°52'W) lies near the western boundary of the São Francisco craton, about 100 km east of the margin of the Braziliano foldbelt (Figure 5). This foldbelt, separating the São Francisco and Guapore cratons, was affected by a major Upper Precambrian tectonomagmatic event notably marked by numerous intrusions of basic and ultrabasic rocks, which yield radiometric ages close to 1000 m.y. (the Uruacuano orogeny). The intercratonic foldbelts were then reactivated in the Braziliano orogeny, the deformation affecting miogeosynclinal deposits in the Brasilia region west of São Francisco. Contemporaneous deformation produced the Caririan foldbelt, separating the São Luiz and São Francisco cratons, on which Natal is situated. The rocks here are schists, phyllites, quartzites, and itabirites, folded with axes striking northwest and yielding rubidium-strontium ages close to 600 m.y., overlain by unfolded Cambro-Ordovician clastic "molasse" sediments of the Jaibaras Group.

The northern part of the São Francisco craton is composed of three metasedimentary units, which are separated by unconformities and are all

older than upper Precambrian. The tectonic strike is close to north–south. The oldest rocks (Carabia Group) are arkosic metasediments associated with basic and ultrabasic eruptives, which were migmatized and metamorphosed to granulite facies about 2000 m.y. ago. Overlying these are the amphibolite facies metamorphics of the Uaua Group, typically schists, quartzites, marbles, and amphibolites, plus several types of paragneisses. Following the Trans-Amazonian orogeny, the Jacobina Group of very thick (more than 8000-m) sediments and eruptives was formed, deposition being controlled by a zone of major north–south faulting of reversed type. Late Precambrian sandstones and limestones cover these three older formations and are only weakly folded and faulted.

No geophysical data are available for the São Francisco craton, but seismicity appears to be very low, though present along the coast (Tarr, 1974).

São Francisco appears to be a rock of stability. And with an annual mean of 40% cloud cover and only 3 months of the year showing greater than 50% cover, São Francisco seems to offer good observing conditions. Operationally, however, this location is a difficult one.

## 7. FORT RESOLUTION, CANADA

Fort Resolution (61°10'N, 113°39'W) is situated on the southeastern shores of Great Slave Lake, near the boundary between the Canadian Shield to the east and the Paleozoic-Quaternary sediments of the Great Plain to the west. The Canadian Shield is composed of two ancient cratons, enwrapped by younger rocks (Stockwell, 1962). The Keewatin craton forms central Canada and Labrador; the smaller Yellowknife craton lies between Great Slave and Great Bear Lakes. The two cratons are separated by the east-northeast-trending, mid-Precambrian Athabascan belt.

The McDonald Lake fault, a great Precambrian transcurrent fault, runs along the southern shores of Great Slave Lake and extends at least 500 km farther east; to the west, it is buried under the Great Plain sediments (Figure 6). The McDonald Lake fault separates cratonic rocks 2700 to 2800 m.y. old to the north from 1900-m.y.-old gneissic rocks to the south (Holmes, 1965). It may possibly mark a Precambrian plate boundary (Hoffman, 1973), but prefault compressional structures have the same northeast–southwest trend on both sides of the fault (Jacobs et al., 1974). A suite of dolerite dikes, younger than the fault, also trends northeast–southwest. The McDonald Lake fault was a line of dextral shear, active perhaps not long after 1900 m.y. ago but extinct before the end of the Precambrian. A few of the minor, associated faults show evidence of post-Devonian and even post-Cretaceous movements of small magnitude (Byers, 1962).

Post-Pleistocene glacial warping of the Canadian Shield has been measured from a study of deformed strand lines and tide-gauge records. The average rate of warping is about 1 mm $yr^{-1}$ over 100 km (Flint, 1971). The maximum (300-m) topographic displacement across the McDonald Lake fault (the southern side is higher) is probably due to differential movement during isostatic readjustment, as well as to differing weathering resistances of the rocks to either side: It does not represent tectonic displacement.

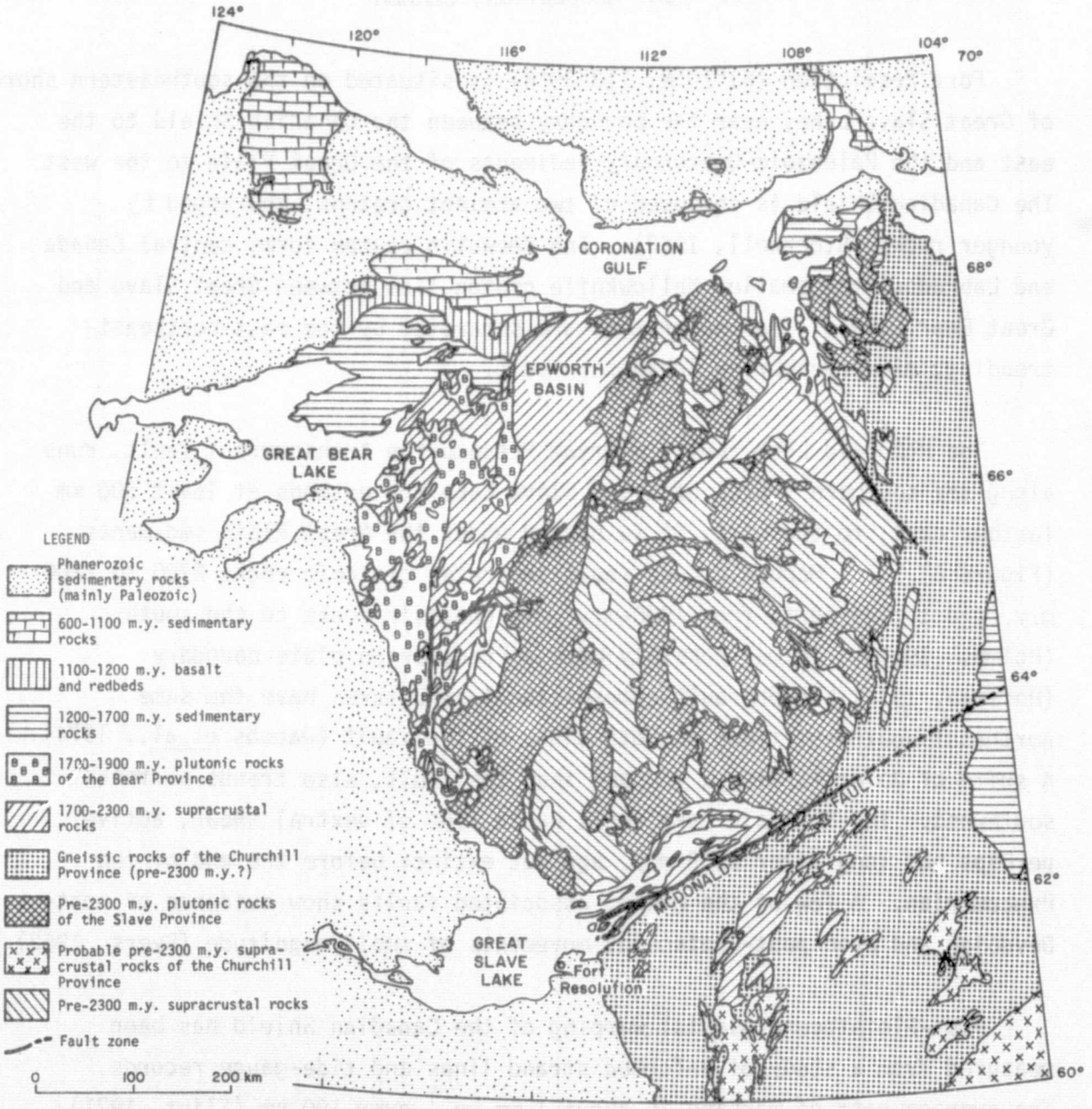


Figure 6. Geological map of the northwestern corner of the Canadian Shield (modified from Hoffman, 1973; Byers, 1962).

Fort Resolution is located 1000 km from the nearest active plate boundary, along the Canadian Pacific coast. However, the broad zone of on-going crustal deformation forming the Rocky Mountains is associated with minor seismicity, and a few $M > 4.5$ earthquakes have been recorded from the McKenzie Mountains, some 400 km west of Fort Resolution. Nevertheless, we regard Fort Resolution as a stable tectonic site.

It also appears favorable according to cloud-cover data, which show the annual average to be 53% and the cover to be less than 50% for 6 months of the year. Unfortunately, Fort Resolution would present operational problems in nearly every category investigated.

## 8. QUITO, ECUADOR

The Andean city of Quito (0°14'S, 78°30'W) lies at an elevation of 2850 m on the southeastern slopes of the volcano Pichincha (4700 m), which last erupted in 1666. The Andes represent the uplifted western margin of the South American plate, above the eastward-subducting Nazca plate, the distribution of earthquakes (Figure 7) according to their focal depth reflecting this fact (Tarr, 1974; Stauder, 1975). The South America-Nazca plate boundary is marked by the Peru-Chile trench for most of its length, but from north of the westernmost "bulge" of the South American continent, at the Peru-Ecuador border, the trench ceases to exist. This is probably related to the proximity, farther west, of the transformed Galapagos Ridge spreading line separating the Nazca and Cocos plates.

The Andes owe their origin essentially to block faulting along ancient lines of weakness. Where folding is present, it has been the result either of gravity sliding of unconsolidated sediments on tilted blocks or of lateral deformation from massive batholithic intrusions (Myers, 1975). During the mid-Cretaceous, the Precambrian basement and its thin sedimentary cover were block-faulted into ribbon-like belts parallel to the present coastline. Oscillatory vertical movements of these belts controlled the deposition of sediments, sometimes several thousands of meters thick, as well as their deformation. The Coastal Batholith was emplaced largely during the interval 105 to 95 m.y. ago, some of the magma breaking through to the surface to form voluminous andesitic volcanics.

The major uplift of the Andes began about 30 m.y. ago and has continued into the present (Myers, 1975). The average rate of uplift has been about 1 mm $yr^{-1}$, but the dynamic picture is not well known and the occurrence of major earthquakes attests to a drastic stop-go geomorphic agency. This seismicity is infracrustal, occurring above the subduction zone, and may be due to the excessive thickness and rigidity of the lithosphere and contained

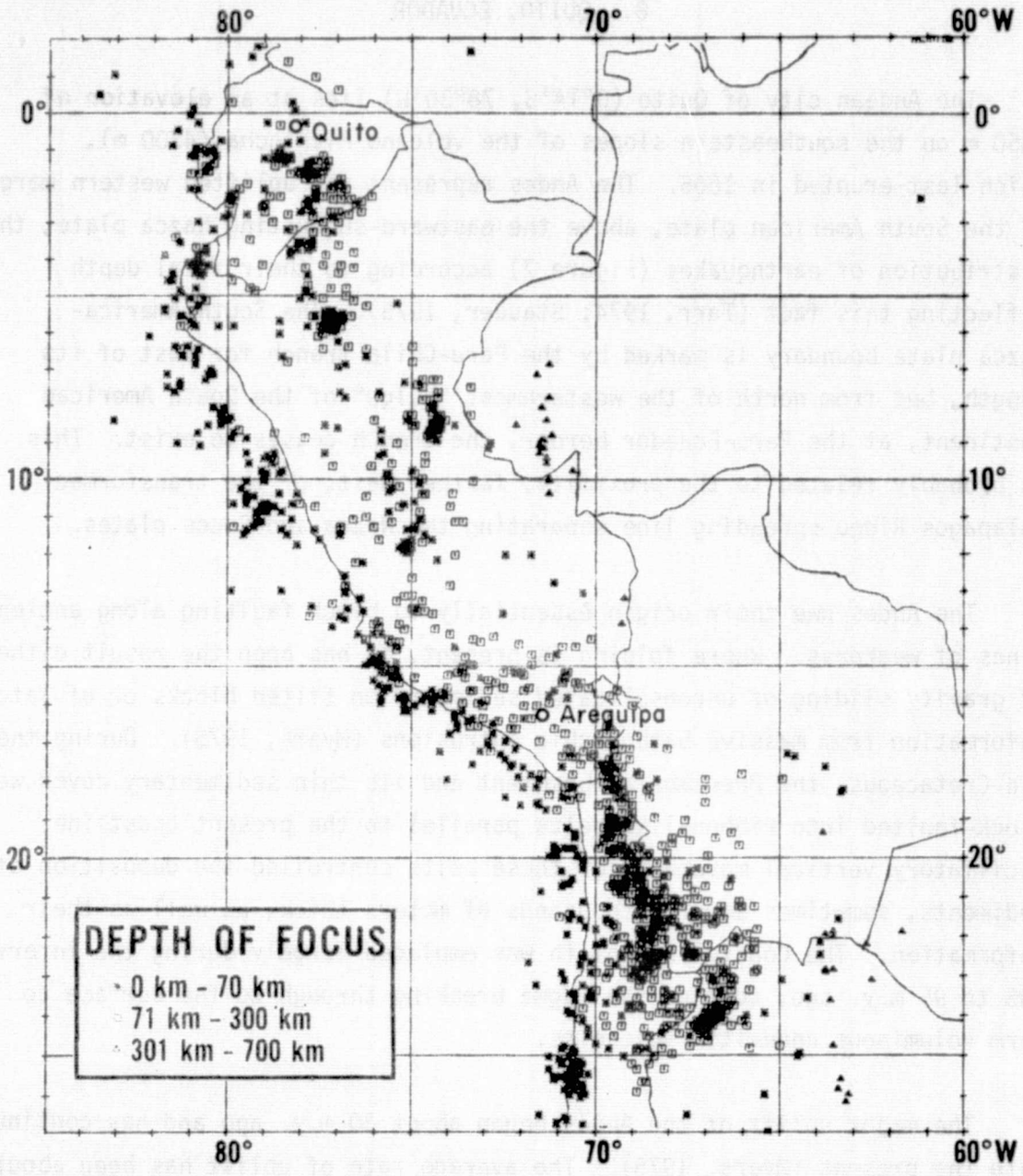


Figure 7. Seismicity of Peru and Ecuador for the years 1961-1968 (Stauder, W., Journ. Geophys. Res., vol. 80, pp. 1053-1064, 1975, copyrighted by the American Geophysical Union).

continental crust demonstrated to exist under the Andes (James, 1971; Cobbing and Pitcher, 1972). Barazangi, Pennington, and Isacks (1975) have identified a zone of sublithospheric high attenuation for seismic waves traveling through the wedge of mantle above the subducting Nazca plate, under central Ecuador. The reason for an unusual degree of partial melting, implied by the attenuation, in this region is not yet known, but there is the awesome presence of the large volcanoes Cotopaxi, Antisana, and Cayambe (Figure 8), as well as Pichincha itself, close to Quito (Whymper, 1892). During the 1929 eruption of Cotopaxi, the world's highest active volcano (5897 m), blocks weighing 200 tons were hurled as much as 15 km from the summit crater (Holmes, 1965, p. 294), and a further violent eruption occurred in 1942.

The convergence rate of the Nazca and South American plates in the Ecuador sector is estimated to be 8.8 cm $yr^{-1}$ (LePichon, Francheteau, and Bonnin, 1973). Major earthquakes in 1906, 1942, and 1958, with magnitudes of 7.8 to 8.9 (Kelleher, 1972), have occurred along the coast of northern Ecuador. The Quito region itself, situated near the southern end of an active volcanic belt of the Andes, experiences shallow and intermediate-depth earthquakes of moderate magnitude — for example, the 2 March 1967, M = 5.8 earthquakes at 0°18'S, 78°42'W, whose focal mechanism indicates normal faulting within the crust here (Stauder, 1975) — and therefore does not meet our geophysical criteria (Table 1).

Cloud-cover data likewise disfavor Quito as a satellite-tracking station, as only 2 months of the year show less than 50% cloud cover, with the annual mean being over 60%. Operational considerations, however, are satisfactory.

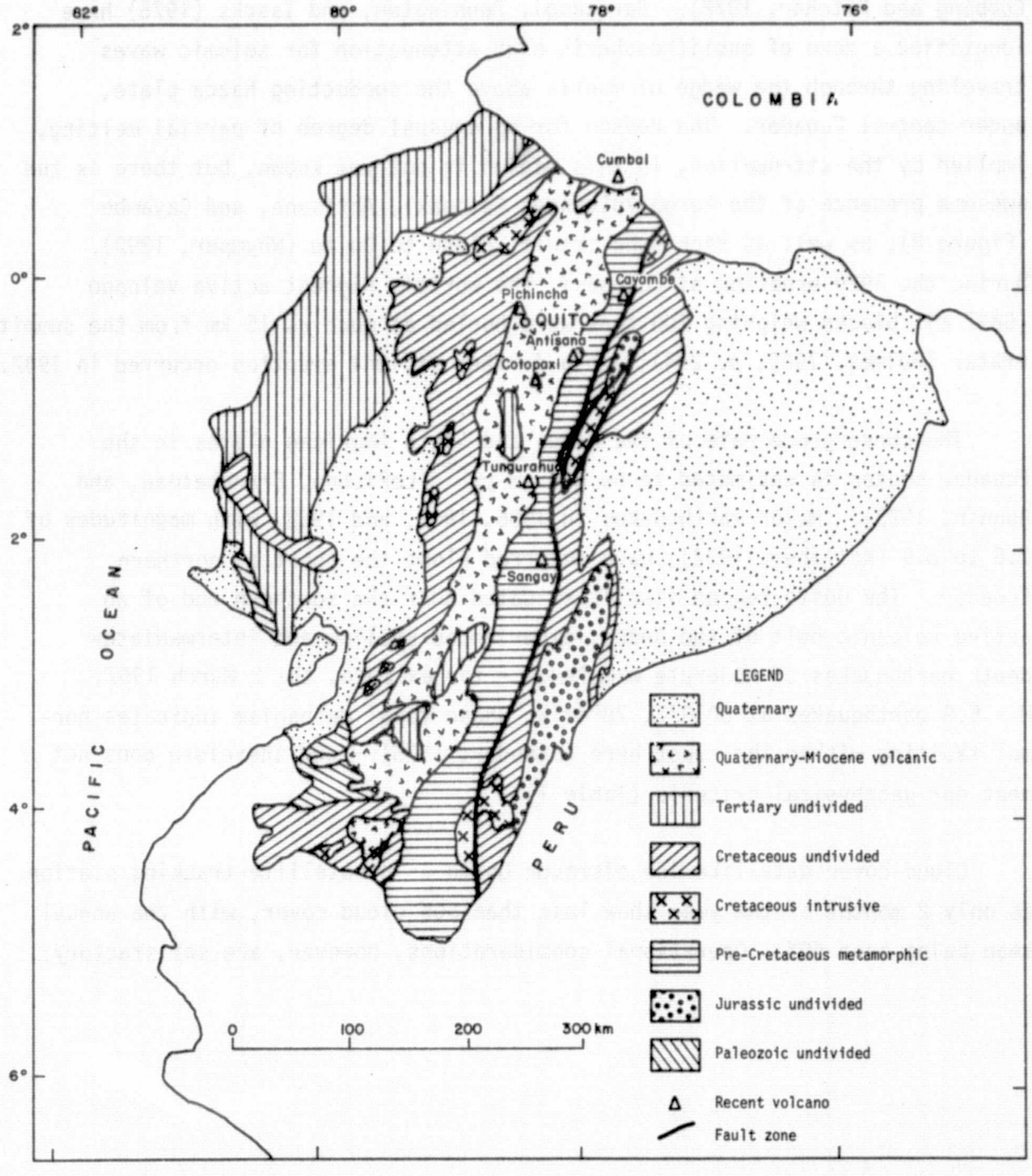


Figure 8. Geological map of Ecuador (modified from Stose, 1970).

## 9. CAIRO, EGYPT

Cairo (El Qahira) (30°03'N, 31°15'E) is situated at the upstream apex of the Nile delta, 150 km south of the Mediterranean coast. Close to the continental margin of north Africa and also to the young Red Sea and its northwesterly offshoot, the Gulf of Suez, the Cairo region was involved in extensive epeirogenic movements, with marine incursions and sedimentation, during the Mesozoic and post-Mesozoic. The last, Pliocene marine incursion up the Nile valley reached almost to Aswan (Said, 1962; Youssef, 1968).

The city of Cairo is on the northwest-trending Cairo graben, now largely buried, whose existence has been inferred from drilling and gravity data. The Precambrian basement lies at 2000-m depth, except in the graben, where it drops to 2500 m (Schürmann, 1971) across a width of about 15 km. The graben, which has the same trend as the Gulf of Suez, also has structural elements controlling the Nile valley (Youssef, 1968). The Gulf of Suez rift was initiated in the Oligocene, with minor associated tholeiitic volcanism; massive synthetic block faulting ensued in the Miocene (Robson, 1971).

The northwest-trending faults of northeastern Egypt are superimposed on older, compressional structures extending west-southwest from the North Sinai foldbelt (Figure 9). Youssef (1968) relates the Mesozoic development of this ancient pattern to the collision of Africa with Europe-Southeast Asia and to the upthrusting of the ocean floor to form Troodos, Cyprus (Gass and Masson-Smith, 1963).

The contemporary plate tectonics of the eastern Mediterranean region is complex (McKenzie, 1972). After neglecting several intervening microplates, the relative rate of convergence of Africa and Eurasia here is 2.5 cm $yr^{-1}$ along a meridional direction (LePichon, 1968). However, the closest plate boundary is that of Africa-Arabia, with a probable cul-de-sac offshoot up the Gulf of Suez. Thus, major seismicity has been

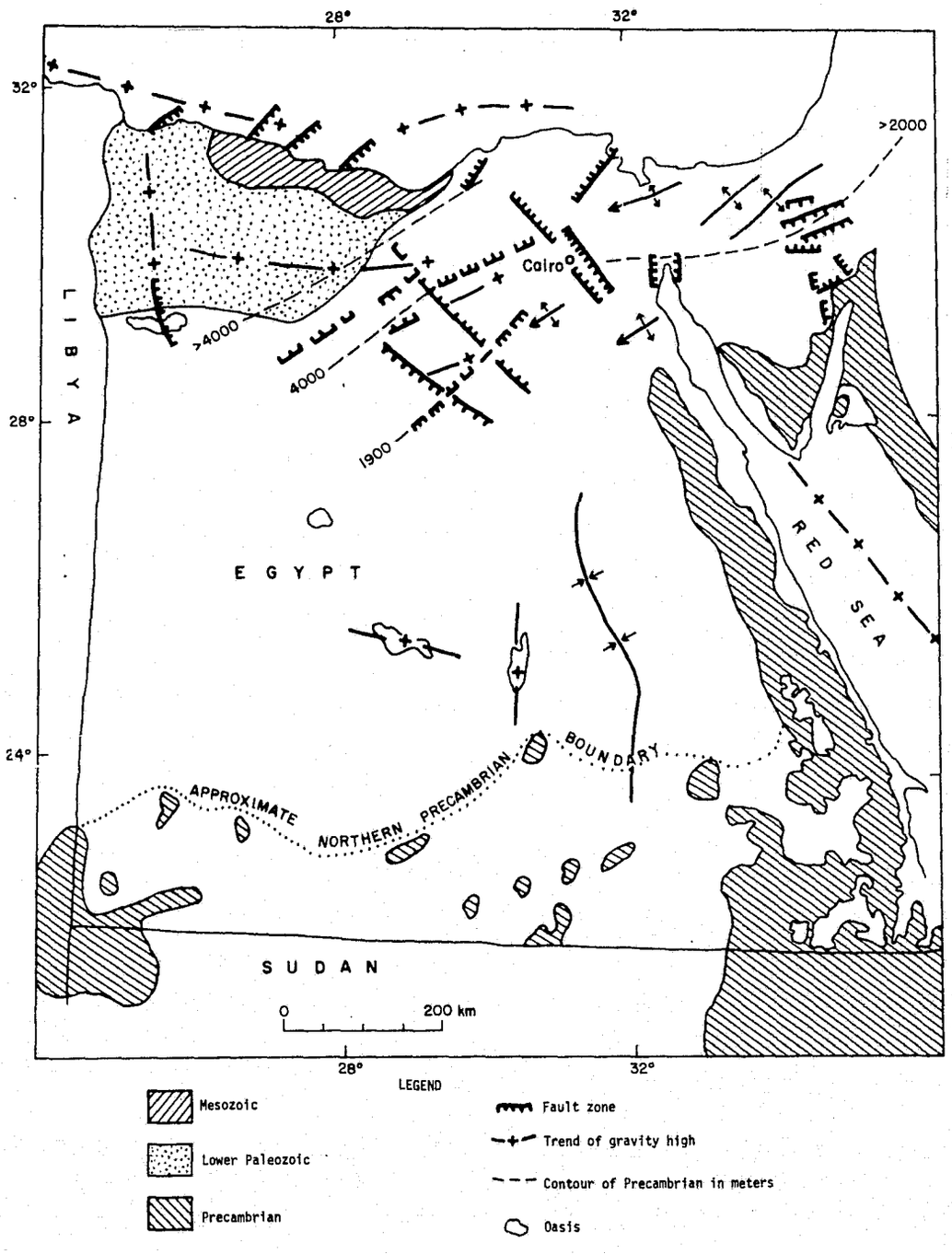


Figure 9. Tectonic map of Egypt (modified from Schürmann, 1971).

a feature of the southern end of the Gulf of Suez; the 1969 seismicity yielded focal mechanisms consonant with northeast–southwest crustal extension (McKenzie, Davies, and Molnar, 1970).

Seismicity in the Cairo region itself is not unknown (McKenzie, 1972), and a magnitude-4.9 earthquake occurred on 29 April 1974, some 60 km northeast of the city.

Cloud-cover conditions over Cairo are excellent; the annual mean is 29%, and all months show less than 50%. Operational considerations are equivocal at present.

## 10. DEBRE ZEIT, ETHIOPIA

The 3000-km-long African rift system is an incipient plate boundary traversing the eastern side of the African continent; it connects in the north with active oceanic spreading zones at the Afar triple junction, Ethiopia. Although the continental rift zones of Africa have a history extending in some places as far back as the Mesozoic (Baker, Mohr, and Williams, 1972), the major development has taken place during the last 4 m.y. The faulting of the rift gräben in Ethiopia, Kenya, and Tanzania, and the accompanying uplift of the plateau shoulders of the rifts through as much as 2000 m, have been dated as being late Pliocene-early Pleistocene in age (Baker and Wohlenberg, 1971; Mohr, 1967, 1975). This episode was preceded, during the mid-late Tertiary, by downwarping of the protorift margins and by emission of flood basalts (Baker, 1963; Mohr, 1971).

Debre Zeit (8°45'N, 38°57'E) lies on one of several parallel fault zones comprising the western margin of the Ethiopian rift valley near the northern end of the African rift system, at the latitude of Addis Ababa (Figure 10). This zone of normal faulting has been associated during the last few thousand years with the formation of a spectacular chain of maars (explosion craters), as well as with basaltic cinder cones and some lava flows (Mohr, 1961, 1974). Earlier, Pleistocene silicic volcanism built up a caldera volcano; it is on the denuded eastern fringes of this that Debre Zeit is situated. Hot springs are still active in the vicinity.

Geophysical parameters emphasize the active rift setting: Negative Bouguer anomalies, a high Poisson's ratio (0.29), the attenuation of teleseismic S-waves, and the delay (average 1.3 sec) in P-wave arrivals confirm the presence of low-density/partially melted upper mantle beneath this region. Attenuated crust under the rift and Afar is reduced to a minimum thickness of about 16 km under north-central Afar, with a transition down into the upper

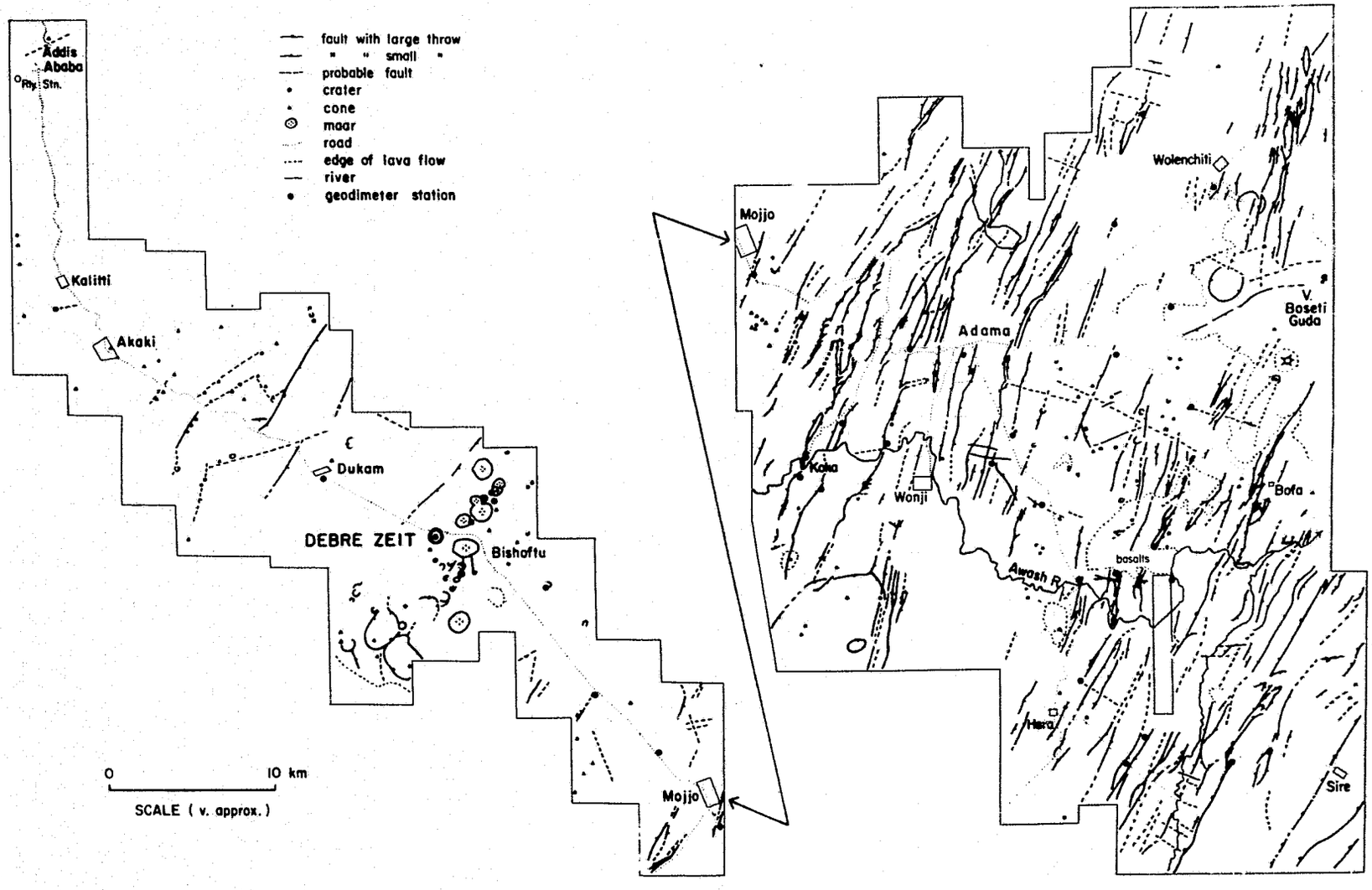


Figure 10. Structural map of the northern sector of the main Ethiopian rift.

mantle with $P_n$ values of 7.2 to 7.6 km $sec^{-1}$ (Searle and Gouin, 1971, 1972; Makris, 1975; Berckhemer, Baier, Bartelsen, Behle, Burkhardt, Gebrande, Makris, Menzel, Miller, and Vees, 1975).

Seismicity is characteristically irregular in this continental rift setting (Gouin, 1970; Thompson and Burke, 1974; see also Figure 11): On 14 July 1960, a magnitude-6.3 earthquake was centered on the volcano Chabbi, 170 km south of Debre Zeit. Frequent microearthquake swarms occur about 200 km north of Debre Zeit, on the Afar margin. On 25 August 1906, a magnitude ∿6.75 earthquake may have been centered within 75 km of Debre Zeit (Gouin, 1975).

Precise geodetic studies confirm the analysis of aggregate fault displacements (Mohr, 1973) — that strain-accumulation rates of up to $10^{-6}$ $yr^{-1}$ are active in the rift (Mohr, 1974, 1975). In view of the geologically recent volcanism and tectonism of the Debre Zeit region, such a rate may apply in this instance also.

Cloud-cover data show Debre Zeit to be good for satellite observations during about 6 months of the year, with an annual mean of 54%. Operationally, this location has been found to be favorable.

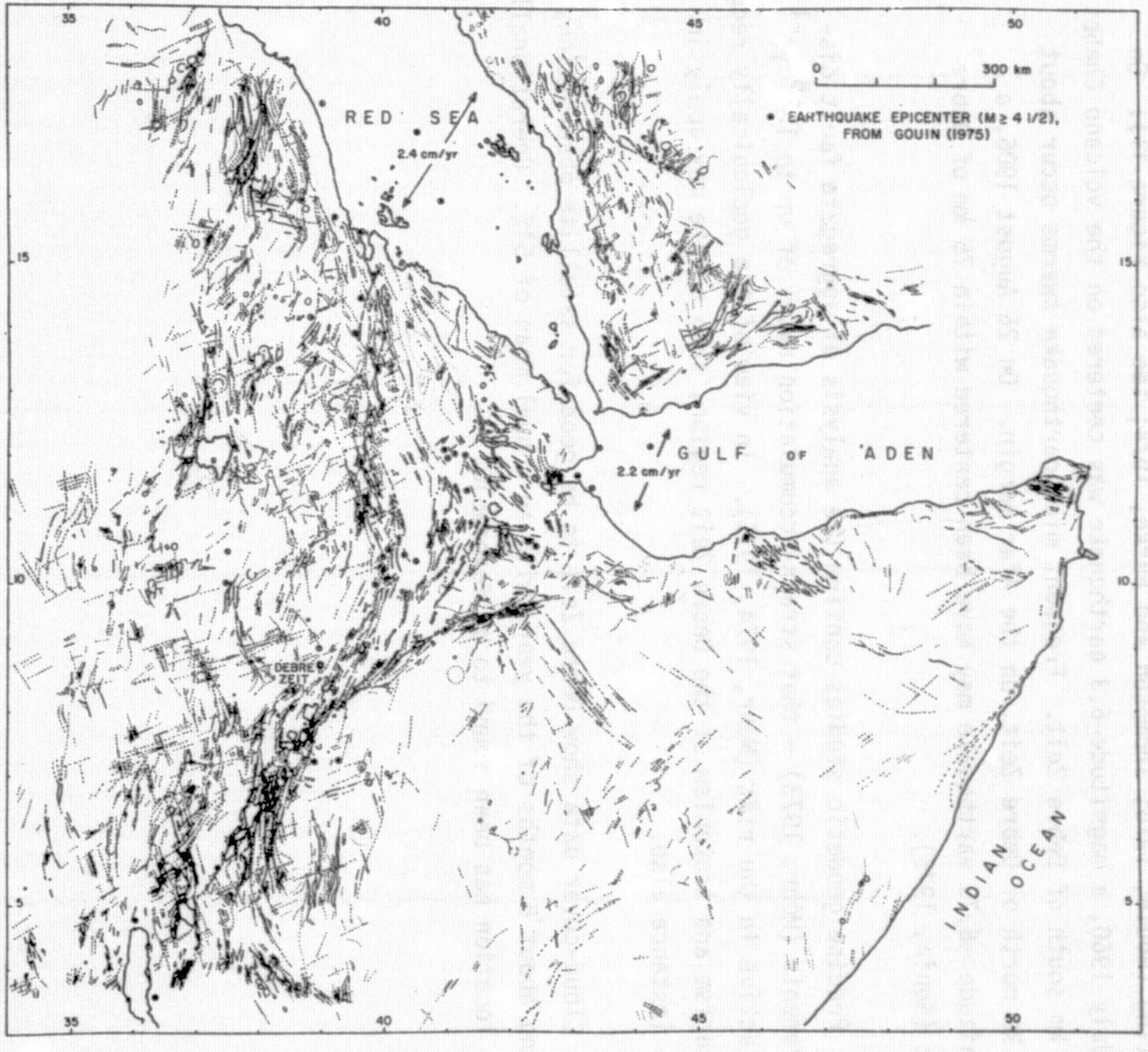


Figure 11. Structural map and present seismicity of Ethiopia.

## 11. ATHENS, GREECE

Athens (38°00'N, 23°44'E) is situated on the Aegean microplate, within the Alpine-Himalayan orogenic belt, which forms the southern boundary of the great Eurasian plate. Athens, and indeed most of Greece, lies on the Hellenide arc, a south-convex zone of compression, seismicity, and volcanism marking the subduction here of the African plate beneath the Aegean microplate (Figure 12). This subduction has been operating since the Jurassic.

Of the various parallel tectonic zones comprising the Hellenide arc (Makris, 1973), the Kyklades massif in the interior of the arc is where Athens is located. This massif is composed of Triassic-Cretaceous marine sediments affected by an intervening late Jurassic metamorphism that produced marbles and mica schists and, later, by block faulting during and after the Miocene.

The seismicity of the Athens region (Figure 1), though not so intense as for the outer zones of the Hellenide arc, where shallow-focus earthquakes are concentrated, is still appreciable, with focal depths between 150 and 180 km (Ninkovich and Hays, 1972; McKenzie et al., 1970). Quaternary volcanoes dot the Aegean (Pichler and Kussmaul, 1972), and Santorini, 220 km southeast of Athens, remains active. The dormant volcano of Aegina lies 30 km southwest of Athens. Depth to the Moho beneath Athens is 30 to 32 km, decreasing to slightly lower values eastward under the Aegean basin and increasing rapidly westward under the deeply rooted Peloponnese Mountains (Makris, 1973; also see Figure 12).

The complex episodic seismic pattern, and the wide variety of focal-plane mechanisms over small areas of the Aegean region, have been analyzed by McKenzie (1972). He concludes that the Aegean microplate is moving southwestward with respect to both Africa and Eurasia: Very tentatively, the relative motions are estimated to be 3.5-cm $yr^{-1}$ convergence between

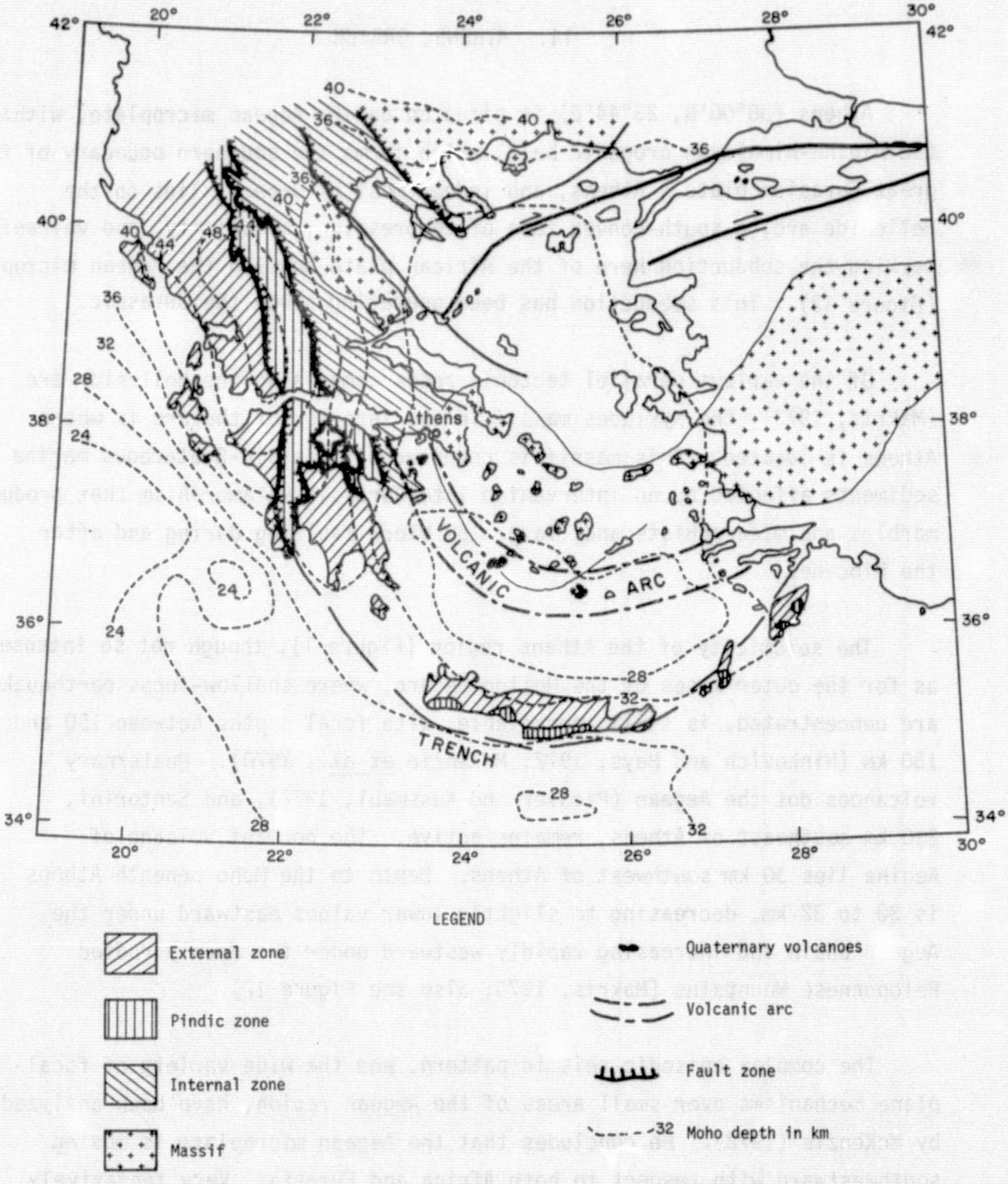


Figure 12. Tectonic map of the Hellenides, with Moho depth computed from gravity and seismic data (modified from Makris, 1973).

the Aegean and Africa and 2-cm $yr^{-1}$ dextral displacement southwestward of the Aegean against Eurasia. Because of the incompletely resolved complexities of active microplate tectonics in the Aegean region, it is difficult to recommend Athens as a laser-station site. Its cloud-cover data suggest favorable observing conditions during 6 months of the year, and its operational data reveal no significant difficulties.

## 12. BANGALORE, INDIA

The Indian subcontinent represents a detached fragment of the ancient Gondwanaland supercontinent. Despite the vagaries of plate motion from Cretaceous times, with India carried rapidly north into collision with the Eurasian continent, the ancient shield fragment comprising most of present-day India has remained unaffected by major tectonism since the end of the Precambrian. Late Precambrian-Phanerozoic crustal deformation has been restricted to mild epeirogeny with associated block faulting (Krishnan, 1968). The current shape of India was determined during the late Mesozoic, when Gondwanaland began to split, and the eastern coastal margin in the Bombay region remains seismically active.

Bangalore (12°58'N, 77°35'E) is in the central southern part of India (Figure 13), where the crustal rocks are Archaean gneisses and schists profusely intruded (radiometric ages are near 3000 m.y.) and overlain by the Precambrian Dharwarian sediments (2300 ± 100 m.y. near Bangalore) (Rogers, 1974; Holmes, 1965; Aswathanarayana, 1964). A charnockite metamorphism affected the region 1350 m.y. ago, and farther north, the shield was pierced by kimberlite pipes during the period 1450 to 840 m.y. ago (Paul, Rex, and Harris, 1975). The Dharwar and Eastern Ghats Archaean foldbelts converge southward and merge in the Bangalore region to give a north–south strike to the major structures. During the post-Mesozoic, the Indian Peninsula has been uplifted, possibly by underplating (Qureshy, 1971), but it remains in isostatic equilibrium.

According to Kaila, Gaur, and Narain (1972) and Varma, Gosavi, and Guha (1970), Bangalore lies on the boundary between a zone of least seismic risk (the Hyderabad region to the north) and one of minor seismic risk (south to Madurai), as shown in Figure 14.

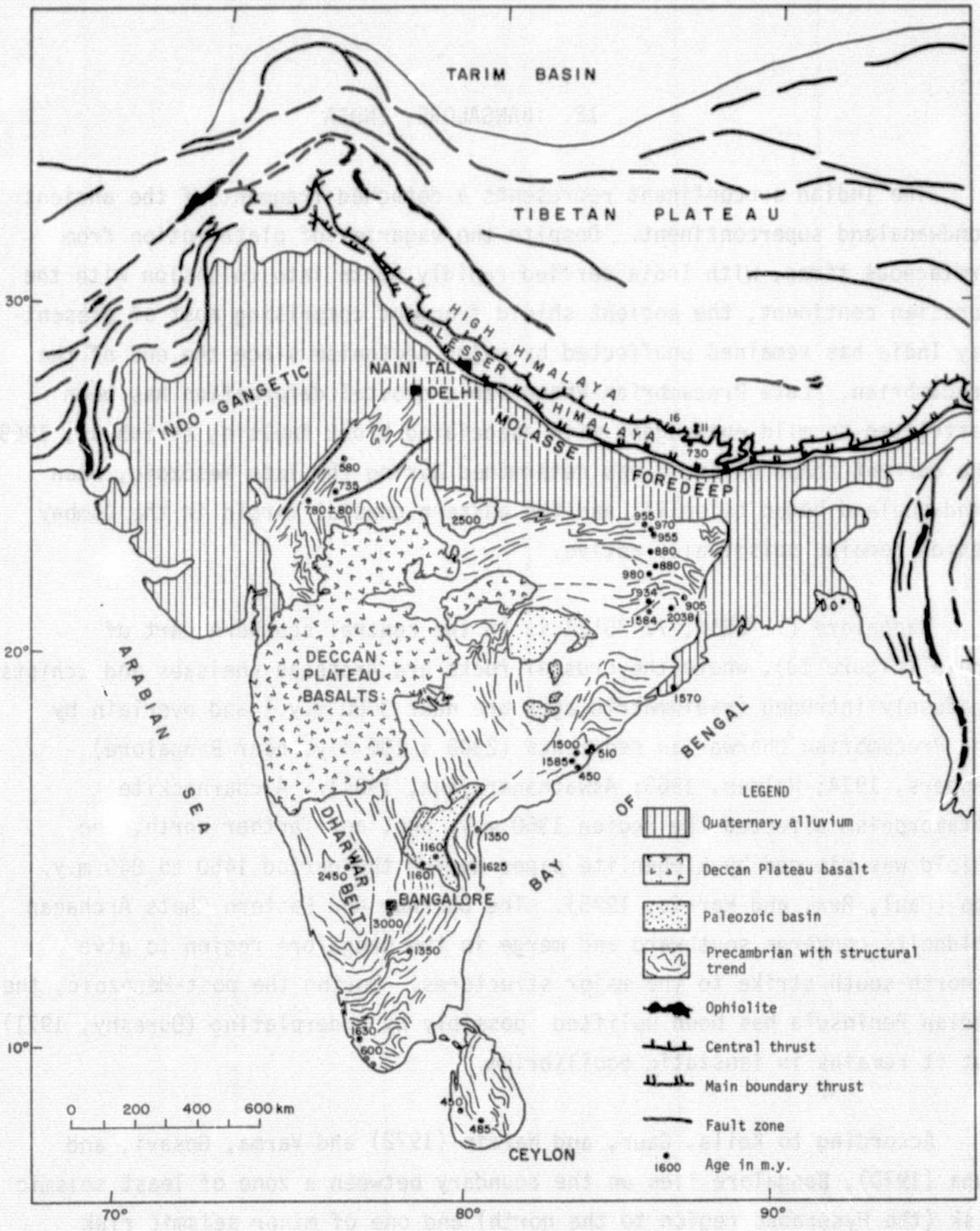


Figure 13. Tectonic map of India and adjoining regions (modified from Holmes, 1965; Powell and Conaghan, 1973).

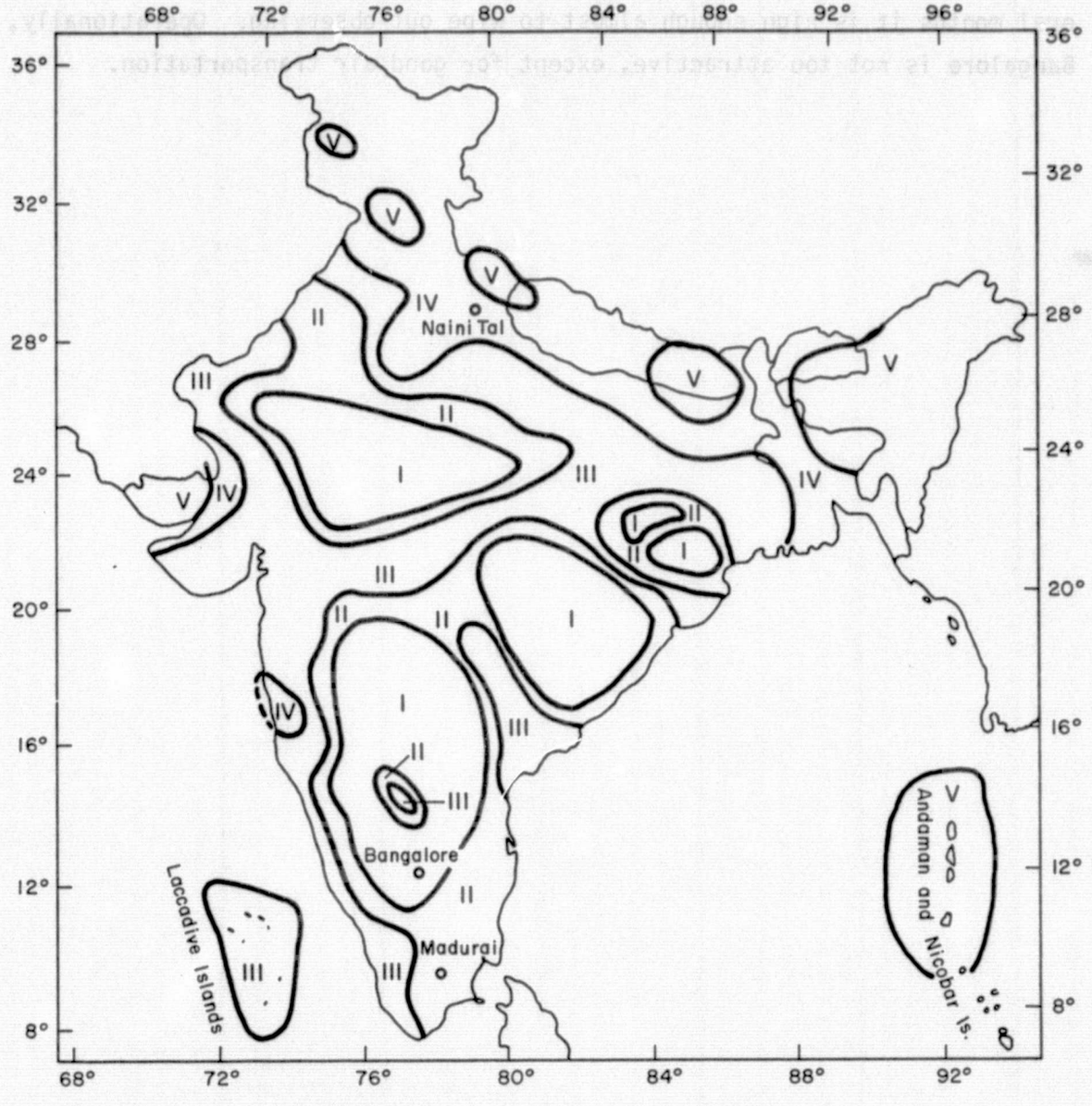


Figure 14. Map of India showing seismic zones. The intensities of future earthquakes, labeled here I, II, III, IV, and V, are associated with seismic zones on the modified Mercalli scale of V or less, VI, VII, VIII, and IX and above, respectively (simplified from Kaila et al., 1972).

Bangalore meets our geophysical requirements in all three areas listed in Table 1. Although the annual mean cloudiness is only 51%, during several months it is high enough almost to wipe out observing. Operationally, Bangalore is not too attractive, except for good air transportation.

## 13. NAINI TAL, INDIA

Naini Tal (29°22'N, 79°26'E) is located on the boundary between the Molasse Foredeep of the Indo-Gangetic plain and the thrusted sheets of the Lesser Himalaya (Gansser, 1964; Powell and Conaghan, 1973; see Figure 13). The Upper Miocene-Recent molasse lies on the underthrusting, northward-traveling Indian continent. The original "prow" of the Indian continent, which began to encounter Asia in the late Cretaceous and collided during the Paleocene, was broken off and, later, was underthrust to form the High Himalaya and, behind these, the Tibetan Himalaya. The front of the original Asian continent runs along the Indus-Brahmaputra suture. After the initial collision of India and Asia, there was lithospheric jamming until, in the early Miocene (20 m.y. ago), India began to underthrust its prow and the attached Asian continent. The Tibetan Plateau has been uplifted nearly 5 km owing to the underlying double thickness of continental crust. On the basis of distance to the northern limits of the Tibetan Plateau, the average rate of plate convergence at the Naini Tal sector, since the early Miocene, has been about 5 cm $yr^{-1}$ (Powell and Conaghan, 1973).

At least five major thrust faults run northwest–southeast near Naini Tal. They are directed south from the Central Gneiss root zone of the Himalaya and dip north at 30° to 40°; they take up most of the movement between India and its prow, now welded to Asia. Secondary tensional and tear faults are associated with these great thrusts (Mehdi, Kumar, and Prakash, 1972).

Quantitative seismicity maps of India (Kaila et al., 1972) show that the greatest concentration of epicenters lies along the High Himalaya, with lesser activity scattered across the Tibetan Plateau. Except at the two ends of the Himalayan arc, all foci are less than 50 km deep. Focal-mechanism solutions (Fitch, 1970) confirm the underthrusting of India beneath the Himalaya, with subordinate tensional mechanisms possibly associated with gräben in the Tibetan Himalaya. The computed seismic slip rate

from four large earthquakes is 6.8 cm $yr^{-1}$ along an idealized fault plane 2900 km long and 100 km wide (Fitch, 1970), in essential agreement with the convergence rate of 5.6 cm $yr^{-1}$ obtained from plate-tectonic synthesis (LePichon, 1968). Although precise geodetic surveys are now being undertaken to determine the actual present-day rates of movement on the boundary thrust faults along the front of the Lesser Himalaya, the situation of Naini Tal causes us to rate it poorly as a potential laser-station site.

Cloud cover over Naini Tal varies from 23 to 92% in different months; although its annual average is around 51%, too many months are almost completely lost to rate it as good for observing. Transportation and local living conditions in Naini Tal, where SAO already operates a Baker-Nunn camera station, are troublesome.

## 14. TOKYO, JAPAN

Five linked island arcs have played a role in the geological evolution of Japan: from north to south, the Kurile arc, the north Honshu arc, the Fossa Magna arc and its southward continuation into the Pacific as the Bonin arc, the southwest Honshu arc, and the Ryukyu arc (Holmes, 1965, p. 1137; Sugimura and Uyeda, 1973; Ludwig, Marauchi, and Houtz, 1975). The arcs are active convergent plate boundaries, marked by a deep trench and an associated negative gravity anomaly on the eastern oceanic side, by west-dipping subduction and associated seismicity, by prominent volcanic activity along the line of intermediate-depth earthquakes, and by some important transcurrent faults paralleling the arcs. Three plates are responsible for this tectonic arrangements: The Pacific plate is subducting west (at an integrated rate of about 9 cm $yr^{-1}$) under the Eurasian and Philippine plates, and the Philippine plate is likewise subducting west under the Eurasian plate. The three plates meet at a triple point in central Honshu. Tokyo (35°40'N, 139°45'E) lies on the outer, eastern side of the north Honshu arc, about 150 km east of the Fossa Magna (Figure 15).

The orogenic history of southwest Japan can be traced back at least as far as the Paleozoic, with strong compressional pulses during the Triassic and Cretaceous. During the Cretaceous, the transcurrent fault known as the Median Line divided southwest Honshu along its length. The formation of Japan as an island arc, and the history of most of the north Honshu region, began 26 m.y. ago in the late Oligocene (Watts and Weissel, 1975). Crustal subsidence during the Miocene initiated the behind-arc Sea of Japan and was accompanied by profuse calc-alkaline volcanism along the Japan Sea side of Honshu and along the Fossa Magna. The Fossa Magna is a narrow, sunken zone that trends meridionally across Honshu and divides the island; it has been formed by sinistral transcurrent faulting, with a total displacement of about 60 km, yielding an integrated rate of movement of about 3 mm $yr^{-1}$.

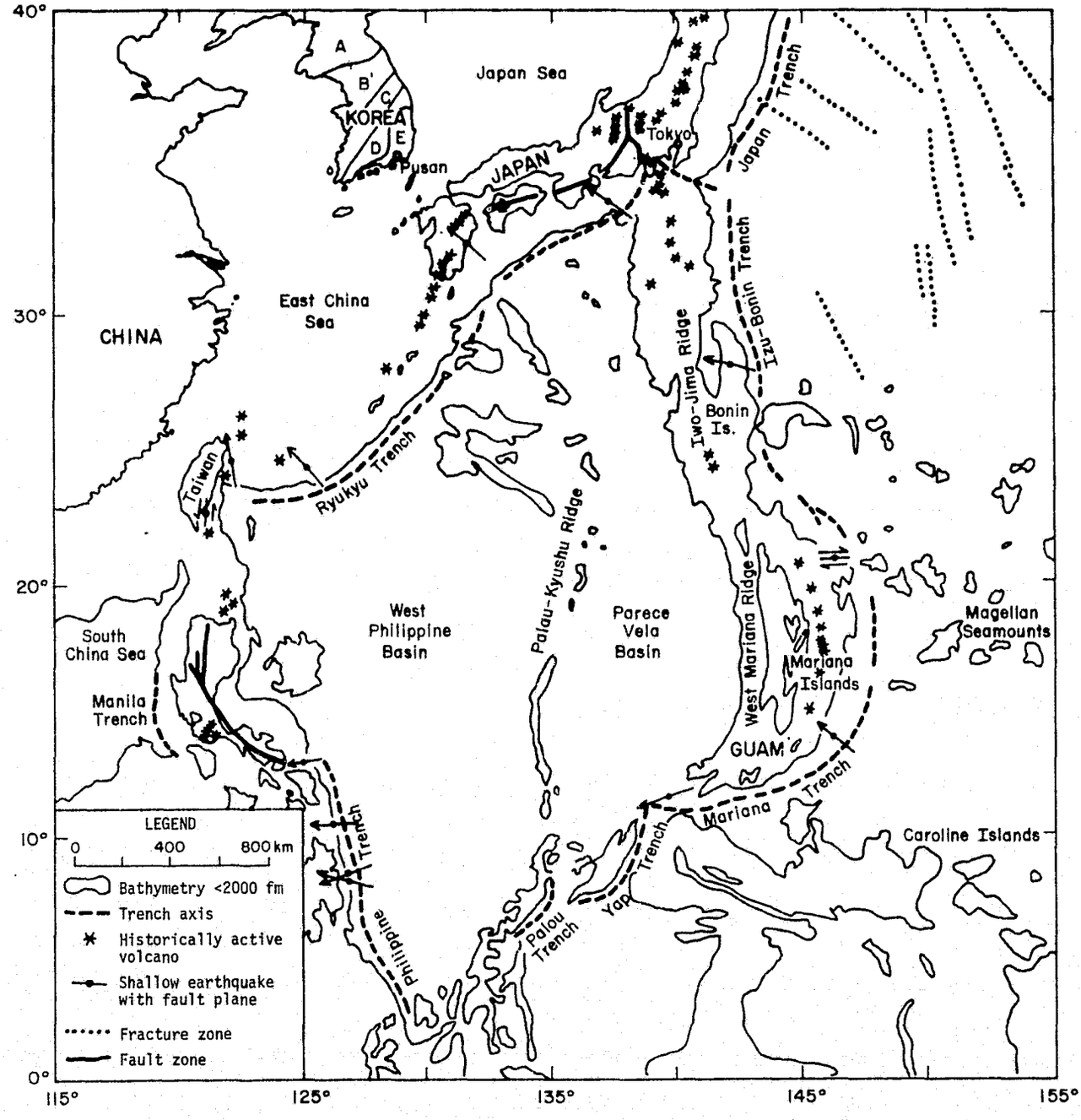


Figure 15. Structural elements of the Philippine Sea (simplified from Watts and Weissel, 1975) with tectonic provinces of Korea (simplified from Kobayashi, 1967). (A) Pyeongnam zone, (B) Kyeonggi massif, (C) Okcheon orogenic zone, (D) Yeongnam massif, and (E) Tsushima Basin.

A fierce renewal of volcanism, this time largely basaltic, during the Pleistocene has been responsible for most of the major calderas of Japan, many of which are still active. The main volcanic line lies along the western side of Japan, passing 120 km northwest of Tokyo (e.g., Asama-yama, 2500 m), but the isolated cones of Fuji-san (3776 m) and Hakone lie closer to the west-southwest of Tokyo.

Vertical tectonic movements during the last 2 m.y. have produced the present strong relief of Japan. The Kanto Plain, on which Tokyo is situated, has subsided during the Quaternary through a maximum height of 1400 m in the center of the plain. This indicates a rate of the order of 1 mm $yr^{-1}$, which conforms with the results of leveling surveys (Miyabe, Miyamuru, and Mizoue, 1966) and studies of dated marine terraces (Sugimura and Uyeda, 1973). The latter results show that this rate has operated on a time scale at least as short as $10^5$ yr, and possibly as short as $10^4$ yr (see Figure 16).

Horizontal-component crustal-deformation studies in western Japan reveal that in regions of active seismic swarms, linear deformation of as much as $10^{-4}$ $yr^{-1}$ can occur and that a change from linearity heralds a change in seismic activity (Kasahara and Sugimura, 1964; Kasahara, Okada, Shibano, Sasaki, and Matsumoto, 1967).

However, the release of crustal strain in sudden large movements is a well-known factor in the present tectonism of Japan (see Figure 1). Although most of the major earthquakes ($M > 18$) of this century have been located off the east coast, the one of 1 September 1923 ($M = 8.3$) was centered on the northern shore of Sagami Bay, 70 km southwest of Tokyo. This disastrous earthquake caused a clockwise rotation of the bay floor relative to the mainland, with a maximum observed displacement of 4 m (Holmes, 1965).

Despite the tectonically unstable setting of Tokyo, the density of geodetic polygons and leveling lines, together with supporting geophysical monitoring (e.g., see Kisslinger, 1975), is such that any crustal movements, on-going or abrupt, should be quantitatively resolvable within a regional setting.

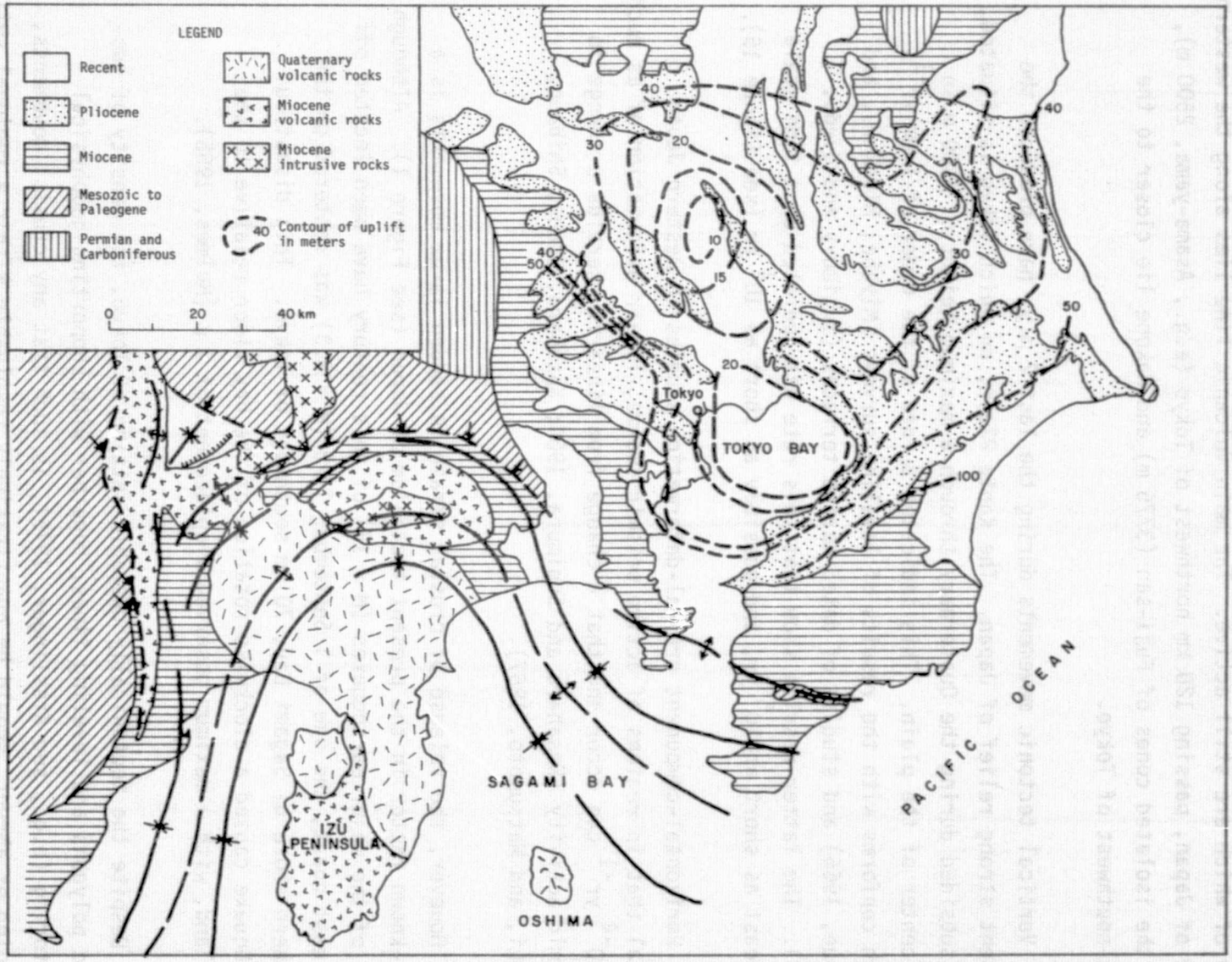


Figure 16. Tectonic map of the south Fossa Magna area and uplift of marine Simosueyosi terrace of the Kanto Plain during the last 125,000 yr (modified from Sugimura and Uyeda, 1973).

Cloud-cover data suggest Tokyo to be a poor observing site, with 10 months of the year having more than 50% cover. On the other hand, all the operational criteria check out favorably.

## 15. PUSAN, KOREA

The later Tertiary and Quaternary history of Korea is bound up with the evolution of the Sea of Japan. Before that, the structural framework of Korea was established by geanticlinal arching, along a northeast–southwest axis, of the Precambrian basement rocks during the Paleozoic. Within this basement, the Okch'eon orogenic zone separates the Kyeonggi massif to the northwest from the Yeongnam massif to the southeast. Farther southeast, the Tsushima Basin impinges on the Korean landmass (Figure 15), and it is here that Pusan (35°05'N, 129°02'E) is situated (Kobayashi, 1967).

Intense Cretaceous-Paleogene tectonism related to the birth of the Sea of Japan was associated with granitic intrusive activity in the present Korean peninsula. Mid-Tertiary granites have intruded Oligocene sediments in the Tsushima Island, between Korea and Japan, a faulted horst in the Tsushima Strait. Related north-northeast-trending faults cut early Tertiary sediments along the coast north of Pusan.

The Sea of Japan, including the Tsushima Basin, is floored with oceanic crust (Ludwig et al., 1975), although layers 2 and 3 are thickened, possibly as a result of excessive volcanic sedimentation during the early Miocene. However, if the western and central Sea of Japan originated from behind-the-arc sea-floor spreading, it must have done so before deposition of the undisturbed cover of ?Miocene sediments.

Present seismicity in the Sea of Japan is almost wholly from deep-focus events due to Pacific plate subduction under the Japanese arc. No equivalent deep-focus earthquakes are resulting from Philippine plate subduction: The northern limit of this subduction is marked by shallow and intermediate seismicity in Kyushu, on the southeastern side of the Tsushima Strait (Tarr, 1974; see Figure 1). The nearest earthquake to Pusan, magnitude $\geq$ 4.5, was recorded about 200 km to the northeast, in the Tsushima Basin.

Four hundred kilometers to the southeast runs the Eurasian-Philippines plate boundary, and a further 300 km southeast is the Unzen volcano, associated with the plate subduction. Less than 500 km northwest of Pusan, the north-northeast-trending boundary between the Liao-Ho syncline and the Liao-Tung uplift is seismically active: The latest large earthquake there was on 4 February 1975, M = 7.4; centered on Ying-k'ou (40°35'N, 122°35'E), it was felt in Seoul. Pusan is therefore located in rather a small eye in the middle of a storm.

Cloud-cover data indicate about 6 months of good observing conditions, with a yearly mean cloudiness of 51%. Air transportation is good, but other operational factors are less favorable.

## 16. RAPA NUI, PACIFIC OCEAN

Rapa Nui (Easter Island) (27°07'S, 109°27'W) lies 3700 km west of Chile and about 500 km east of the crest of the East Pacific Rise. It is situated near the western edge of the Nazca plate. The Nazca plate is bounded by some of the most active plate boundaries on the planet; it is separated by the East Pacific Rise from the Pacific plate in the west, by the Peru-Chile trench from the South American plate in the east, by the Chile Ridge from the Antarctic plate in the south, and by the Galapagos rift zone from the Cocos plate in the north (Figure 17).

Rapa Nui is one of only two reasonably large islands exposing the Nazca plate above sea level (the other is Juan Fernandez). It is roughly triangular in shape, with an area of 160 $km^2$ and a maximum width of 24 km. Although it is bounded in places by very high cliffs, especially in the north and southwest, much of the southern coastline is formed by single lava flows only a few meters thick. Inland relief is subdued, and the highest point, on Maunga Terevaka, is only 511 m above sea level (Baker, Buckley, and Holland, 1974; see Figure 18).

The island is the product of three principal volcanic structures: Maunga Terevaka in the north, Poike in the east, and Rano Kau in the southwest (Baker et al., 1974). Potassium-argon ages on single samples from the first two centers give values of 300,000 yr and 3 m.y., respectively, but there are even younger, undated lavas on Maunga Terevaka. The village on Rapa Nui, on the west coast, reclines on hawaiite lavas derived from the north-northeast-aligned fissure system of Maunga Terevaka.

Rapa Nui lies on the Easter Island fracture zone, which extends from 85°W west via a large transform fault (of which the fracture zone is the fossil trace) on the East Pacific Rise to 130°W on the Pacific plate (Figure 17). The fracture zone has only rare, and then usually small,

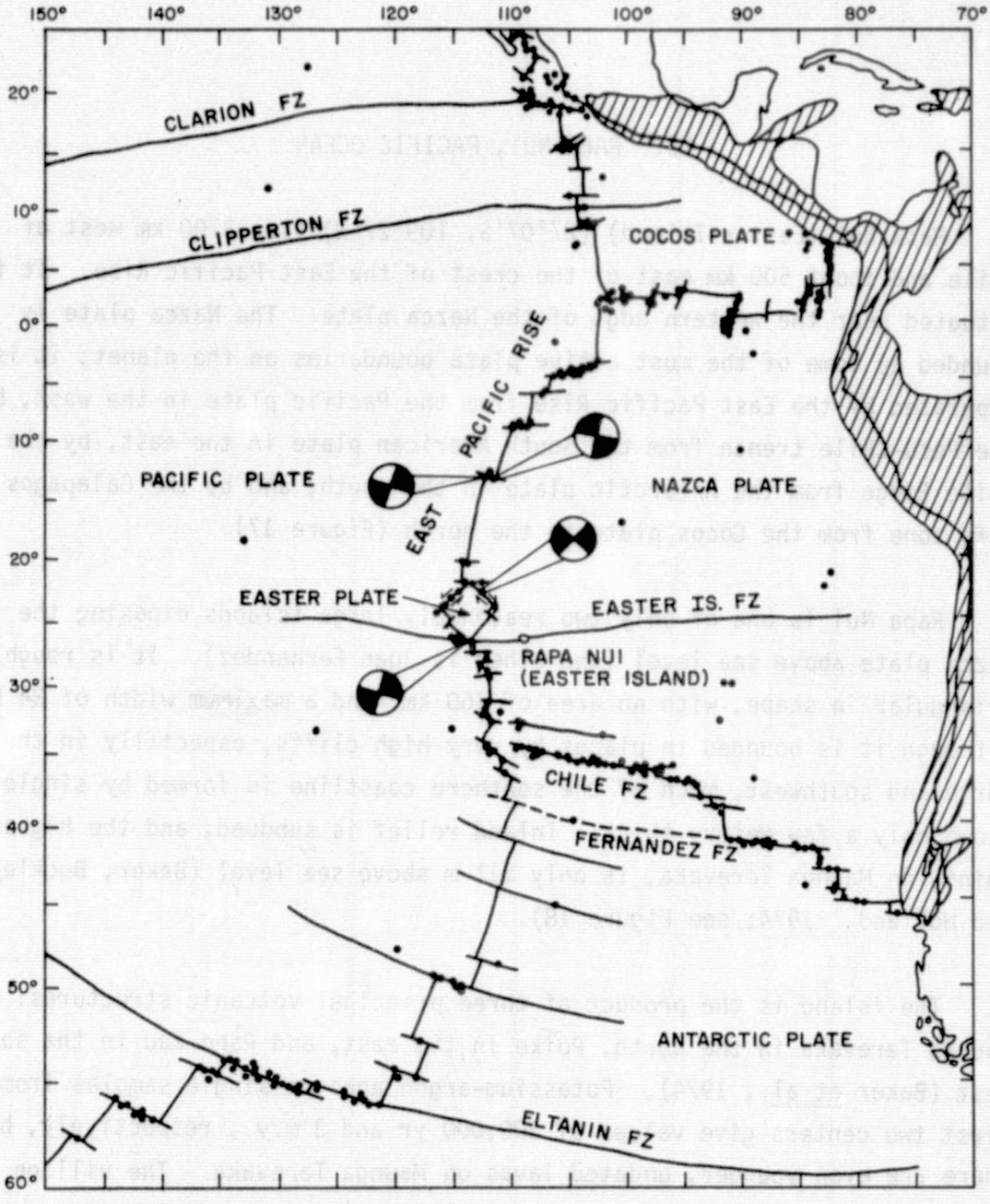


Figure 17. Map showing epicenters of earthquakes for 1961-1972, physiographic features (FZ represents fracture zones) of the east Pacific Ocean (modified from Stover, 1973), and earthquake focal-mechanism solutions (after Anderson, Forsyth, Molnar, and Mammerickx, 1974). Black quadrants of focal-mechanism solutions indicate compressional first motions; white quadrants, dilatational first motions. The cross-hatched area is the areal extent of the continental seismic zone.

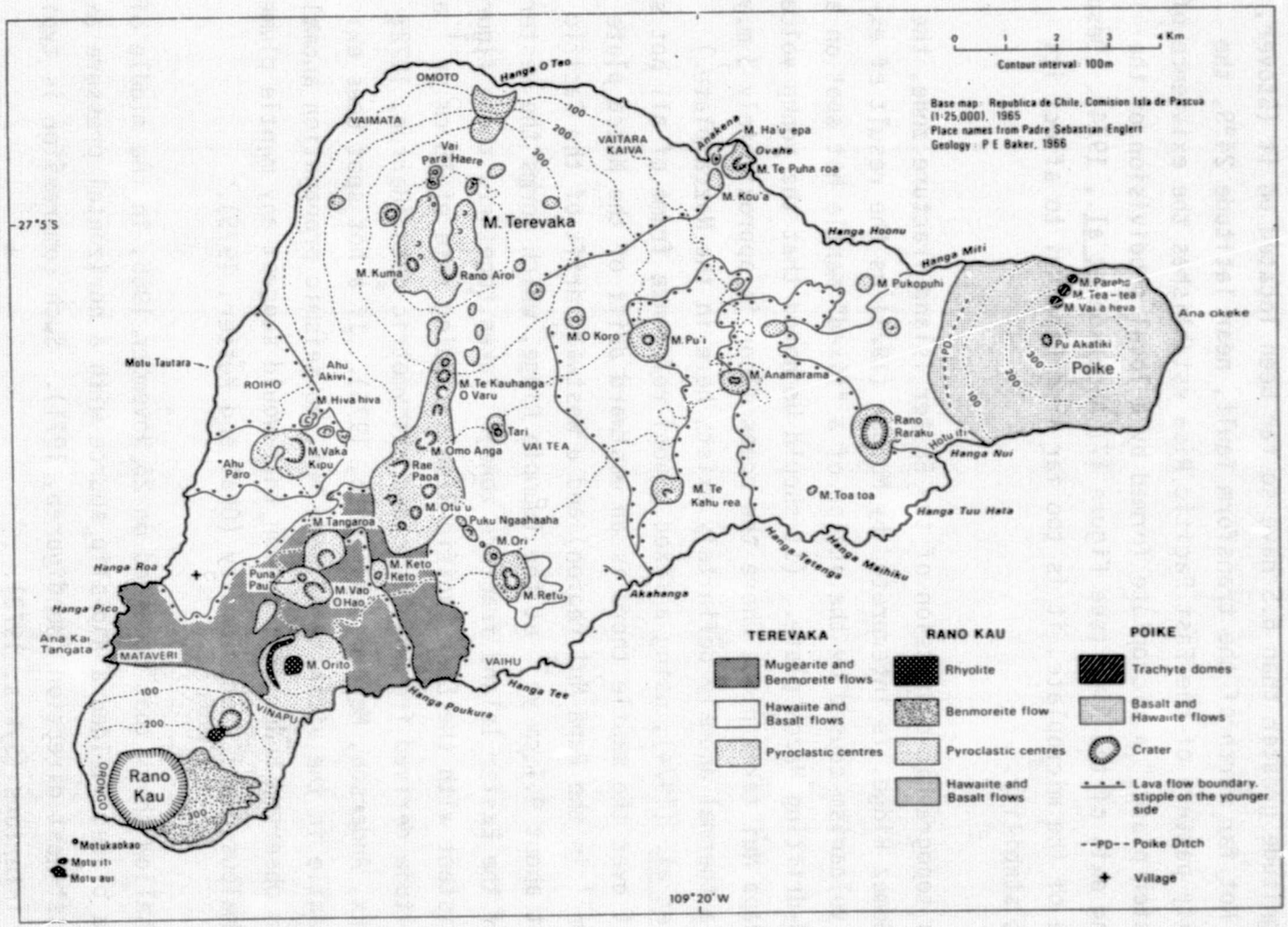


Figure 18. Geological map of Rapa Nui (Easter Island) (after Baker et al., 1974).

earthquakes, except of course along the transform sector. There, as close as 300 km to Rapa Nui, seismicity is high, although only three earthquakes with magnitude greater than 6.5 have so far been located on it (Stover, 1973). Not far north of the transform fault, near latitude 24°S, the seismicity pattern of the East Pacific Rise establishes the existence of the "Easter plate," a microplate formed by a local subdivision of the spreading axis of the Rise (see Figure 17; Anderson et al., 1974). Despite the name of the microplate, it is too far from Rapa Nui to affect its tectonic stability.

The topographic expression of the Easter Island fracture zone, the Sala y Gomez Ridge, is interpreted by Morgan (1971) as the result of excessive volcanism caused by the action of a "fixed" mantle hot spot on a westward-drifting Nazca plate. (It should be noted that the young volcanism of Rapa Nui takes place where the ocean floor is approximately 5 m.y. old, so a thermal anomaly definitely exists here in the Nazca plate.) Minster et al. (1974), using a fixed global reference frame of all hot spots, show that over the mantle there is an eastward drift of the Nazca plate (at 9.3 cm $yr^{-1}$ in the Rapa Nui region) and a westward drift of the Pacific plate (at about 9.1 cm $yr^{-1}$ at the Tuamoto Ridge, which forms the western sector of the Easter Island fracture zone). Taken together, these figures are consistent with the East Pacific Rise spreading rate of 18 cm $yr^{-1}$ at this latitude derived from magnetic and bathymetric data (Herron, 1972; Mammerickx, Anderson, Menard, and Smith, 1975). If a hot spot does exist in the mantle in the vicinity of Rapa Nui, no seismic propagation anomalies have been observed under this region that would suggest any mantle plume with anomalous density or rigidity (Okal and Kuster, 1975).

A shallow shock that occurred on 25 November 1965, in the middle of the Nazca plate, yielded a dip-slip source with a horizontal pressure axis in the east–west direction (Mendiguren, 1971). Such compression is typical of plate interiors (Sykes, 1973).

In summary, Rapa Nui shows moderate risk in all categories listed in Table 1 except for strain rate, which is suspected to be low.

From cloud-cover data, only 2 months of the year exhibit less than 50% cover; the annual mean is 59%. Operating a laser would be rendered difficult by the remoteness of the location plus the poor facilities and semitrained personnel in Rapa Nui.

## 17. GUAM, PACIFIC OCEAN

Guam (13°30'N, 166°40'E) is situated near the southern end of the Mariana arc (Figure 15), one of a chain of arcs extending from Kamchatka in the north to New Guinea in the south. The chain bifurcates around the Philippine Sea, with the Mariana arc forming part of the eastern branch (Watts and Weissel, 1975). The arcs represent the surface mark of subduction zones and are associated with active volcanism and major seismicity.

Guam is an island 50 km by 10 to 20 km, elongated northeast–southwest along the strike of the Mariana arc. It is block-faulted into three regions (Figure 19): late Tertiary reef limestones in the north, Eocene volcanic rocks in the central part, and Miocene volcanic rocks in the south (Tracey, Schlanger, Stark, Doan, and May, 1964). The separating fault zones trend mainly northwest–southeast, perpendicular to the arc strike.

The Mariana arc is formed of four structural units: from east to west, the Mariana Trench, the Mariana Ridge (on which Guam is situated), the Mariana Trough, and the West Mariana Ridge. The Mariana Trench marks the line where the Pacific plate is being subducted down to the west under the Philippine plate. West of the West Mariana Ridge lies the broad Parece Vela Basin, which forms the eastern half of the Philippine Sea. The basins get progressively younger toward the east: late Eocene in the western Philippine Sea, early Miocene for the Parece Vela Basin, and late Pliocene-Quaternary for the Mariana Trough and Trench.

The Philippine Sea is considered to have come into existence in the Eocene as the result of a change in the direction of Pacific plate movement (Karig, 1971). Karig proposes that the Mariana arc is continuing its development through a discontinuous tectonism, a typical pulse being 1) trench formation, 2) volcanism, and 3) extensional basin development. The present extensional basin is represented by the Mariana Trough, termed by Karig an interarc basin.

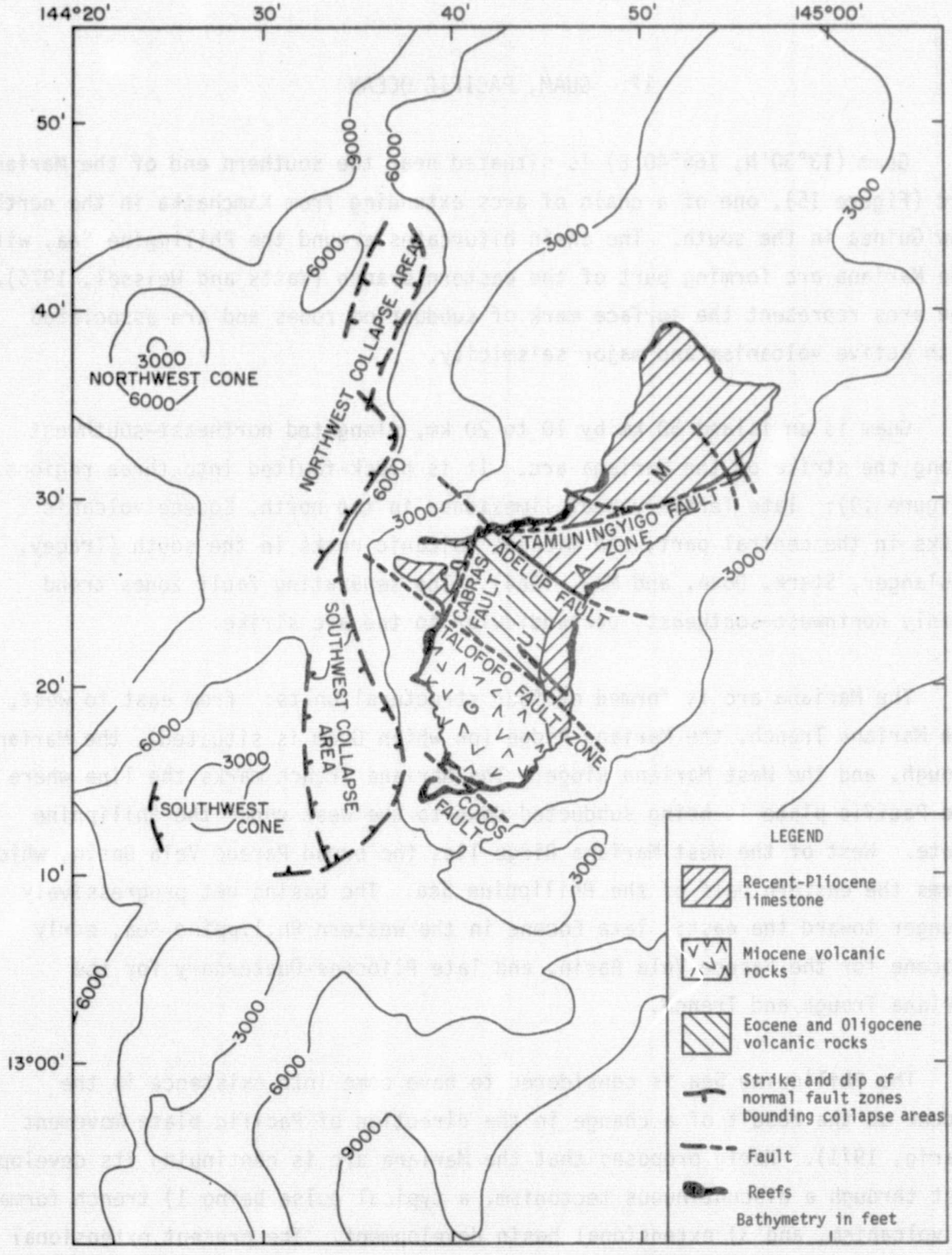


Figure 19. Structural map of Guam and vicinity (modified from Tracey et al., 1964).

The Mariana Trough is the locus of Quaternary pillow basalt volcanism and high heat flow, and earthquake focal mechanisms confirm that the Trough is being subjected to crustal tension.

The rate of plate convergence at the Mariana arc is considered by Bracey and Ogden (1972) to be 8 to 9 cm $yr^{-1}$, but LePichon et al. (1973) computed values between 2.3 and 4.9 cm $yr^{-1}$. Seismicity shows the typical pattern of a west-dipping Benioff zone, and Guam lies on the boundary between shallow (< 70 km) and intermediate-depth earthquakes. A possible fracture zone extends east from the north end of Guam to the Trench (Figure 1). Major earthquakes (M > 8.0) have been experienced in the southern Mariana arc since 1900. Thus, Guam is located in a tectonically unstable region. Its cloudiness record is no more promising, with the lowest month having 65% cover and the yearly mean being almost 72%. Operationally, however, Guam appears favorable in all considerations except for obtaining local help.

## 18. MAUI, HAWAII, PACIFIC OCEAN

The Hawaiian archipelago forms a broadly linear chain of islands and seamounts extending about 3000 km across the central Pacific, from the island of Hawaii in the east to the Colahan seamount in the west (Figure 20). While the pattern of the chain as a whole is linear, the individual volcanoes lie on short, sigmoidal loci that are arranged en echelon left with respect to each other. These subparallel loci may represent extensional features in the lithosphere (Jackson, Silver, and Dalrymple, 1972).

The origin of the Hawaiian chain has been proposed by Wilson (1963) as resulting from motion of the Pacific plate over a fixed hot spot in the mantle, and by Jackson et al. (1972) as due to a slowly southeastward-propagating fracture that repeatedly taps mantle magma. Certainly, the age of the volcanic islands increases from southeast to northwest, and the rate of lateral propagation of the chain can be estimated from a plot of radiometric (potassium-argon) ages of the oldest lavas versus distance from Kilauea (the most active volcano on Hawaii). Jackson et al. (1972) thus obtained a mean propagation rate of 14.7 cm $yr^{-1}$ for the last 17 m.y. Minster et al. (1974) produced a consistent model of global plate motions, relating these to a fixed hot-spot reference frame. Their AM1 model predicts that the Pacific plate is moving over a Hawaiian hot spot at a rate of 8.9 cm $yr^{-1}$. As pointed out by Minster et al., the rate calculated from radiometric ages versus distance is biased toward faster rates because of the difficulties of sampling and dating the oldest lavas, especially the seamounts, and because of argon loss in weathered rocks.

The island of Maui (21°N, 156°W), the second youngest of the Hawaiian chain, lies about 200 km northwest of Kilauea on the youngest island, Hawaii itself. Two major volcanoes have built up the island of Maui (Figure 21). West Maui is joined by an isthmus to the younger and larger cone of Haleakala; since it last erupted in 1750, Haleakala must be regarded as a dormant volcano (Macdonald and Abbott, 1970). The oldest potassium-argon ages so far obtained are 0.84 m.y. for Haleakala and 1.5 m.y. for West Maui (McDougall, 1964).

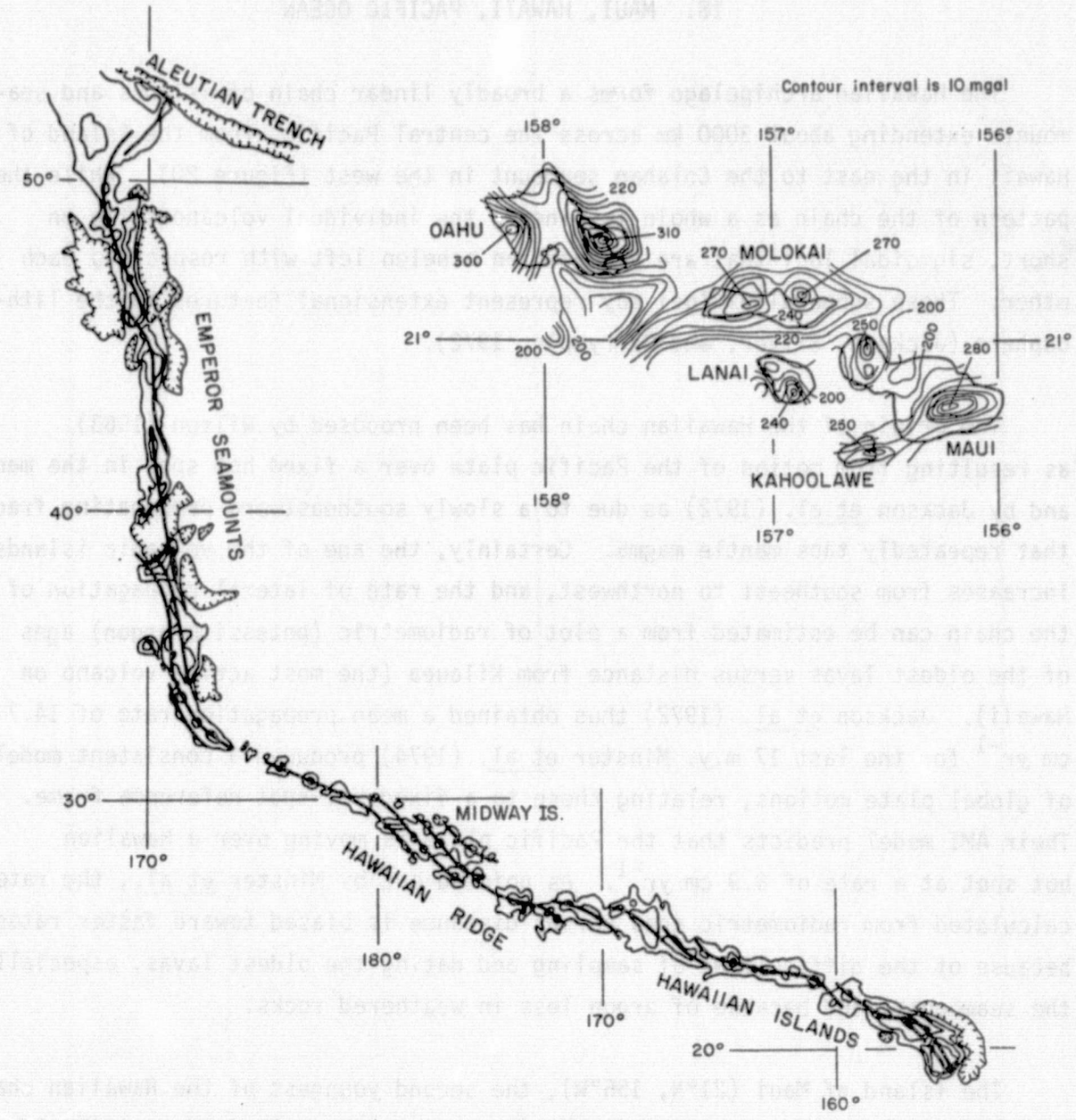


Figure 20. Loci of shield volcanoes (heavy lines) in the Hawaiian-Emperor chain (simplified from Jackson et al., 1972). Inset shows the Bouguer gravity anomalies, in milligals, of the southern Hawaiian ridge (after Malahoff, 1969).

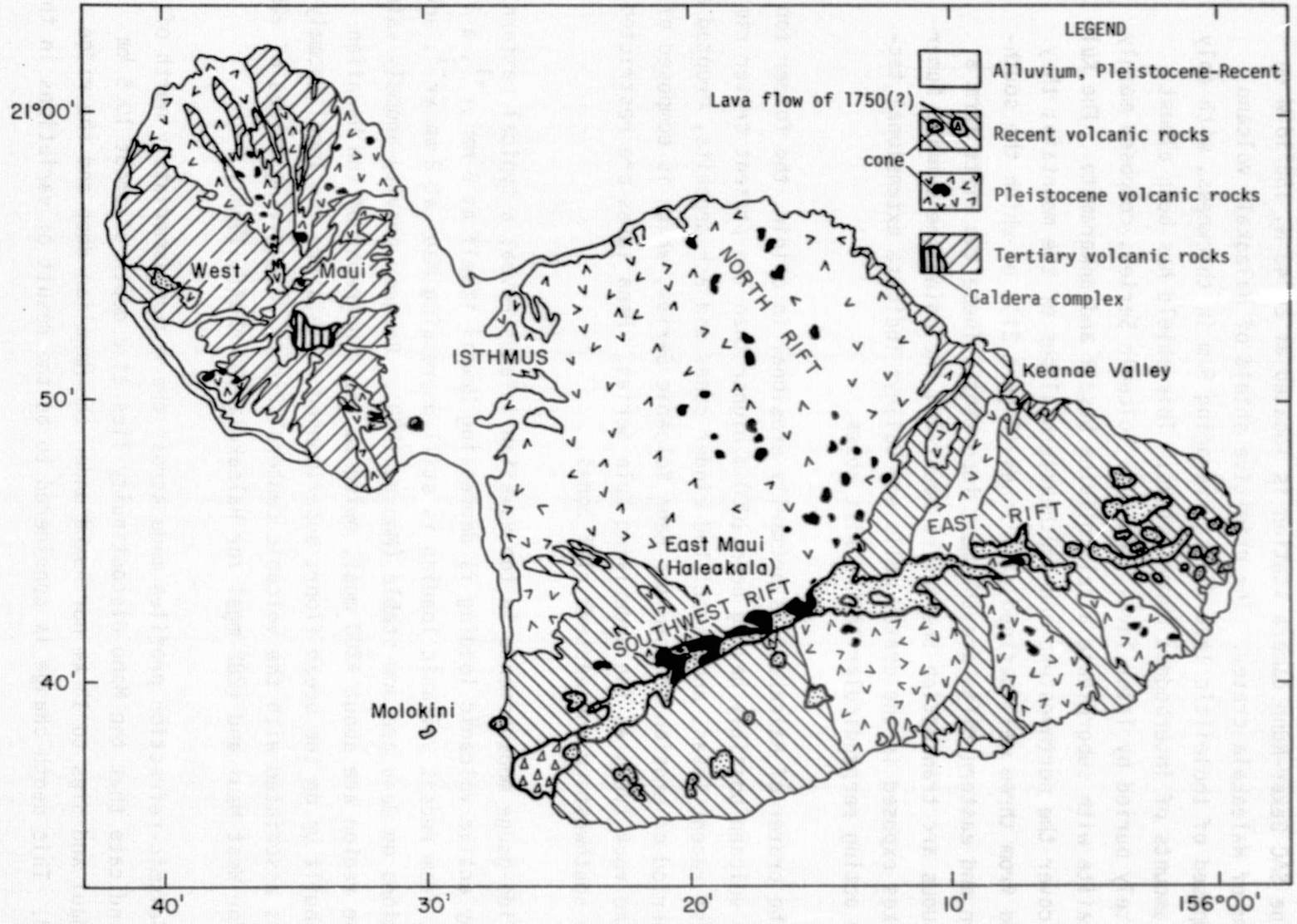


Figure 21. Geological map of the island of Maui (modified from Macdonald and Abbott, 1970).

The SAO Baker-Nunn camera station is located at 20°43'N, 156°16'W on the rim of Haleakala crater. The primitive shield of Haleakala volcano is composed of tholeiitic lava flows, averaging 5 m in thickness, with only minor amounts of interbedded pyroclastics. This shield has been almost completely buried by later lavas, the Kula Volcanic Series, composed mainly of hawaiite with subordinate alkali olivine basalt and ankaramite. The Kula lavas cover the northwestern and southeastern slopes of the mountain; they erupted from three well-defined rift zones (Figure 21), of which the southwestern and eastern rifts are the most important. These two rifts form a continuous arc transecting the entire mountain, including the summit. Numerous dikes exposed in the crater walls and valleys indicate extensional tectonism acting perpendicular to the rift zones.

The crater of Haleakala is primarily erosional in origin, the former top of the volcano possibly having been 1000 m higher than the present crater rim. The most recent lavas, and associated cinder cones and ash deposits, erupted after this period of erosion to form the Hana Volcanic Series, which is composed of the same rock types as the underlying Kula Series. Hana lavas are restricted to the southwestern and eastern rift zones.

Tide-gauge measurements in the Hawaiian islands reveal a typical pattern, whereby active volcanic loading is depressing Hawaii itself at 5 mm $yr^{-1}$, a lag effect from recent volcanic loading is still depressing Maui at 2 mm $yr^{-1}$, and conditions on Oahu are now stable (Moore, 1970). Bouguer gravity-anomaly values for the region are about +200 mgal, owing to the topography of the Hawaiian ridge built up on the ocean floor; superimposed on this are the local-anomaly effects associated with the volcanic centers (Figure 20), giving values of +252 mgal for West Maui and +282 mgal for Haleakala (Malahoff, 1969).

Seismic-refraction profiles made across the region immediately north of Maui indicate that the Moho discontinuity lies at a depth of about 10.5 km near Maui and dips to 13 km northward under the Hawaiian deep and the ridge beyond. This depth change is considered to be the result of variations in the

thickness of sedimentary and volcanic cover (Shor and Pollard, 1964). Under the shelf northwest of Kahului, Maui, is a small area in which high-velocity material occurs within 7 km of sea level; this area may represent upfaulting or magmatic ascent of mantle rocks.

A search for seismic-propagation anomalies under the Hawaiian islands, to try and detect any mantle plume, has yielded controversial results. Kanasewich, Ellis, Chapman, and Gutowski (1972) interpreted Canadian array seismograms for Tongan and Samoan earthquakes as indicating a heterogeneous region of high velocity in the mantle near the interface with the core, beneath the Hawaiian archipelago. More precisely, Kanasewich and Gutowski (1975) have claimed to identify a 150-km-diameter cylindrical-shaped volume, occurring about 400 km above the core-mantle boundary, with anomalously high-velocity seismic-wave propagation and surrounded by an anomalously low-velocity penumbra. But no such anomalies could be detected by Okal and Kuster (1975) from data recorded at the French Polynesia seismic array.

Except for the island of Hawaii itself, the Hawaiian islands do not comprise a highly seismic area. However, the 1938 Maui earthquake (M = 6.8) had an epicenter about 40 km north of Pauwela Point on the north coast of Haleakala, damaging roads and buildings on Maui and Molokai. Thus, we have to consider Maui as situated in a fringe tectonic zone.

From the operational and cloud-cover standpoint, Maui rates quite well. Its annual mean cloudiness is about 47%, with 5 months of the year showing near or greater than 50% cloud cover. SAO has been on location at Maui for 18 years and finds no real operational difficulties, although local help is hard to obtain.

## 19. TUTUILA, SAMOA, PACIFIC OCEAN

The Samoa island chain is situated at the northern end of the Tonga arc, to which it trends perpendicularly in an east-southeast direction. The Tonga arc marks a vigorous subduction zone, where the Pacific plate is descending west under the Indian plate. Along with numerous nearby seamounts, the Samoa chain forms a broadly linear feature 1200 km long, whose east-southeast trend is notably concentric with that of other Pacific island chains (Figure 22).

The island of Tutuila (14°S, 171°W) consists of five principal volcanic centers (Stearns, 1944, illustrated in Figure 23). The Samoa islands as a whole are composed of Pliocene-Quaternary basalts overlain by trachytes (Daly, 1924). These basalts, alkaline olivine basalts, are quite distinctive from the calc-alkaline basalts of the island arcs and the tholeiites of the ocean floors (Macdonald, 1944; Peterman and Hedge, 1971). They are akin to the late-stage alkaline lavas of Hawaii and Tahiti and show greater resemblance to the latter in the associated presence of undersaturated lavas, such as basanites and olivine nephelinites. Such rocks comprise the youngest lavas of the Samoa islands, including some seamounts, erupted after the main basalt calderas had become appreciably eroded, and their petrology indicates an origin from the base of the lithosphere (Hawkins and Natland, 1975), here estimated to be 90 to 100 km thick.

The Samoa islands appear to be an exception to the rule that the Pacific island chains show progressively younger volcanism to the east (Chubb, 1957; Holmes, 1965). Thus, Savai'i, in the west, is largely covered with Holocene lavas, compared with Pliocene lavas on Tutuila and Manu'a to the east. However, the youngest eruption in Samoa is a historical submarine one in the Manu'a islands. Furthermore, $^{87}Sr/^{86}Sr$ values for Samoa basalts, some of the highest yet found in the ocean basins, increase progressively from Manu'a to Savai'i (Hedge, Peterman, and Dickinson, 1972). Difficult to interpret in terms of the hot-spot concept, this direction of progression is better attributed to lateral changes in mantle composition along a constant melting depth. Penecontemporaneous volcanism running the length of the Samoa chain suggests an

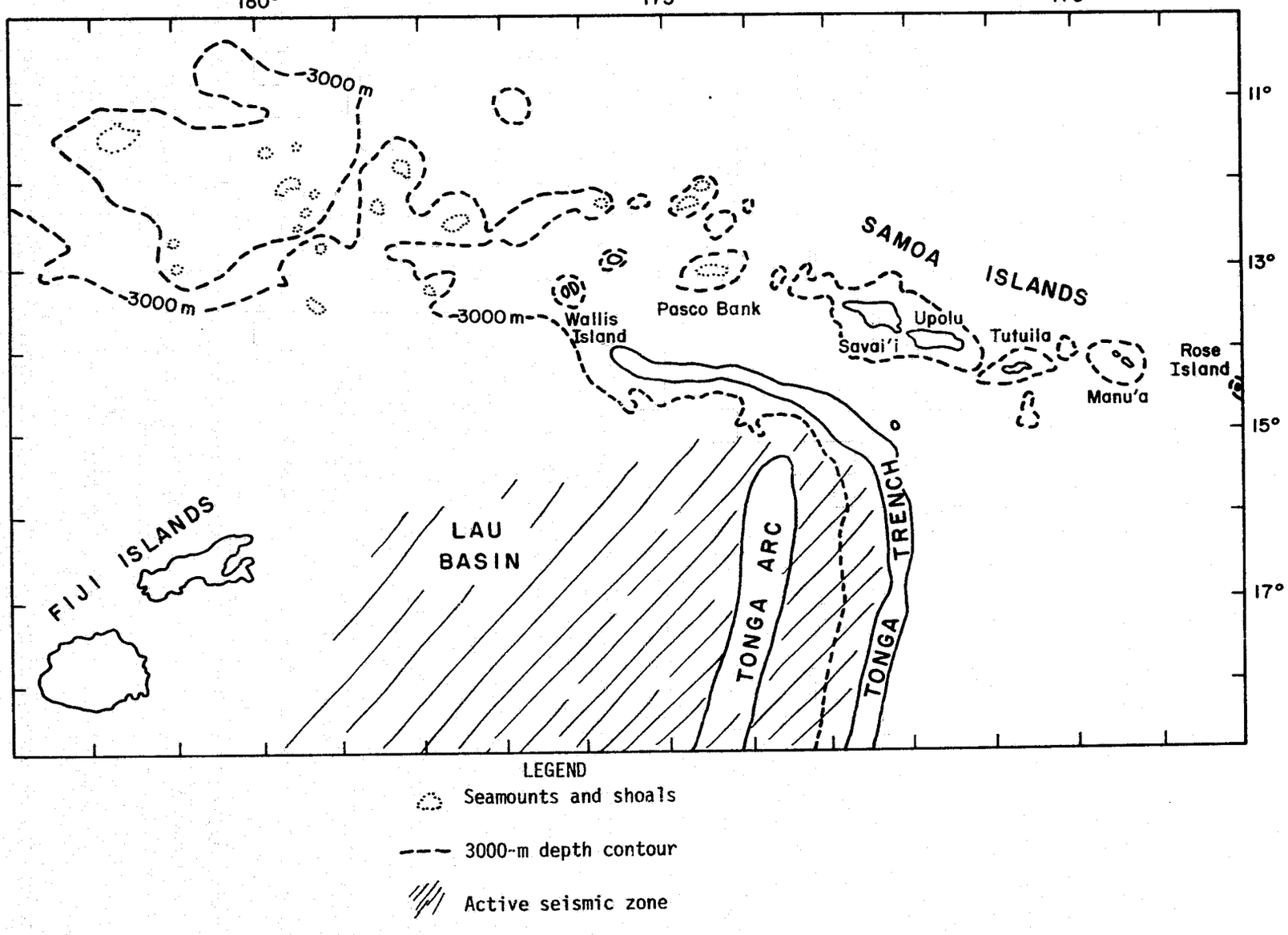


Figure 22. Sketch map of Samoa islands region (modified from Hawkins and Natland, 1975).

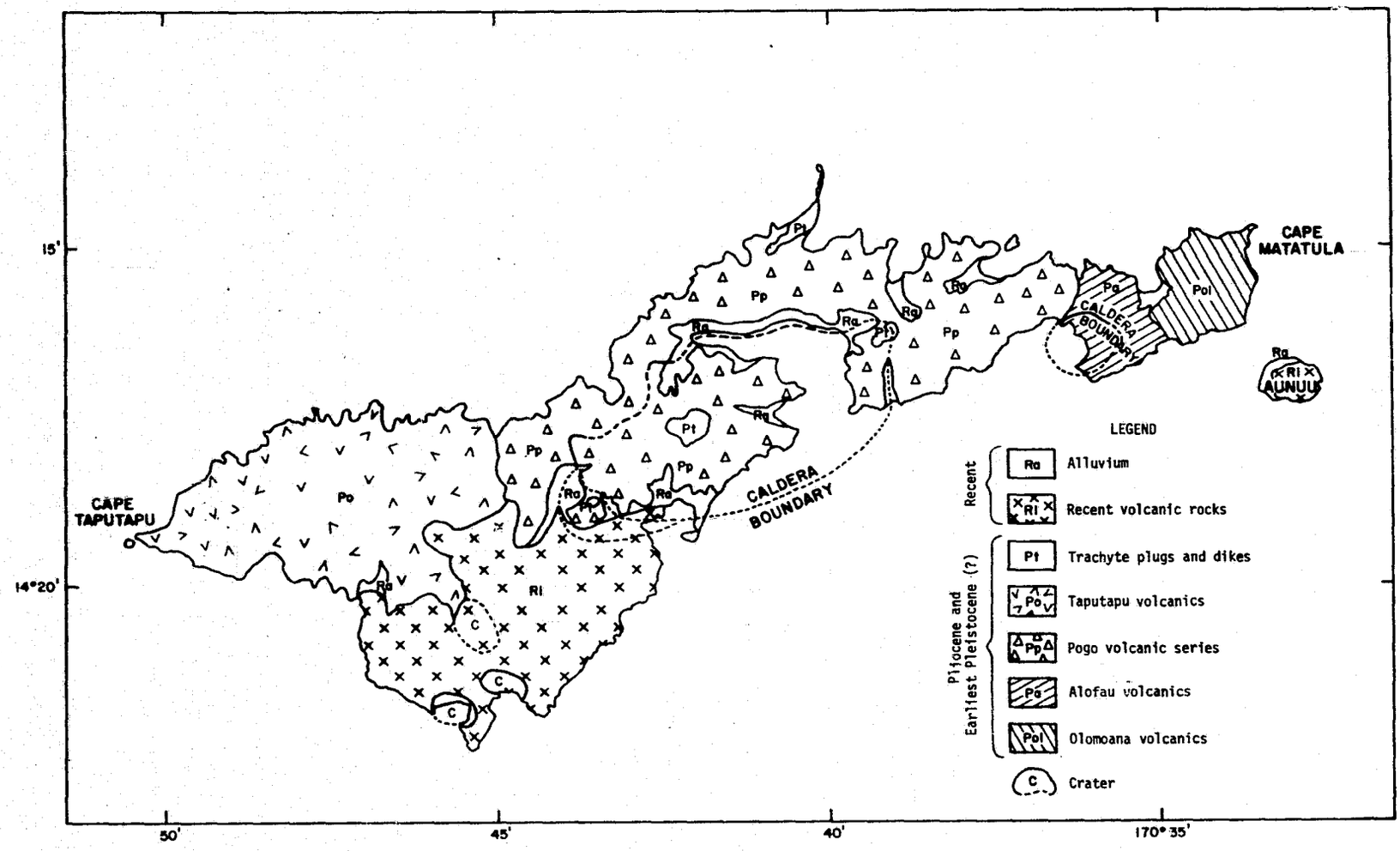


Figure 23. Geological map of Tutuila Island (simplified from Stearns, 1944).

association with lithospheric deformation along a necessary hinge line at the northern end of the down-going sector of the Pacific plate.

The complex history of plate tectonics in this region has been described by Chase (1971). The Tonga and New Hebrides arcs were continuous 45 m.y. ago, but they have become progressively separated by a transform fault with which the Samoa chain is now closely associated, if not identified. The transform fault has shifted southward during the last 1.5 m.y., and six microplates have developed between the two arcs, involving three very active spreading lines in the Fiji region. This last is a necessary geometrical consequence of the opposing directions of subduction in the Tonga and New Hebrides arcs. These arcs are currently releasing more seismic energy than is any other equal length on the planet. LePichon et al. (1973) computed that the east–west convergence rate here is 9 to 10 cm $yr^{-1}$.

The position of the Samoa island chain in proximity to the Tonga arc is coincidental according to Chase (1971), who reckons that the chain is probably of Cretaceous initiation, like the sea floor on which it rests, and is a passive passenger on the Pacific plate now being carried past a highly active plate margin. He thus envisages the volcanism of the chain as a reactivation resulting from the propagation of end-of-arc lithospheric stresses. Hawkins and Natland (1975) see the origin of the chain as entirely due to the necessary lithospheric flexing as the transform fault is approached, with magma generation from viscous shear melting.

Recent tectonism in Samoa includes Quaternary faulting along a possible graben between Savai'i and Tutuila. Although the major seismicity of the Tonga trench terminates a few hundred kilometers south of the Samoa islands, weaker, shallow seismicity extends into Savai'i. No epicenters with M > 4.5 have been recorded from Tutuila (see Figure 1), which nevertheless is clearly on the fringes of a tectonic storm.

Neither cloud-cover nor operational considerations recommend Tutuila as an observing site; only 3 months of the year find less than 50% cloud cover.

## 20. TAHITI, PACIFIC OCEAN

Tahiti lies near the southeastern end of the Society Islands chain, at 17°40'S, 149°30'W. The island of Tahiti is formed by two deeply eroded volcanic centers 35 km apart, which rise abruptly from the Pacific floor (-4000 m) to a maximum elevation of 2237 m on the larger, more northwesterly center of Tahiti-nui (Figure 24). Tahiti is geologically renowned for the highly undersaturated and alkaline character of its lavas (Lacroix, 1928; Williams, 1933; McBirney and Aoki, 1968), with basanites and ankaramites predominating. Subordinate silicic differentiates include phonolites and trachytes. The cores of the two volcanoes now expose plutonic equivalents of the lavas.

The age of the Pacific floor in the Tahiti region is late Cretaceous (Pitman et al., 1974). Potassium-argon ages for the Tahiti Island rocks (Dymond, 1975) give mean values of 1.65 ± 0.13 m.y. for Moorea (the next island west of Tahiti-nui), 0.65 ± 0.22 m.y. for Tahiti-nui, and 0.48 ± 0.10 m.y. for Tahiti-iti (attached to the southeastern flanks of Tahiti-nui). The Tahiti volcanoes therefore get progressively younger to the east, as with the Hawaiian, Marquesas, and other Pacific island chains (Figure 25). According to the radiometric ages given above, the present location of the Tahiti melting spot should lie about 100 km east of Tahiti-iti, near the manifestly recently active volcanic island of Mehetia. The rates of Pacific plate rotation implied by age data for Tahiti and other island chains are greater than those derived from plate-tectonic analysis (see, e.g., Minster et al., 1974), suggesting hot-spot migration in the direction opposite plate motion (McDougall, 1971; Forristall, 1974; Dymond, 1975).

The closest plate boundary is 2000 km west of Tahiti. The nearest recorded intraplate seismicity ($M > 4.5$) occurred 1000 km north of Tahiti (Tarr, 1974; also see Figure 1). We thus consider Tahiti to provide a stable site.

Conditions of cloud cover are favorable, too, with a yearly mean average of 52% and only 1 month of the year exceeding 60%. Operationally, however, there may be some difficulties, particularly in freight handling and living conditions.

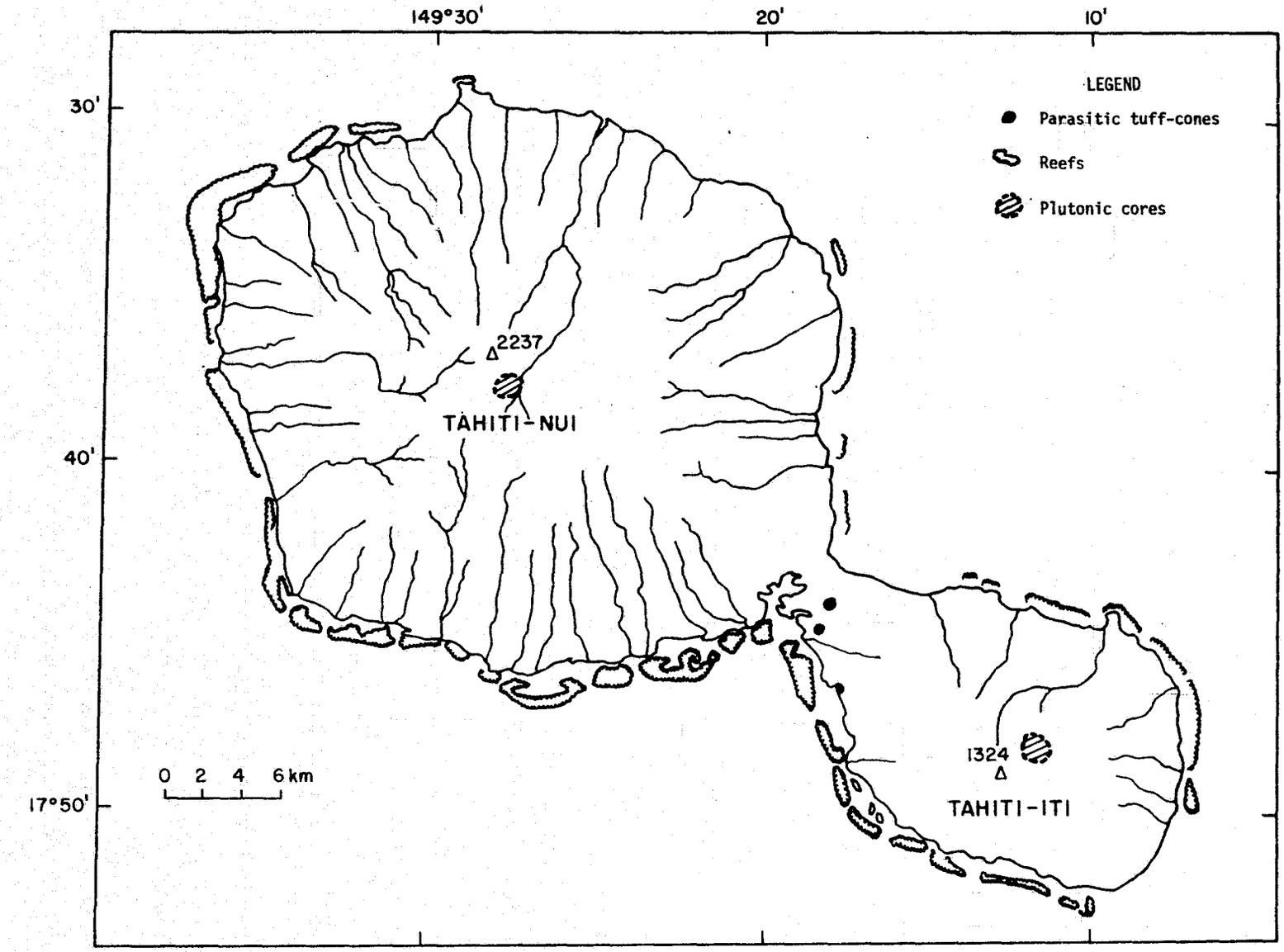


Figure 24. Sketch map of Tahiti (simplified from Williams, 1933).

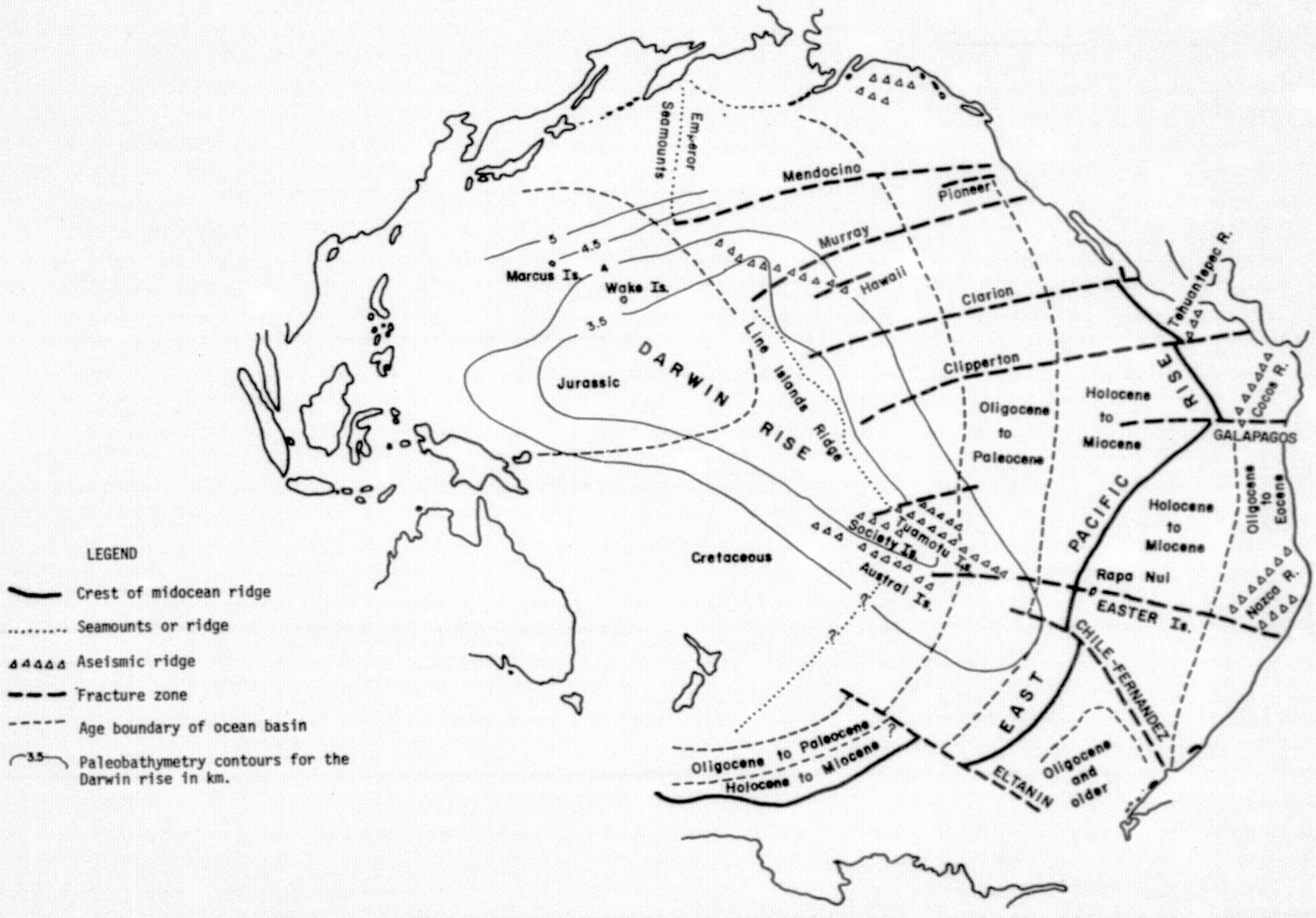


Figure 25. Sketch map of the Pacific Ocean showing tectonic features and the age boundary of the ocean basin (modified from Jacobs et al., 1974).

## 21. WAKE ISLAND, PACIFIC OCEAN

Wake Island (19°18'N, 166°36'E) is situated in the far-reaching tectonic calm of the northwest Pacific (Tarr, 1974). The island lies 2000 km east of the Mariana arc (Figure 25), which contains the nearest active plate boundary and the nearest seismicity, and is one of numerous seamounts on the northwest end of the Darwin Rise (Menard, 1964; Jacobs et al., 1974). The age of the ocean floor in this region is about 150 m.y., mid-Jurassic (Pitman et al., 1974).

The ocean depth, crustal structure, and heat flow of the Darwin Rise are consonant with a sea floor of this age (Woollard, 1975). Water to a depth of 5.5 km lies on a multilayered, 6-km-thick crust, in turn upon mantle with a high P-wave velocity of 8.4 km $sec^{-1}$. Heat flow averages 1.0 HFU. The history of the Darwin Rise and its place in the plate-tectonic evolution of the Pacific are not yet clearly understood, nor is the reason for the present singular elevation of Wake Island, although coral atoll building began in the Upper Cretaceous (Hamilton, 1956). The age of the rocks forming the island is still undetermined.

We consider Wake to provide a stable site. Cloud cover is light or nonexistent for 3 months out of the year, and only 1 month has as much as 54% cloud cover. Operationally, though, air transportation may present problems.

## 22. AREQUIPA, PERU

The Andes of Peru and Bolivia consist of two subparallel foldbelts: That of late Paleozoic age constitutes the eastern cordillera; the other, of Mesozoic-Tertiary age, makes up the western cordillera (Bellido, 1969; Cobbing and Pitcher, 1972). These two foldbelts are separated by the Altiplano, which is a broad intermontane plateau filled with Tertiary molasse and on which Lake Titicaca is situated at 3812 m. The western cordillera can be divided into an eastern miogeosynclinal belt of folded carbonate and clastic sediments and a western eugeosynclinal belt of relatively undeformed volcaniclastics.

Arequipa (16°25'S, 71°32'W) lies on the eugeosynclinal belt, here of Mesozoic age, although it is largely covered with late Tertiary-Quaternary volcanics. The belt runs parallel to the coast, about 100 km inland; near Ica, it runs into and forms the coast of northern Peru. Intimately associated with the eugeosynclinal belt is the upper Cretaceous-lower Tertiary (110 to 60 m.y.) Coastal Batholith; in the Arequipa region, these essentially granodioritic rocks lie on the coastward side of the belt and contain faulted inliers of Precambrian gneiss (Figure 26). Similar gneisses constitute the Arequipa massif, forming the coast of southern Peru; their structural strike is perpendicular to the present Andes, and their radiometric ages fall close to 640 m.y.

The proved immobility of the Arequipa massif with respect to the Andean zone immediately to the east, at least since the Devonian, implies the important fact that Mesozoic-Tertiary sedimentation and tectonism have taken place and acted on continental basement. The folding in the eugeosynclinal belt is gentle and associated with upward movement on vertical faults: No thrusting has occurred (Cobbing and Pitcher, 1972; Myers, 1975). This block faulting is a feature peculiar to the Andes and has raised them to their present elevation during the last 30 m.y., and in particular during a late Tertiary-Quaternary episode (Bellido, 1969). Thus, the late Miocene-early Pliocene "Puna" erosion surface now lies between 4200 and 4500 m. The absence of major thrusts and nappes from the Andes is

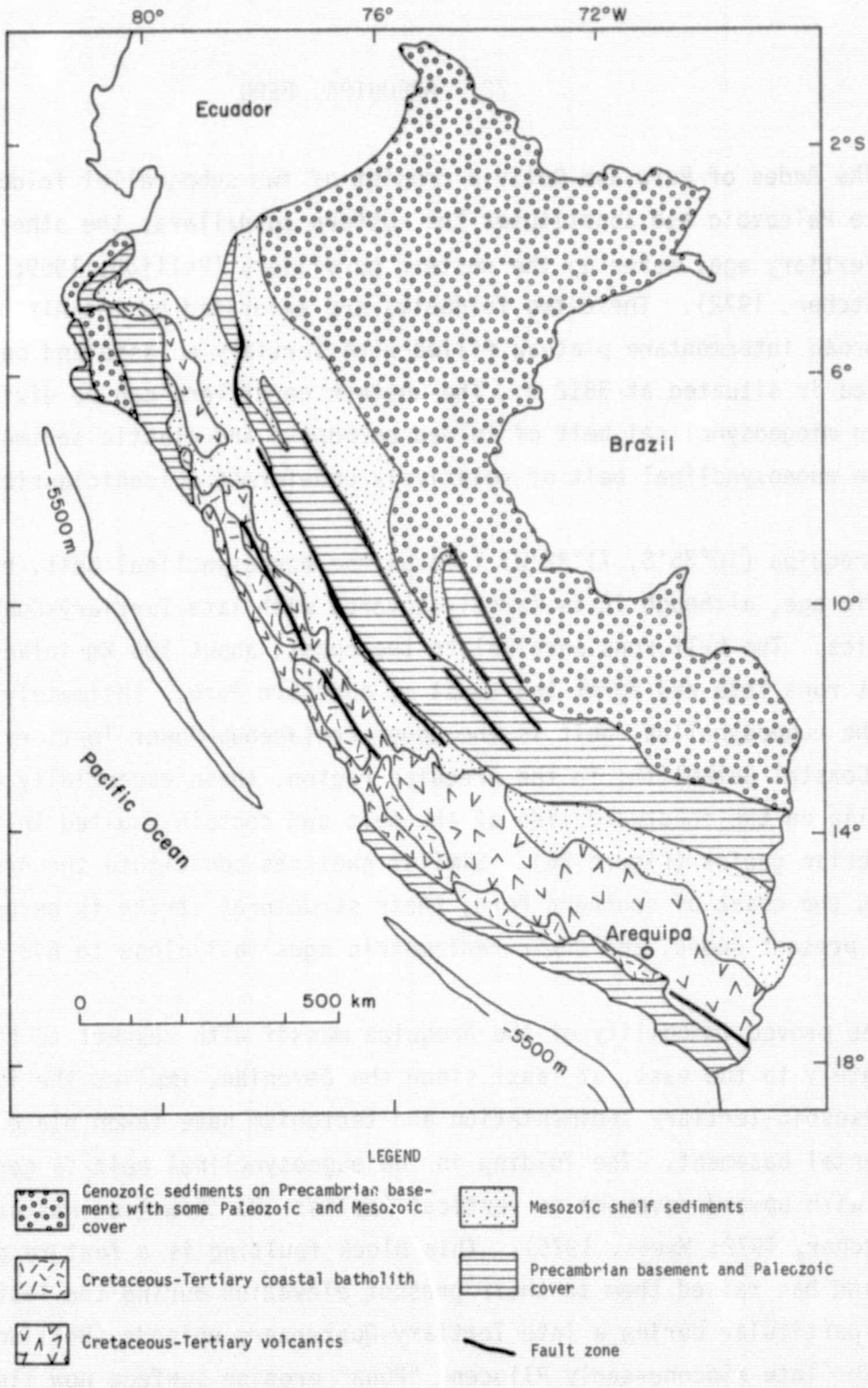


Figure 26. Geological map of Peru (modified from Myers, 1975).

attributed to an unusual thickness of underlying sialic crust, estimated to be 60 km in the Arequipa region (James, 1971; Myers, 1975).

Tertiary and Quaternary volcanism, and possibly tectonism too, have been episodic in the history of the Peruvian Andes (Noble, McKee, Farrar, and Petersen, 1974). Volcanism during the late Eocene was followed by quiescence during the Oligocene. Resumption of activity in the early Miocene may have been related to an increase in the rate of drift of the Pacific plate over the mantle and to a major pulse of tectonic deformation in the mid-Miocene with the start of rapid spreading from the East Pacific Rise. Intense volcanism and plutonism have endured throughout the Pliocene and Quaternary.

Arequipa is situated at the northern end of a 1000-km-long line of historically active volcanoes in northern Chile-southern Peru. Nevada-Chachani (6075 m) lies only 20 km north of Arequipa, and the perfect cone of El Misti (5822 m) is a similar distance to the northeast (Guevara, 1969; Vargas, 1970). El Misti erupted in 1878 and 1949.

The seismicity of Peru accords with active subduction of oceanic lithosphere, which acts as a stress guide, beneath the possibly west-migrating continental lithosphere of South America (Stauder, 1975). Whereas in northern Peru and Ecuador the subducted slab is virtually shoaling beneath the continent, in southern Peru it is dipping at about 35°, a change that is accompanied by a change in the pattern of active volcanism along the Andes.

Arequipa sits on a zone of intermediate-depth (90 to 100 km) earthquakes (Figure 7); in this region, these yield tensional focal mechanisms representing failure under gravitational sinking (Stauder, 1975). One of the most recent shocks (M = 5.9) was that of 17 June 1970, whose epicenter was about 60 km northwest of Arequipa. Major earthquakes in southernmost Peru include the shallow-focus, coastal earthquakes of 6 August 1913 (M = 7.9) and 24 August 1942 (M = 8.6) and the deep-focus earthquake north of Lake Titicaca on 15 August 1963 (M = 8.0).

Kelleher (1972) has developed a theory of major seismic behavior along compressional plate boundaries, whereby historically quiet "gaps" between recorded rupture zones of large-magnitude earthquakes are predicted as sites for future such earthquakes. Along the western coast of South America, two gaps extend between latitudes 12°5 to 14°S and 17° to 25°S. Kelleher (1972) states that "There is good reason to assume that much of these regions are now under great tectonic strain." Consequently, Arequipa seems an unsuitable site for a laser station.

During January, February, and March, there is $\sim$ 85% cloud cover over Arequipa; the other months, however, are clear enough to lower the annual average to 51%. Operationally, Arequipa ranks very well; SAO is already established there.

## 23. SAN FERNANDO, SPAIN

San Fernando (36°28'N, 6°12'W) is less than 100 km north of the active Eurasian-Africa plate boundary. This boundary, termed the Azores-Gibraltar fracture, extends eastward from the Azores triple junction on the mid-Atlantic ridge. As far east as longitude 24°W, it has the character of an elevated, obliquely spreading ridge, marked by numerous low-magnitude, shallow-focus earthquakes. From 24°W to about 12°W, the fracture shows strain release in the form of few but large earthquakes, the focal mechanisms indicating dextral shear along the fracture. This motion of Europe eastward relative to Africa was also predicted from the bend in the mid-Atlantic ridge at the Azores according to known spreading rates north and south of the triple junction.

From longitude 12°W eastward to the Strait of Gibraltar, seismicity again becomes more common and includes major earthquakes like that of 1755 (which destroyed Lisbon) and 28 February 1969 (M = 8.0). Focal mechanisms indicate dextral shear along the fracture (Figure 27), but with a component of steeply inclined underthrusting of Spain beneath Africa (Udias and Lopez Arroyo, 1972).

East of the Strait of Gibraltar, geological evidence combined with seismic studies indicates the existence of an intervening plate, the Alboran plate, between Eurasia and Africa (Andrieux, Fontbote, and Mattauer, 1971). The margins of the Alboran plate are formed by the Guadalquivir flexure of the Cordillera Betica of southern Spain (the Cordillera are regarded as produced by sheets of Alboran plate crust thrust north over the Spanish Meseta) and by the Er Rif range of Morocco, also produced by overthrusting of the Alboran plate onto Africa.

Deep drilling in the Sevilla-Cadiz region has revealed the Paleozoic Hercynian basement of the Meseta to be dipping south at about 4% (consistent with the underthrusting of Spain beneath Africa) and to be more than 3000 m deep under Cadiz. The basement there is overlain by thick Triassic-Eocene

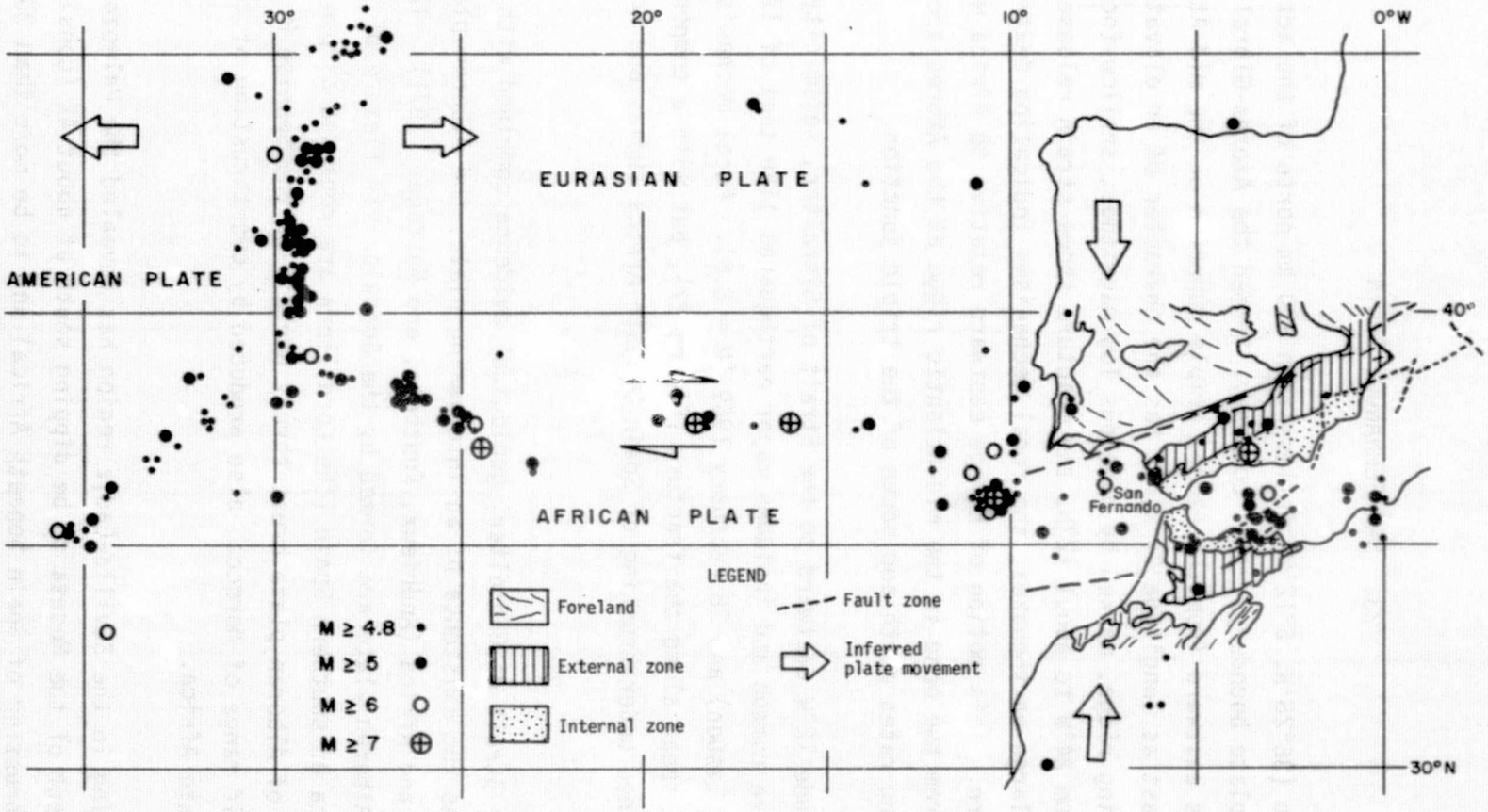


Figure 27. Map showing seismic activity ($M \geq 4.8$) in the Azores-Gibraltar region between 1910 and 1970 (after Udias and Lopez Arroyo, 1972), and the tectonic divisions of the westernmost part of the Alpine chain (simplified from Kampschuur and Rondeel, 1975).

sediments affected by Alpine tectonism and by surficial mid-Pliocene marine conglomeratic sands on which the present SAO tracking station is sited. These sands are exposed by Quaternary uplift.

Seismic-refraction profiling across the Portugal-Spain border indicates a southward thickening of the crust to about 35 km under the Algarve, with normal mantle ($P_n$ = 8.15 km $sec^{-1}$) below (Mueller, Prodehl, Mendes, and Moreira, 1973). Cadiz lies on one of the rare sectors of the Iberian coast to have negative Bouguer anomalies, here probably related to a west-southwest extension of the strongly negative values of the Cordillera Betica.

According to a 1968 Spanish Government report, San Fernando falls within a zone of median seismic risk (intensity VI to VIII maximum). Plate theory predicts a slow buildup of strain in this region, with 0.4-cm $yr^{-1}$ convergence between Spain and Africa (Minster et al., 1974).

Meteorological conditions look good. Cloud cover exceeds 50% during only 2 months, and the yearly mean is low, 39%. Operational aspects are adequate, with the only problem being air transportation.

## 24. UPPSALA, SWEDEN

Sixty kilometers north of Stockholm, Uppsala (59°55'N, 17°38'E) is situated in the southwestern part of the Precambrian Baltic Shield (Figure 28). The shield is bordered to the northwest, along the length of Norway, by the mid-Paleozoic Caledonian orogenic belt and to the south and east by an essentially undeformed cover of Phanerozoic sediments on the subsided Russian platform (Holmes, 1965). The southwestern, Svecofennian province of the shield is characterized by late granites and pegmatites yielding radiometric ages close to 1850 m.y.

The post-Pleistocene glacial history of Scandinavia is quite well known (Holmes, 1965) and evidences important vertical movements due to isostatic readjustment (Figure 28). During the last fluctuating recession of the Scandinavian ice sheet (∿ 13500 yr B.P.), the present Baltic Sea was presaged by a series of marginal glacial lakes, which coalesced and drained wherever they could find an outlet. Sea level remained low, but the depressed land in front of the receding ice sheet was beginning to rise, and this movement induced the Baltic Ice Lake to drain into the North Sea by 10275 B.P.

The sea, some 40 m below its present level, now began to rise more quickly than the land, widening the outlet of the Baltic Ice Lake and encouraging infiltration of sea water, so that by the time the ice front had withdrawn to Uppsala (9800 B.P.), the Baltic was definitely marine (Yoldia Sea). However, after another two centuries, the land was again rising faster than the sea, the connection with the North Sea was narrowed to a short river, and the Baltic again became a fresh-water lake (Ancylus Lake). This lake lasted some 2000 years, until the isostatic rise of Denmark lagged behind the eustatic rise of sea level and a second marine influx occurred. This ancestral Baltic Sea (7500 B.P.) was more extensive than its present-day descendant, which is still shrinking as the land rises in the north.

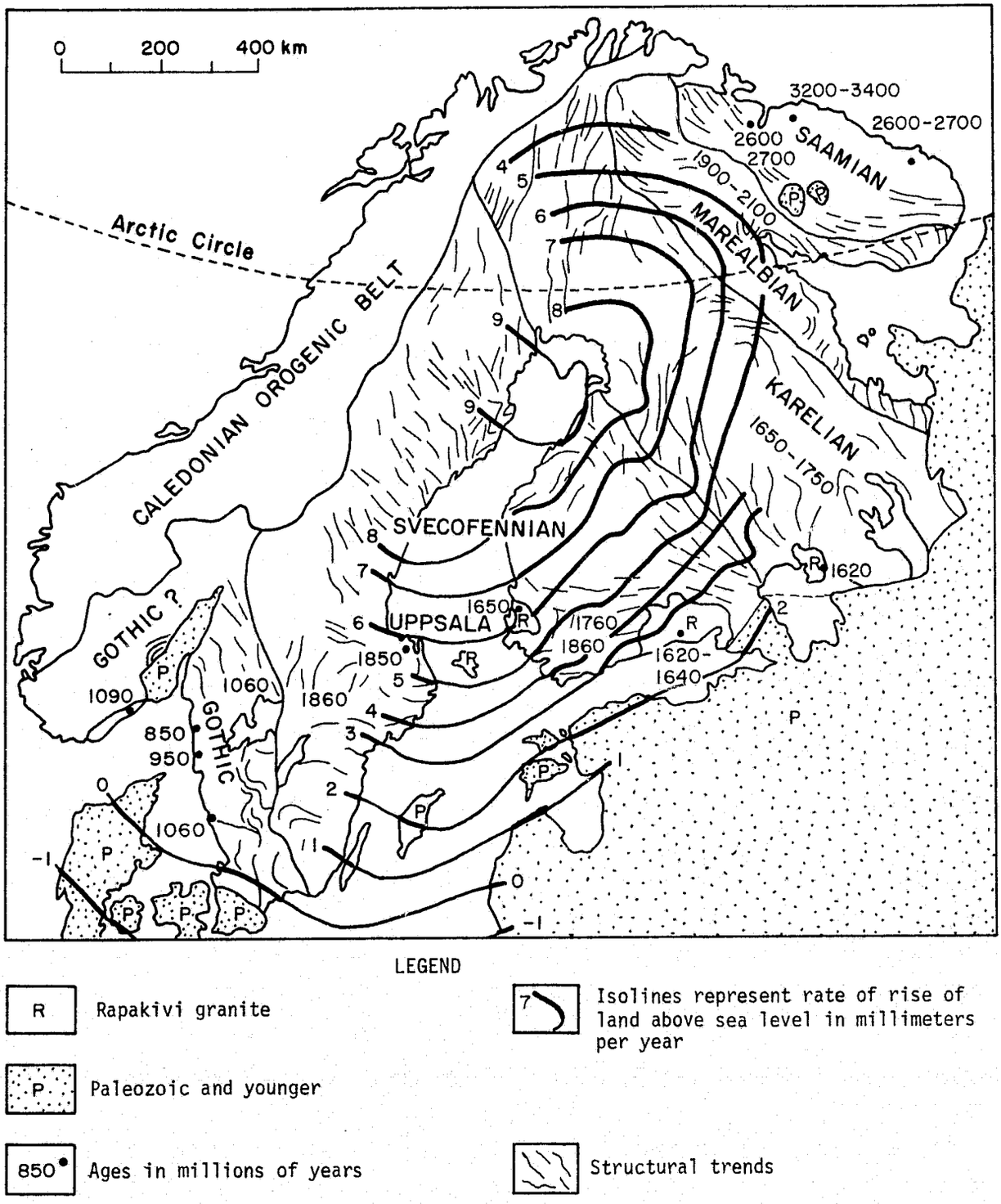


Figure 28. Tectonic map of the Baltic Shield (after Holmes, 1965), with contemporary uplift (after Flint, 1971).

Total uplift of the ancient shore lines of the Baltic Ice Lake reaches more than 250 m above present sea level. Uplift continues in Finland at rates of 1 mm $yr^{-1}$ (southeast) to 9 mm $yr^{-1}$ (northwest); in the Uppsala region, the rate of uplift is close to 5 mm $yr^{-1}$ (Flint, 1971; also see Figure 28).

The closest recorded seismicity consists of scattered epicenters along the continental shelf of Norway (Tarr, 1974; Figure 1).

We classify Uppsala as a stable site. Operational conditions appear excellent, but observing conditions leave much to be desired: The best month of the year has 51% cloud cover, and the yearly average is 64%.

## 25. BANGKOK, THAILAND

Bangkok (Krung Thep) is located at the southern end of the Central Thai Plain (13°44'N, 100°30'E), a 500-km (north–south) by 100-km (east–west) basin of Quaternary alluvial sedimentation at least 3000 m deep. The Plain forms a single structural unit with the Gulf of Siam, which is underlain by thick late-Tertiary sediments. A north–south line of Tertiary andesitic volcanoes, along the eastern margin of the Central Plain (Figure 29), can be considered to separate the Paleozoic Burma-Malaya geosynclinal arc to the west from the stable Mesozoic block to the east (Takaya, 1968).

Southeast Asia is now considered to have been part of Gondwanaland, proximate to India, before continental drift commenced in the Jurassic (Ridd, 1971). A change in the Indian Ocean spreading pattern initiated the subduction of the Indian plate northeastward under the Asian plate, to which Southeast Asia became welded. This subduction, in the late Jurassic, at first operated only in the Andaman-Nicobar sector; subduction under the present-day Sunda arc did not begin until the early Cretaceous. In the intervening period, a transform fault existed, which can now be identified with the northeast–southwest Khlong Marui fault (Figure 29). This fault is responsible for the prominent bend in peninsular Thailand and extends across the Gulf of Siam to pass not far southeast of Bangkok. A 200-km sinistral displacement has been identified along this fault during mapping of the associated swarm of subparallel tin-bearing pegmatites (Garson and Mitchell, 1970), although the Khlong Marui fault bears no evidence of still being active.

The present plate boundary between the Indian and the Eurasian plates forms the Burman, Andaman-Nicobar, and Sunda arcs. Active seismicity here is mild compared to the subduction zones of the Pacific margins, a fact that led Molnar, Fitch, and Wu (1973) to postulate that Indian subduction under Eurasia has slowed or stopped in Recent times (Figure 1). The present seismicity pattern, with intermediate-depth ($< 180$ km) earthquakes immediately northeast of

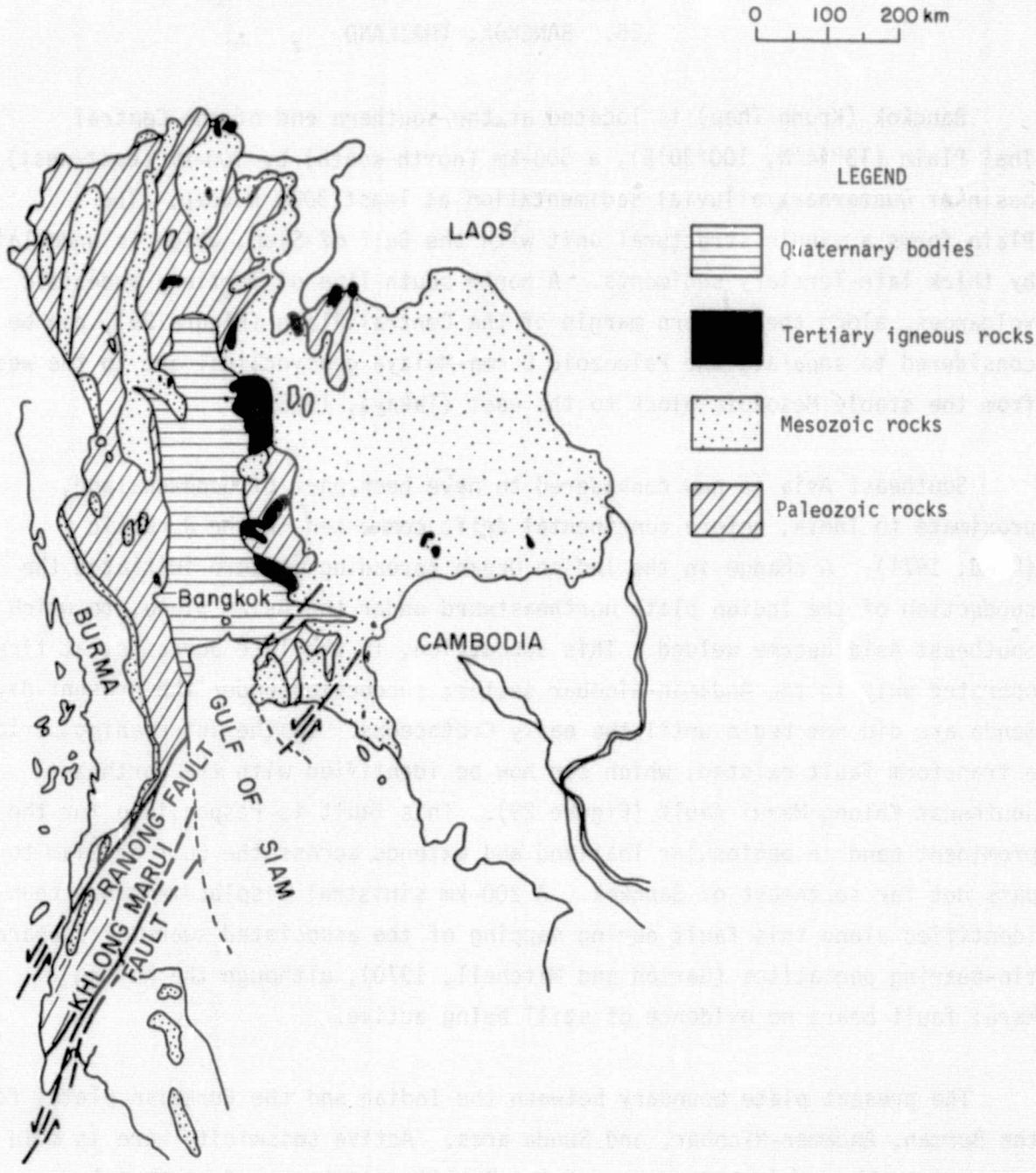


Figure 29. Geological map of Thailand (modified from Takaya, 1968; Garson and Mitchell, 1970).

a line of shallow earthquakes, suggests 200 km of Indian plate subduction during the last 10 m.y. — equivalent to a rate of 2 cm $yr^{-1}$ (Molnar et al., 1973).

A branching line of shallow-focus epicenters, possibly marking a microplate boundary, runs from the Andaman Islands north-northeast into the Gulf of Martaban and then along the Burmese border with Thailand and Laos, on to the K'un-ming region of Yunan Province, China. Focal mechanisms for two earthquakes on this line yielded solutions indicative of normal faulting (Fitch, 1970). On 17 February 1975, an earthquake (M = 5.5 to 6) occurred on the Thai-Burma border at 17.6N, 97.9E; it was felt throughout northern and central Thailand and caused slight damage and injuries in Bangkok. Nevertheless, Bangkok is far enough from major plate and microplate boundaries to escape major strain-release hazard.

Bangkok has 5 months a year with greater than 50% cloud cover, but several pretty clear months bring the annual mean down to 47%. Difficulties may occur in operating a station there: Utilities are available only near the city; communications could be very expensive; and living conditions may be prickly.

## 26. MT. HOPKINS, ARIZONA, USA

The complex geology of the Santa Rita Mountains in southwestern Arizona essentially consists of Mesozoic plutonic and volcanic rocks, formed during the Laramide orogeny, overlain and intruded by Paleocene and Oligocene rhyolites. The mountains were uplifted along northeast-trending faults during the Oligocene, and further regional uplift and minor faulting and volcanicity have continued into the Quaternary (Drewes, 1972a,b; also see Figure 30).

SAO has a camera and laser station at Mt. Hopkins (31°41'N, 110°53'W), some 60 km south of Tucson and only a few kilometers southwest of the Santa Rita fault. However, this fault, recording considerable vertical movements with subordinate lateral movements, was chiefly active in the Triassic-Paleocene and can now be regarded, on the evidence of its almost complete obliteration by subsequent plutonic intrusions, as extinct. Associated with the Santa Rita fault are the Sawmill fault zone 8 km to the northeast and the Montosa thrust faults and related Paleocene dikes of the Cottonwood canyon southwest of Mt. Hopkins, all trending northwest–southeast like the Santa Rita fault itself (Figure 30).

Later, Oligocene tectonism formed the Elephant Head fault, along which the present mountains were raised on the southeast upthrown side of the northeast-trending fault. Closely contemporaneous with this major faulting was the emplacement of the northeast-trending Gardner canyon and Box canyon dike swarms in response to northwest–southeast crustal tension; some sectors of the swarms were associated with graben subsidence (Drewes, 1972a,b). Pliocene and Pleistocene faulting, of the order of a few tens of meters, is shown in tilting and displacement of piedmont gravels along a range-front fault.

Southwestern Arizona, containing the Santa Rita Mountains, lies within the southern Basin and Range province, a broad region of late Tertiary-Quaternary crustal extension along the axis of the mountainous western USA passing to both

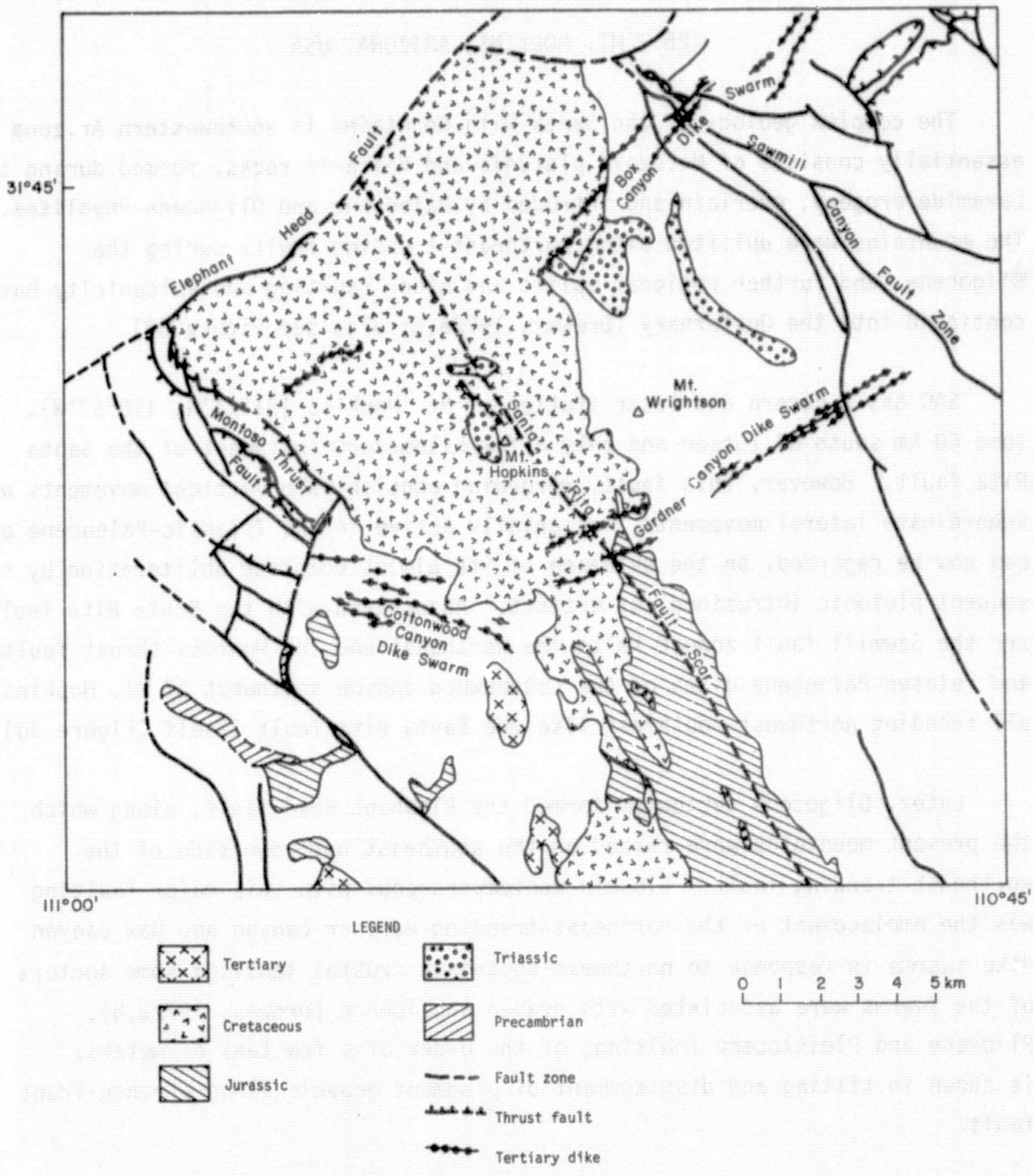


Figure 30. Tectonic map of the Mt. Hopkins area (simplified from Drewes, 1972b).

sides of the stable Colorado plateau (which occupies northeastern Arizona) (Figure 31). The overall east–west extension of the Basin and Range province probably results from differential movement focused on the North American-Pacific plate interaction along the San Andreas fault farther west (Atwater, 1970). Before the late Oligocene (34 to 28 m.y.) in south-central Arizona, subduction of the Farallon plate under the North American plate was responsible for strong compressive tectonism (various episodes of the Laramide orogeny) and associated andesitic igneous activity. Consumption of the Pacific-Farallon plate boundary in the subduction zone, and the resulting development of the San Andreas fault, changed the Arizona regime to one of regional uplift, crustal extension, and basalt-rhyolite volcanism, all of which are essentially still operating (Christiansen and Lipman, 1972).

Seismicity maps of Arizona (Duda, 1965; Woollard, 1969) reveal that earthquake activity is commonest along the boundary of the Colorado plateau, but it is also a feature of the southeastern corner of Arizona and the Mexican border. A few epicenters are dispersed through central and southwest Arizona and are probably related to Basin and Range faulting. The maximum observed magnitude is about 3. The south-central part of Arizona, including the Santa Rita Mountains, has been seismically quiet during the last few decades.

Various geophysical observations confirm the Basin and Range setting and its connotation of slow crustal extension of continental-rift type. Depth to the Moho under central Arizona is 20 km, compared with 40 km under the Colorado plateau. The $P_n$ velocity under central Arizona is 7.8 km $sec^{-1}$ (Warren, 1969), indicating the presence of low density and/or partially melted mantle: This is confirmed by S-wave attenuation studies (Yasar and Nuttli, 1974), which show that the low-velocity layer under the western USA is thickest, and probably closest to the surface ($\sim$ 40-km depth), under southern Utah and central Arizona. The depth of this layer under the Santa Rita Mountains is probably about 120 km, however. An average crustal cross section for the Basin and Range province in Arizona is given by Langston and Helmberger (1974) and Roy et al. (1972), which shows the thinner crust, the presence of partially melted upper mantle, and the relatively high heat flow (Figure 31).

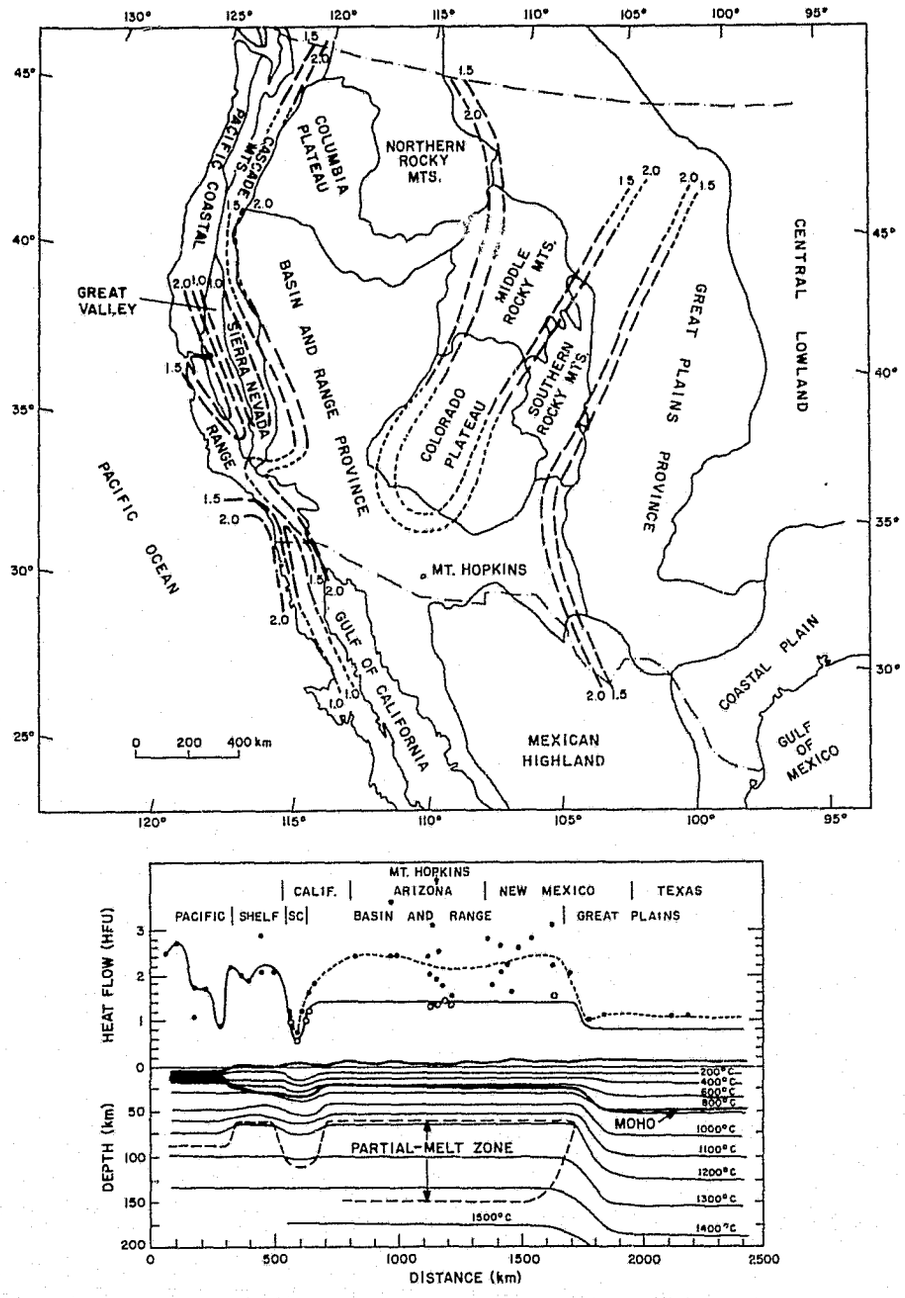


Figure 31. Map showing heat flow and physiographic provinces in the western United States. The contours are in units of HFU. The bottom figure represents a cross section of southwestern United States and part of northern Mexico at approximately 32°N latitude. Solid dots represent the observed heat flow at the surface, and open circles, the reduced heat flow. The region denoted by SC is the Peninsular Ranges of Southern California (modified from Roy, Blackwell, and Decker, 1972).

In summary, the site of Mt. Hopkins is associated with geophysical and tectonic characteristics indicative of minor instability, with rare, long-term episodes of greater magnitude.

Meteorologically (Pearlman et al., 1972) and operationally, Mt. Hopkins rates very well. July and August are the only months to suffer cloudiness in excess of 50%, and the annual mean is 38%. SAO has operated a camera station on Mt. Hopkins for several years.

## 27. CONCLUSIONS

The quality as well as the quantity of available geological and geophysical information varies greatly from one site to another. Although we have established certain criteria as a measure of the stability of a site, these criteria generally apply more to regional than to local stability; local data can be obtained only through detailed geophysical and geodetic monitoring of a site. Of the 26 stations studied, only Tokyo, one of the most unstable sites, has sufficient recorded local data. It is not only the stability of a site that matters, but also — and more importantly — an understanding of any instability of a site. Consequently, we recommend that supplementary geophysical (microseismic, tidal gravimetric, and tiltmetric) and geodetic surveys be made at all sites to be selected as laser tracking stations.

Table 4 is a brief summary of our evaluations, in which each station is ranked from 1 to 3 in the categories studied: tectonic, cloud-cover, and operational considerations. It can be seen at a glance that some locations — such as Quito, Arequipa, Naini Tal, and Guam — would not make good ranging-station sites because of tectonic instability. Others can be eliminated because of consistently poor weather or possible operating difficulties.

Table 4. Summary of factors for evaluation of laser stations.

| Station number* | Station locations | Geophysical considerations† | Cloud-cover considerations‡ | Operational considerations** |
|---|---|---|---|---|
| 1 | Argentina, Comodoro Rivadavia | 1 | 1 | 2 |
| 2 | Atlantic Ocean, Bermuda | 1 | 1 | 1 |
| 3 | Australia, Orroral Valley | 2 | 1 | 1 |
| 4 | Brazil, Natal | 1 | 3 | 1 |
| 5 | Brazil, Porto Alegre | 1 | 1 | 1 |
| 6 | Brazil, São Francisco | 1 | 2 | 3 |
| 7 | Canada, Fort Resolution | 1 | 1 | 3 |
| 8 | Ecuador, Quito | 3 | 3 | 1 |
| 9 | Egypt, Cairo | 2 | 1 | 2 |
| 10 | Ethiopia, Debre Zeit | 3 | 2 | 2 |
| 11 | Greece, Athens | 2 | 2 | 1 |
| 12 | India, Bangalore | 1 | 2 | 3 |
| 13 | India, Naini Tal | 3 | 2 | 2 |
| 14 | Japan, Tokyo | 3 | 3 | 1 |
| 15 | Korea, Pusan | 1 | 2 | 3 |
| 16 | Pacific Ocean, Rapa Nui | 2 | 3 | 3 |
| 17 | Pacific Ocean, Guam | 3 | 3 | 1 |
| 18 | Pacific Ocean, Maui, Hawaii | 2 | 1 | 1 |
| 19 | Pacific Ocean, Tutuila, Samoa | 2 | 3 | 2 |
| 20 | Pacific Ocean, Tahiti | 1 | 1 | 3 |
| 21 | Pacific Ocean, Wake Island | 1 | 1 | 2 |
| 22 | Peru, Arequipa | 3 | 2 | 1 |
| 23 | Spain, San Fernando | 2 | 1 | 1 |
| 24 | Sweden, Uppsala | 1 | 3 | 1 |
| 25 | Thailand, Bangkok | 2 | 2 | 2 |
| 26 | USA, Mt. Hopkins, Arizona | 2 | 1 | 1 |

*The code number ascribed to each station is the same as indicated in Figure 1.

†Relative stability of the location: 1 = stable, 2 = some activity, 3 = unstable.

‡Relative observing conditions: 1 = good most of the year, 2 = good about 6 months of the year, 3 = poor.

**Relative ease of setting up and operating a station: 1 = no problem, 2 = difficult, 3 = very difficult.



C·2

## 28. ACKNOWLEDGMENTS

We wish to thank Mr. John M. Thorp and Mr. Preston R. Clark for collecting, from disparate and sometimes obscure sources, the cloud-cover and operational data reproduced in Tables 2 and 3. We especially thank Ms. Cynthia B. Wong for efficient editorial labors that have reduced the entropy of our compendium.

## 29. REFERENCES


ANDERSON, R. N., FORSYTH, D. W., MOLNAR, P., and MAMMERICKX, J.

1974. Fault plane solutions of earthquakes on the Nazca plate boundaries and the Easter plate. Earth Planet. Sci. Lett., vol. 24, pp. 188-202.

ANDRIEUX, J., FONTBOTE, J.-M., and MATTAUER, M.

1971. Sur un modèle explicatif de l'arc de Gibraltar. Earth Planet. Sci. Lett., vol. 12, pp. 191-198.

ASWATHANARAYANA, U.

1964. Age determination of rocks and geochronology of India. In International Geology Congress, 22nd Session, ed. by B. C. Roy, New Delhi, India, 27 pp.

ATWATER, T.

1970. Implications of plate tectonics for the Cenozoic tectonic evolution of western North America. Geol. Soc. Amer. Bull., vol. 81, pp. 3513-3536.

AUMENTO, F., REYNOLDS, P. H., and GUNN, B. M.

1974. The Bermuda seamount: A reactivated section of an older ocean crust (abstract). Trans. Amer. Geophys. Union, vol. 55, p. 455.

BAKER, B. H.

1963. Geology of the Baragoi area. Geol. Surv. Kenya Rep. No. 53, 74 pp.

BAKER, B. H., MOHR, P. A., and WILLIAMS, L. A. J.

1972. Geology of the Eastern Rift system of Africa. Geol. Soc. Amer. Spec. Paper No. 136, 67 pp.

BAKER, B. H., and WOHLENBERG, J.

1971. Structure and evolution of the Kenya rift valley. Nature, vol. 229, pp. 538-542.

BAKER, P. E., BUCKLEY, F., and HOLLAND, J. G.

1974. Petrology and geochemistry of Easter Island. Contr. Min. Petrol., vol. 44, pp. 85-100.

BARAZANGI, M., and DORMAN, J.

1969. World seismicity maps compiled from ESSA Coast and Geodetic Survey epicenter data, 1961-1967. Bull. Seism. Soc. Amer., vol. 59, pp. 369-380.

BARAZANGI, M., PENNINGTON, W., and ISACKS, B.

1975. Global study of seismic wave attenuation in the upper mantle behind island arcs using pP waves. Journ. Geophys. Res., vol. 80, pp. 1079-1092.

BELLIDO, E. B.

1969. Sinopsis de la geologia del Peru. Bol. Serv. Geol. Min. Peru, no. 22, 54 pp.

BERCKHEMER, H., BAIER, B., BARTELSEN, H., BEHLE, A., BURKHARDT, H., GEBRANDE, H., MAKRIS, J., MENZEL, H., MILLER, H., and VEES, R.

1975. Deep seismic soundings in the Afar region and on the highland of Ethiopia. In Symposium on the Afar Region of Ethiopia, ed. by A. Pilger and A. Rösler, Schweizerbart, Stuttgart, in press.

BRACEY, D. R., and OGDEN, T. A.

1972. Southern Mariana arc: Geophysical observations and hypothesis of evolution. Bull. Geol. Soc. Amer., vol. 83, pp. 1509-1522.

BYERS, A. R.

1962. Major faults in western part of Canadian Shield with special reference to Saskatchewan. In The Tectonics of the Canadian Shield, ed. by J. S. Stevenson, Roy. Soc. Canada Spec. Publ. No. 4, pp. 40-59.

CHASE, C. G.

1971. Tectonic history of the Fiji plateau. Bull. Geol. Soc. Amer., vol. 82, pp. 3087-3110.

CHRISTIANSEN, R. L., and LIPMAN, P. W.

1972. Cenozoic volcanism and plate tectonic evolution of the western United States. II. Late Cenozoic. Phil. Trans. Roy. Soc. London, vol. A271, pp. 249-284.

CHUBB, L. J.

1957. The pattern of some Pacific island chains. Geol. Mag., vol. 94, pp. 221-228.

CLEARY, J. R., and SIMPSON, D. W.

1971. Seismotectonics of the Australian continent. Nature, vol. 230, pp. 239-241.

COBBING, E. J., and PITCHER, W. S.

1972. Plate tectonics and the Peruvian Andes. Nature, Phys. Sci., vol. 240, pp. 51-53.

DALY, R. A.

1924. The Geology of American Samoa. Geophys. Lab., Carnegie Inst., Washington, Publ. No. 340, pp. 95-143.

de ALMEIDA, F. F. M., AMARAL, G., CORDANI, U. G., and KAWASHITA, K.

1973. The Precambrian evolution of the South American cratonic margin south of the Amazon river. In The Ocean Basins and Margins, vol. 1, The South Atlantic, ed. by A. E. M. Nairn and G. Stehli, Plenum Press, New York, pp. 411-446.

DONN, W. L., and EWING, M.

1972. Resonant coupling of ocean Rayleigh waves to atmospheric shock waves from Apollo rockets. Journ. Geophys. Res., vol. 77, pp. 7010-7021.

DREWES, H.

1972a. Cenozoic rocks of the Santa Rita Mountains, southeast of Tucson, Arizona. U. S. Geol. Surv. Prof. Paper 746, 66 pp.

1972b. Structural geology of the Santa Rita Mountains, southeast of Tucson, Arizona. U. S. Geol. Surv. Prof. Paper 748, 35 pp.

DUDA, S. J.

1965. Regional seismicity and seismic wave propagation from records at the Tonto Forest Seismological Observatory, Payson, Arizona. Ann. di Geofis., vol. 18, pp. 365-397.

DYMOND, J.

1975. K-Ar ages of Tahiti and Moorea, Society Islands, and implications for the hot-spot model. Geology, vol. 3, pp. 236-240.

FITCH, T. J.

1970. Earthquake mechanisms in the Himalayan, Burmese and Andaman region and continental tectonics in central Asia. Journ. Geophys. Res., vol. 75, pp. 2699-2709.

FLINT, R. F.

1971. Glacial and Quaternary Geology. J. Wiley & Sons, New York, 892 pp.

FORRISTALL, G. Z.

1974. The thickness of the asthenosphere deduced from the motion of the Hawaiian hot-spot. Geophys. Res. Lett., vol. 1, pp. 131-133.

GANSSER, A.

1964. Geology of the Himalayas. J. Wiley & Sons, London, 289 pp.

GARSON, M. S., and MITCHELL, A. H. G.

1970. Transform faulting in the Thai Peninsula. Nature, vol. 228, pp. 45-47.

GASS, I. G., and MASSON-SMITH, D.

1963. The geology and gravity anomalies of the Troodos massif, Cyprus. Phil. Trans. Roy. Soc. London, vol. A225, pp. 417-467.

GEOLOGICAL SOCIETY OF AUSTRALIA

1971. Tectonic map of Australia and New Guinea (1:5,000,000). Geol. Soc. Australia, Sydney, Australia.

GOUIN, P.

1970. Seismic and gravity data from Afar in relation to surrounding areas. Phil. Trans. Roy. Soc. London, vol. A267, pp. 339-358.

1975. Catalogue of Ethiopian earthquakes. Bull. Geophys. Obs. Addis Ababa, no. 16 (in press).

GUEVARA, C.

1969. Geologia del cuadrangulo de Characato. Bol. Serv. Geol. Min. Peru, no. 23, 53 pp.

HALPERN, M.

1973. Regional geochronology of Chile south of 50 degrees latitude. Bull. Geol. Soc. Amer., vol. 84, pp. 2407-2422.

HAMILTON, E. L.

1956. Sunken islands of the mid-Pacific Mountains. Geol. Soc. Amer. Mem., no. 64, 97 pp.

HAWKINS, J. W., and NATLAND, J. H.

1975. Nephelinites and basanites of the Samoan linear volcanic chain: Their possible tectonic significance. Earth Planet. Sci. Lett., vol. 24, pp. 427-439.

HEDGE, C. E., PETERMAN, Z. E., and DICKINSON, W. R.

1972. Petrogenesis of lavas from western Samoa. Bull. Geol. Soc. Amer., vol. 83, pp. 2709-2714.

HERRON, E. M.

1972. Sea-floor spreading and the Cenozoic history of the east-central Pacific. Bull. Geol. Soc. Amer., vol. 83, pp. 1671-1692.

HOFFMAN, P.

1973. Evolution of an early Proterozoic continental margin: The Coronation geosyncline and associated aulacogens of the northwestern Canadian Shield. Phil. Trans. Roy. Soc. London, vol. A273, pp. 547-581.

HOLMES, A.

1965. Principles of Physical Geology. 2nd ed., Ronald Press Co., New York, 1288 pp.

HYNDMAN, R. D., and AUMENTO, F.

1973. Deep drill — 1972: Heat flow in Bermuda (abstract). Trans. Amer. Geophys. Union, vol. 54, p. 486.

JACKSON, E. D., SILVER, E. A., and DALRYMPLE, G. B.

1972. Hawaiian-Emperor chain and its relation to Cenozoic circumpacific tectonics. Bull. Geol. Soc. Amer., vol. 83, pp. 601-618.

JACOBS, J. A., RUSSELL, R. D., and WILSON, J. T.

1974. Physics and Geology. 2nd ed., McGraw-Hill Book Co., New York, 622 pp.

JAMES, D. E.

1971. Plate tectonic model for the evolution of the central Andes. Bull. Geol. Soc. Amer., vol. 82, pp. 3325-3346.

KAILA, K. L., GAUR, V. K., and NARAIN, H.
1972. Quantitative seismicity maps of India. Bull. Seism. Soc. Amer., vol. 62, pp. 1119-1132.

KAMPSCHUUR, W., and RONDEEL, H. E.
1975. The origin of the Betic orogen, Southern Spain. Tectonophys., vol. 27, pp. 39-56.

KANASEWICH, E. R., ELLIS, R. M., CHAPMAN, C. H., and GUTOWSKI, P. R.
1972. Teleseismic array evidence for inhomogeneities in the lower mantle and the origin of the Hawaiian islands. Nature, Phys. Sci., vol. 239, pp. 99-100.

KANASEWICH, E. R., and GUTOWSKI, P. R.
1975. Detailed seismic analysis of a lateral mantle inhomogeneity. Earth Planet. Sci. Lett., vol. 25, pp. 379-384.

KARIG, D. E.
1971. Structural history of the Mariana island arc system. Bull. Geol. Soc. Amer., vol. 82, pp. 323-344.

KASAHARA, K., OKADA, A., SHIBANO, M., SASAKI, K., and MATSUMOTO, S.
1967. Electro-optical measurement of horizontal strains accumulating in the swarm earthquake area (3). Bull. Earthquake Res. Inst., vol. 45, pp. 225-239.

KASAHARA, K., and SUGIMURA, A.
1964. Spatial distribution of horizontal secular strain in Japan. Journ. Geol. Soc. Japan, vol. 10, pp. 139-145.

KELLEHER, J.
1972. Rupture zones of large South American earthquakes and some predictions. Journ. Geophys. Res., vol. 77, pp. 2087-2103.

KISSLINGER, C.
1975. Processes during the Matsushiro, Japan, earthquake swarm as revealed by leveling, gravity, and spring-flow observations. Geology, vol. 3, pp. 57-62.

KOBAYASHI, T.

1967. Geology of South Korea. In Geology and Mineral Resources of the Far East, ed. by T. Ogura, Univ. of Tokyo Press, Tokyo, vol. 1, pp. 25-138.

KRISHNAN, M. S.

1968. Geology of India and Burma. 5th ed., Higginbothams Ltd., Madras, India, 536 pp.

LACROIX, A.

1928. La constitution lithologique des îles volcaniques de la Polynésie australe. Acad. Sci. Paris Mem., vol. 5, pp. 1-80.

LANGSTON, C. A., and HELMBERGER, D. V.

1974. Interpretation of body and Rayleigh waves from NTS to Tucson. Bull. Seism. Soc. Amer., vol. 64, pp. 1919-1929.

LePICHON, X.

1968. Sea-floor spreading and continental drift. Journ. Geophys. Res., vol. 73, pp. 3661-3697.

LePICHON, X., FRANCHETEAU, J., and BONNIN, J.

1973. Plate Tectonics. Elsevier Sci. Publ. Co., New York, 300 pp.

LUDWIG, W. J., MARAUCHI, S., and HOUTZ, R. E.

1975. Sediments and structure of the Japan Sea. Bull. Geol. Soc. Amer., vol. 86, pp. 651-664.

MACDONALD, G. A.

1944. Petrography of the Samoan Islands. Bull. Geol. Soc. Amer., vol. 55, pp. 1333-1362.

MACDONALD, G. A., and ABBOTT, A. T.

1970. Volcanoes in the Sea: The Geology of Hawaii. Hawaii Univ. Press, Honolulu, Hawaii, 441 pp.

MAKRIS, J.

1973. Some geophysical aspects of the evolution of the Hellenides. Bull. Geol. Soc. Greece, vol. 10, pp. 206-213.

1975. Afar and Iceland — A geophysical comparison. In Symposium on the Afar Region of Ethiopia, ed. by A. Pilger and A. Rösler, Schweizerbart, Stuttgart, in press.

MALAHOFF, A.

1969. Gravity anomalies over volcanic regions. In The Earth's Crust and Upper Mantle, ed. by P. J. Hart, Amer. Geophys. Union, Geophys. Mono. No. 13, pp. 364-378.

MAMMERICKX, J., ANDERSON, R. N., MENARD, H. W., and SMITH, S. M.

1975. Morphology and tectonic evolution of the east-central Pacific. Bull. Geol. Soc. Amer., vol. 86, pp. 111-118.

McBIRNEY, A.R., and AOKI, K.

1968. Petrology of the island of Tahiti. Geol. Soc. Amer. Mem., no. 116, pp. 523-556.

McDOUGALL, I.

1964. Potassium-argon ages of lavas from the Hawaiian islands. Bull. Geol. Soc. Amer., vol. 75, pp. 107-128.

1971. Volcanic island chains and sea floor spreading. Nature, Phys. Sci., vol. 231, pp. 141-144.

McELHINNY, M. W.

1973. Earth sciences and the Australian continent. Nature, vol. 246, pp. 264-268.

McKENZIE, D. P.

1972. Active tectonics of the Mediterranean region. Geophys. Journ., vol. 30, pp. 109-185.

McKENZIE, D. P., DAVIES, D., and MOLNAR, P.

1970. Plate tectonics of the Red Sea and East Africa. Nature, vol. 226, pp. 243-248.

MEHDI, S. H., KUMAR, G., and PRAKASH, G.

1972. Tectonic evolution of eastern Kumann Himalaya: A new approach. Himalayan Geol., vol. 2, pp. 481-501.

MENARD, H. W.

1964. Marine Geology of the Pacific. McGraw-Hill Book Co., New York, 271 pp.

MENDIGUREN, J. A.

1971. Focal mechanism of a shock in the middle of the Nazca plate. Journ. Geophys. Res., vol. 76, pp. 3861-3879.

MINSTER, J. B., JORDAN, T. H., MOLNAR, P., and HAINES, E.

1974. Numerical modelling of instantaneous plate tectonics. Geophys. Journ. Roy. Astron. Soc., vol. 36, pp. 541-576.

MIYABE, N., MIYAMURU, S., and MIZOUE, M.

1966. A map of secular vertical movements of the earth's crust in Japan. Ann. Acad. Sci. Fenn., Ser. AIII, Geol. Geogr., pp. 287-289.

MOHR, P. A.

1961. The geology, structure and origin of the Bishoftu explosion craters. Bull. Geophys. Obs. Addis Ababa, no. 4, pp. 65-101.

1967. The Ethiopian rift system. Bull. Geophys. Obs. Addis Ababa, no. 11, pp. 1-65.

1971. Ethiopian Tertiary dike swarms. Smithsonian Astrophys. Obs. Spec. Rep. No. 339, 53 pp.

1973. Crustal deformation rate and the evolution of the Ethiopian rift. In Implications of Continental Drift to the Earth Sciences, ed. by D. H. Tarling and S. K. Runcorn, Academic Press, London, pp. 767-776.

1974. 1973 Ethiopian rift geodimeter survey. Smithsonian Astrophys. Obs. Spec. Rep. No. 358, 110 pp.

1975. The Sagatu Ridge dike swarm, Ethiopian rift margin. J. Volcanology, in press.

MOLNAR, P., FITCH, T. J., and WU, F. T.

1973. Fault plane solutions of shallow earthquakes and contemporary tectonics in Asia. Earth Planet. Sci. Lett., vol. 19, pp. 101-112.

MOORE, J. G.

1970. Relationship between subsidence and volcanic load, Hawaii. Bull. Volc., vol. 34, pp. 562-576.

MORGAN, W. J.

1971. Convection plumes in the lower mantle. Nature, vol. 230, pp. 42-43.

MUELLER, S., PRODEHL, C., MENDES, A. S., and MOREIRA, V. S.

1973. Crustal structure in the southwestern part of the Iberian Peninsula. Tectonophys., vol. 20, pp. 307-318.

MYERS, J. S.

1975. Vertical crustal movements of the Andes in Peru. Nature, vol. 254, pp. 672-674.

NINKOVICH, D., and HAYS, J. D.

1972. Mediterranean island arcs and origin of high potash volcanoes. Earth Planet. Sci. Lett., vol. 16, pp. 331-345.

NOBLE, D. C., McKEE, E. H., FARRAR, E., and PETERSEN, U.

1974. Episodic Cenozoic volcanism and tectonism in the Andes of Peru. Earth Planet. Sci. Lett., vol. 21, pp. 213-220.

OKAL, E., and KUSTER, G.

1975. A teleseismic array study in French Polynesia: Implications for distant and local structure. Geophys. Res. Lett., vol. 2, pp. 5-8.

OVERSBY, B.

1971. Palaeozoic plate tectonics in the southern Tasman geosyncline. Nature, Phys. Sci., vol. 234, pp. 45-60.

PAUL, D. K., REX, D. C., and HARRIS, P. G.

1975. Chemical characteristics and K-Ar ages of Indian kimberlite. Bull. Geol. Soc. Amer., vol. 86, pp. 364-366.

PEARLMAN, M. R., HOGAN, D., GOODWIN, K., and KURTENBACH, D.

1972. A meteorological report for the Mt. Hopkins Observatory: 1968-1971. Smithsonian Astrophys. Obs. Spec. Rep. No. 345, 53 pp.

PETERMAN, Z. E., and HEDGE, C. E.

1971. Related strontium isotopic and chemical variations in oceanic basalts. Geol. Soc. Amer. Bull., vol. 82, pp. 493-499.

PICHLER, H., and KUSSMAUL, S.

1972. The calc-alkaline volcanic rocks of the Santorini group (Aegean Sea, Greece). Neues Jahrb. Miner. Abh., vol. 116, pp. 268-307.

PITMAN, W. C., LARSON, R. L., and HERRON, E. M.

1974. The age of the ocean basins (two charts and summary statement). Geol. Soc. Amer., Boulder, Colorado.

POWELL, C. McA., and CONAGHAN, P. J.

1973. Plate tectonics and the Himalayas. Earth Planet. Sci. Lett., vol. 20, pp. 1-12.

QURESHY, M. N.

1971. Relation of gravity to elevation and rejuvenation of blocks in India. Journ. Geophys. Res., vol. 76, pp. 545-554.

REYNOLDS, P. H., and AUMENTO, F.

1973. Deep drill — 1972: Geochronology of the Bermuda drill core (abstract). Trans. Amer. Geophys. Union, vol. 54, p. 485.

RIDD, M. F.

1971. South-east Asia as a part of Gondwanaland. Nature, vol. 234, pp. 531-533.

ROBSON, D. A.

1971. The structure of the Gulf of Suez (Clysmic) rift, with special reference to the eastern side. Journ. Geol. Soc. (London), vol. 127, pp. 247-276.

ROGERS, J. J. W.

1974. Problems concerning the evolution of the Precambrian Shield of peninsular India. Geophys. Res. Bull., Hyderabad, India, vol. 12, pp. 103-118.

ROY, R. F., BLACKWELL, D. D., and DECKER, E. R.

1972. Continental heat flow. In The Nature of the Solid Earth, ed. by E. C. Robertson, McGraw-Hill Book Co., New York, pp. 506-543.

SAID, R.

1962. The Geology of Egypt. Elsevier Publ. Co., New York, 377 pp.

SCHÜRMANN, H. M. E.

1971. Gulf of Suez and northern Red Sea area. In Tectonics of Africa, UNESCO (Paris) Earth Sci. Ser., no. 6, pp. 417-427.

SEARLE, R. C., and GOUIN, P.

1971. An analysis of some local earthquake phases originating near the Afar triple junction. Bull. Seism. Soc. Amer., vol. 61, pp. 1061-1071.

1972. A gravity survey of the central part of the Ethiopian rift valley. Tectonophys., vol. 15, pp. 41-52.

SHOR, G. G., and POLLARD, D. D.

1964. Mohole site selection studies north of Maui. Journ. Geophys. Res., vol. 69, pp. 1627-1637.

SOLOMON, M., and GRIFFITHS, J. R.

1972. Tectonic evolution of the Tasman orogenic zone, eastern Australia. Nature, Phys. Sci., vol. 237, pp. 3-6.

STAUDER, W.

1975. Subduction of the Nazca plate under Peru as evidenced by focal mechanisms and by seismicity. Journ. Geophys. Res., vol. 80, pp. 1053-1064.

STEARNS, H. T.

1944. Geology of the Samoan Islands. Bull. Geol. Soc. Amer., vol. 55, pp. 1279-1332.

STEWART, I. C. F., and DENHAM, D.

1974. Simpson desert earthquake Central Australia, August 1972. Geophys. Journ. Roy. Astron. Soc., vol. 39, pp. 335-341.

STOCKWELL, C. H.

1962. A tectonic map of the Canadian Shield. In The Tectonics of the Canadian Shield, ed. by J. S. Stevensen, Roy. Soc. Canada Spec. Publ. No. 4, pp. 6-15.

STOSE, G. W.

1950. Geological map of South America. Geol. Soc. Amer., New York.

STOVER, C. W.

1973. Seismicity and tectonics of the east Pacific Ocean. Journ. Geophys. Res., vol. 78, pp. 5209-5220.

SUGIMURA, A., and UYEDA, S.

1973. Island Arcs. Japan and Its Environs. Elsevier Developments in Geotectonics No. 3, 247 pp.

SYKES, L. R.

1973. Intraplate earthquakes, lithospheric stresses and the driving mechanism of plate tectonics. Nature, vol. 245, pp. 298-302.

TAKAYA, Y.

1968. Quaternary outcrops in the Central Plain of Thailand. In Geology and Mineral Resources in Thailand and Malaya, ed. by K. Takimoto, Center for Southeast Asian Studies, Kyoto Univ., Kyoto, Japan, pp. 7-68.

TARR, A. C.

1974. World seismicity map. Prepared by U. S. Geological Survey from earthquake data from the National Oceanic and Atmospheric Administration up to 1972.

THOMPSON, G. A., and BURKE, D. B.

1974. Regional geophysics of the Basin and Range province. Ann. Rev. Earth Planet. Sci., vol. 2, pp. 213-238.

THORP, J. M., BUSH, M. A., and PEARLMAN, M. R.

1974. An evaluation of SAO sites for laser operations. Tech. Rep. RTOP 161-01-03, Supplement No. 57 to NASA Grant NGR 09-015-002, October, 37 pp.

TRACEY, J. I., Jr., SCHLANGER, S. O., STARK, J. T., DOAN, D. B., and MAY, H. G.

1964. General geology of Guam. U. S. Geol. Surv. Prof. Paper 403-A, 104 pp.

UDIAS, A., and LOPEZ ARROYO, A.

1972. Plate tectonics and the Azores-Gibraltar region. Nature, Phys. Sci., vol. 237, pp. 67-69.

VARGAS, L.

1970. Geologia del cuadrangulo de Arequipa. Bol. Serv. Geol. Min. Peru, no. 24, 64 pp.

VARMA, M. M., GOSAVI, P. D., and GUHA, S. K.

1970. Kothagudem (Andhra Pradesh) earthquake of April 13, 1969, Broach (Gujarat) earthquake of March 23, 1970 and seismicity of peninsular India. Bull. Indian Soc. Earthquake Tech. (Roorkee), vol. 7, pp. 207-218.

WARREN, D. H.

1969. Seismic refraction survey of crustal structure in central Arizona. Bull. Geol. Soc. Amer., vol. 80, pp. 257-282.

WATTS, A. B., and WEISSEL, J. K.

1975. Tectonic history of the Shikoku marginal basin. Earth Planet. Sci. Lett., vol. 25, pp. 239-250.

WHYMPER, E.

1892. Travels amongst the Great Andes of the Equator. Longmans, London, 456 pp.

WILLIAMS, H.

1933. Geology of Tahiti, Moorea, and Maiao. Bernice P. Bishop Museum Bull. No. 105, 89 pp.

WILSON, J. T.

1963. Evidence from islands on the spreading of ocean floors. Nature, vol. 197, pp. 536-538.

WOOLLARD, G. P.

1969. Tectonic activity in North America as indicated by earthquakes. In The Earth's Crust and Upper Mantle, ed. by P. J. Hart, Amer. Geophys. Union, Geophys. Mono. No. 13, pp. 125-133.

1975. The interrelationships of crustal and upper mantle parameter values in the Pacific. Rev. Geophys. Space Phys., vol. 13, pp. 87-137.

YASAR, T., and NUTTLI, O. W.

1974. Structure of the shear-wave low-velocity channel in the western United States. Geophys. Journ. Roy. Astron. Soc., vol. 37, pp. 353-364.

YOUSSEF, M. I.

1968. Structural pattern of Egypt and its interpretation. Bull. Amer. Assoc. Petrol. Geol., vol. 52, pp. 601-614.

ZAMBRANO, J. J., and URIEN, C. M.

1970. Geological outline of the basins in southern Argentina and their continuation off the Atlantic shore. Journ. Geophys. Res., vol. 75, pp. 1363-1396.

APPENDIX A

GEOLOGICAL TIME SCALE

| Period | Epoch | Millions of years |
|---|---|---|
| Quaternary | Holocene | |
| | Pleistocene | 2 |
| Tertiary | Pliocene | 5 |
| | Miocene | 25 |
| | Oligocene | 40 |
| | Eocene | 60 |
| | Paleocene | 70 |
| | Cretaceous | 135 |
| | Jurassic | 180 |
| | Triassic | 225 |
| | Permian | 280 |
| | Carboniferous | 350 |
| | Devonian | 400 |
| | Silurian | 440 |
| | Ordovician | 500 |
| | Cambrian | 600 |
| | Precambrian | |